

ELECTRON SPIN RESONANCE STUDIES OF  
RADICALS IN IRRADIATED ACETATES

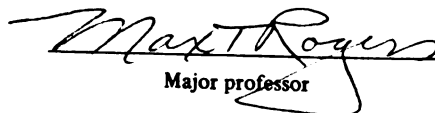
Dissertation for the Degree of Ph. D.  
MICHIGAN STATE UNIVERSITY  
RICHARD CLARK SCHOENING  
1973



This is to certify that the  
thesis entitled  
ELECTRON SPIN RESONANCE STUDIES OF  
RADICALS IN IRRADIATED ACETATES

presented by  
Richard Clark Schoening

has been accepted towards fulfillment  
of the requirements for  
Ph.D. degree in Chemistry

  
Major professor

Date 1973 December 11

## ABSTRACT

### ELECTRON SPIN RESONANCE STUDIES OF RADICALS IN IRRADIATED ACETATES

By

Richard Clark Schoening

Electron spin resonance studies of radicals produced in irradiated single crystals of sodium acetate have been carried out. In  $\text{CH}_3\text{COONa} \cdot 3\text{D}_2\text{O}$  crystals three radicals are formed; the methyl radical predominates at  $77^\circ \text{K}$ , the  $\cdot\text{CH}_2\text{COO}^-$  radical becomes the dominant species at  $198^\circ \text{K}$  and at room temperature the  $\cdot\text{CO}_2^-$  radical is found. The ESR parameters for each radical were determined. In addition,  $\cdot\text{CD}_3$  was studied in irradiated single crystals of  $\text{CD}_3\text{COONa} \cdot 3\text{D}_2\text{O}$  at  $77^\circ \text{K}$ . Both the  $\cdot\text{CH}_3$  and  $\cdot\text{CD}_3$  radicals are  $\pi$ -electron radicals undergoing rotation about their threefold axes at  $77^\circ \text{K}$ . Changes in relative intensities of the lines of the spectra on cooling to  $4.2^\circ \text{K}$  indicate some restriction of rotation at low temperatures.

Anhydrous sodium acetate single crystals produce only  $\cdot\text{CH}_2\text{COO}^-$  radicals at  $77^\circ \text{K}$ . In addition, a triplet spectrum was observed which was attributed to a radical pair with approximately  $5.77 \text{ \AA}$  distance between the two unpaired electrons. Although the components of the pair appeared

to be different the spectra did not permit their positive identification.

The electron spin resonance spectra of radicals produced in irradiated fluorine-substituted ammonium acetates were also studied. Irradiation of single crystals of ammonium monofluoroacetate produced  $\cdot\text{CH}_2\text{COO}^-$  and  $\cdot\text{CFHCOO}^-$  in the approximate ratio of 4:1. On warming to room temperature only  $\cdot\text{CFHCOO}^-$  was present. This room-temperature radical was found to occupy two magnetically inequivalent sites. On cooling, two  $\cdot\text{CFHCOO}^-$  radicals were observed each with different  $A(\text{F})$  and  $A(\text{H})$  tensors and each occupying two magnetically distinct sites. The  $g$ , and the fluorine and the hydrogen hyperfine splitting tensors, were evaluated for both radicals at  $-140^\circ\text{C}$  and for the radical at room temperature. In addition, the  $^{13}\text{C}$  hyperfine interaction tensor was also obtained for the room-temperature radical.

An oscillation of the CHF group of the  $\cdot\text{CFHCOO}^-$  radical about the C-C bond was postulated to account for the dependence of the ESR spectra on temperature. However, changes in crystal structure may also occur.

Irradiated single crystals of ammonium difluoroacetate produced two radicals,  $\cdot\text{CFHCOO}^-$  and  $\cdot\text{CF}_2\text{COO}^-$ , in approximately equal proportions at room temperature. Measurements of the maximum components of the  $^{13}\text{C}$  hyperfine splitting tensors gave estimates of the isotropic components. The  $\cdot\text{CFHCOO}^-$  radical was found to be planar, while the  $\cdot\text{CF}_2\text{COO}^-$



radical is bent approximately  $8^\circ$  from a planar structure. At  $77^\circ$  K, relatively low concentrations of  $\cdot\text{CF}_2\text{H}$  are believed present in addition to more abundant  $\cdot\text{CFHCOO}^-$  and possibly a third radical. A maximum fluorine coupling of 211 G was assigned to the  $A_{zz}(\text{F})$  principal component of  $\cdot\text{CF}_2\text{H}$  by analysis of the powder spectrum.

The  $\cdot\text{CF}_3$  radical has been tentatively identified as probably arising from irradiation of  $\text{CF}_3\text{COOND}_4$ . A long-range coupling of 14.7 G from a neighboring atom was not eliminated in the deuterated salt as would be expected from a previous assignment of the radical to  $[\text{CF}_3\text{COOH}\cdot\cdot\text{NH}_3]^-$ .

Single crystals of ammonium chlorodifluoroacetate were irradiated, and the ESR spectra observed, at  $77^\circ$  K. These show the presence of at least two radicals, one showing chlorine and fluorine hyperfine splitting and the second fluorine hyperfine splitting only. The radicals were assigned the structures  $\cdot\text{CF}_2\text{Cl}$  and  $\cdot\text{CF}_2\text{COO}^-$ .

ELECTRON SPIN RESONANCE STUDIES OF  
RADICALS IN IRRADIATED ACETATES

By

Richard Clark Schoening

A DISSERTATION

Submitted to

Michigan State University

in partial fulfillment of the requirements

for the degree of

DOCTOR OF PHILOSOPHY

Department of Chemistry

1973

To  
My wife, Margaret

## ACKNOWLEDGMENTS

The author wishes to thank Dr. Max T. Rogers for his guidance, encouragement and patience during the course of this investigation.

Special thanks also go to Dr. S. Subramanian of the Indian Institute of Technology, Madras, India and to Dr. Roger V. Lloyd of the University of Connecticut for assistance with some experimental parts of this work. To Dr. William G. Waller, appreciation is expressed for use of computer programs and for helpful discussions.

Financial support provided by Michigan State University, Department of Chemistry and by the Atomic Energy Commission is gratefully acknowledged.

Thanks also go to my colleagues and in particular, to Robert F. Picone for helpful discussions and constant encouragement throughout this study.

Finally, I am indebted to my parents for their understanding and support and to my wife without whose encouragement and love this study could not have been possible.

# TABLE OF CONTENTS

	Page
LIST OF TABLES . . . . .	vi
LIST OF FIGURES . . . . .	vii
CHAPTER	
I. Introduction . . . . .	1
II. Theoretical Considerations . . . . .	20
A. Spin Hamiltonian . . . . .	20
B. Hyperfine Interactions . . . . .	26
III. Experimental Aspects . . . . .	32
A. Sample Preparation . . . . .	32
B. Crystal Morphology . . . . .	33
C. Sample Handling. . . . .	33
D. Instrumentation. . . . .	36
E. Studies Below 77° K. . . . .	37
F. Analysis of Data . . . . .	41
IV. Irradiated Sodium Acetates . . . . .	44
A. $\text{CH}_3\text{COONa} \cdot 3\text{D}_2\text{O}$ . . . . .	44
1. Analysis of Spectra at 77° K . .	44
2. Analysis of Spectra at 198° K. .	50
3. Analysis of Room Temperature Spectra. . . . .	53
4. Analysis of Reaction Scheme. . .	59
B. $\text{CD}_3\text{COONa} \cdot 3\text{D}_2\text{O}$ . . . . .	60
C. ENDOR Studies. . . . .	61

	Page
D. Anhydrous Sodium Acetate. . . . .	62
1. The Doublet ESR Spectrum. . . . .	63
2. The Triplet ESR Spectrum. . . . .	66
E. Methyl Radical Below 77° K. . . . .	73
V. Irradiated Fluoroacetates . . . . .	80
A. Ammonium Monofluoroacetate. . . . .	81
1. Analysis of Room Temperature Spectra . . . . .	81
2. Analysis of Spectra at 77° K. . . . .	94
3. Variable Temperature Studies. . . . .	95
B. Ammonium Difluoroacetate. . . . .	114
1. Room Temperature Radicals . . . . .	114
2. Analysis of $\cdot\text{CFHCOO}^-$ and $\cdot\text{CF}_2\text{COO}^-$ Spectra. . . . .	119
3. Spectra at 77° K. . . . .	122
C. Ammonium Trifluoroacetate . . . . .	123
D. Ammonium Chlorodifluoroacetate. . . . .	125
E. Radical Formation . . . . .	125
VI. Summary . . . . .	129
REFERENCES. . . . .	133

# LIST OF TABLES

Table		Page
1	A summary of motional averaging effects observed for radicals in irradiated organic single crystals by ESR methods . . . . .	9
2	Summary of ESR results obtained for radicals trapped in irradiated single crystals of fluorine-containing organic compounds . . . . .	14
3	Isotropic hyperfine coupling constants and $g$ values for fluorinated methyl radicals. . . . .	18
4	ESR parameters for radicals produced in $\gamma$ -irradiated single crystals of $\text{CH}_3\text{COONa} \cdot 3\text{D}_2\text{O}$ . . . . .	47
5	Summary of ESR results reported for methyl radical. . . . .	48
6	Summary of ESR results reported for $\cdot\text{CH}_2\text{COO}^-$ radical found in single-crystal matrices. . . . .	54
7	Principal hyperfine splitting values and direction cosines for the $\cdot\text{CH}_2\text{COO}^-$ radical produced at $77^\circ\text{K}$ in irradiated single crystals of anhydrous sodium acetate . . . . .	65
8	ESR studies of radical pairs found in irradiated single crystals. . . . .	70
9	Principal values and direction cosines for $A(\text{F})$ , $A(\text{H})$ , $g$ and $A(^{13}\text{C})$ for the $\cdot\text{CFHCOO}^-$ radical produced by room temperature irradiation of ammonium monofluoroacetate . . . . .	87
10	Principal values and direction cosines for $A(\text{F})$ and $A(\text{H})$ for the two $\cdot\text{CFHCOO}^-$ radicals produced at room temperature and observed at $-140^\circ\text{C}$ by irradiation of ammonium monofluoroacetate . . . . .	108

# LIST OF FIGURES

Figure		Page
1	Liquid helium quartz Dewar for "flow-method" studies below 77° K. . . . .	39
2	Schematic diagram of the Andonian Associates variable-temperature throttle-system Dewar. . . . .	40
3	Second-derivative ESR spectra of $\cdot\text{CH}_3$ radical in $\gamma$ -irradiated single crystals of $\text{CH}_3\text{COONa}\cdot 3\text{D}_2\text{O}$ at 77° K. . . . .	46
4	Second-derivative ESR spectra for two orientations of the magnetic field with respect to the $\cdot\text{CH}_2\text{COO}^-$ radical produced in irradiated $\text{CH}_3\text{COONa}\cdot 3\text{D}_2\text{O}$ single crystals which have been warmed to $\sim 198^\circ$ K for five minutes. . . . .	52
5a	Second-derivative ESR spectrum of $\cdot\text{CO}_2^-$ radical produced in irradiated single crystals of $\text{CH}_3\text{COONa}\cdot 3\text{D}_2\text{O}$ at room temperature. . . . .	56
5b	Second-derivative ESR spectrum of $\cdot\text{CD}_3$ radical produced in irradiated single crystals of $\text{CD}_3\text{COONa}\cdot 3\text{D}_2\text{O}$ at 77° K . . . .	56
6	Structure of the $\cdot\text{CO}_2^-$ radical . . . . .	57
7	ESR spectra of radicals produced in irradiated anhydrous sodium acetate at 77° K . . . . .	67
8(a-c)	Second-derivative ESR spectra for $\cdot\text{CH}_3$ and $\cdot\text{CD}_3$ radicals at temperatures below 77° K. . . . .	76
9	Second-derivative ESR spectra for $\cdot\text{CFHCOO}^-$ radical produced in irradiated single crystals of ammonium monofluoroacetate at room temperature. . . . .	82
10(a-c)	Variation with magnetic field orientation of the ESR hyperfine lines for the $\cdot\text{CFHCOO}^-$ radical in irradiated single crystals of ammonium monofluoroacetate at room temperature. . . .	84



Figure		Page
11	Plot of hyperfine splitting with respect to magnetic field direction for fluorine coupling in the $\cdot\text{CFHC}\text{OO}^-$ radical in irradiated single crystals of ammonium monofluoroacetate at room temperature . . . . .	88
12	Plot of hyperfine splitting with respect to magnetic field direction for proton coupling in the $\cdot\text{CFHC}\text{OO}^-$ radical in irradiated single crystals of ammonium monofluoroacetate at room temperature . . . . .	89
13	Plot of g values with respect to magnetic field direction for the $\cdot\text{CFHC}\text{OO}^-$ radical in irradiated single crystals of ammonium monofluoroacetate at room temperature. . . .	90
14	Plot of hyperfine splitting with respect to magnetic field direction for carbon-13 coupling in the $\cdot\text{CFHC}\text{OO}^-$ radical in irradiated single crystals of ammonium monofluoroacetate at room temperature . . . . .	92
15(a-i)	Variation with temperature of the fluorine and proton hyperfine splittings for the $\cdot\text{CFHC}\text{OO}^-$ radical . . . . .	97
16	Second-derivative ESR spectra for $\cdot\text{CFHC}\text{OO}^-$ radical produced in single crystals of ammonium monofluoroacetate irradiated at room temperature and observed at $-140^\circ\text{C}$ . . . . .	102
17(a-c)	Variation with magnetic field orientation of the ESR hyperfine lines for the $\cdot\text{CFHC}\text{OO}^-$ radical in irradiated ammonium monofluoroacetate at $-140^\circ\text{C}$ . . . . .	104
18	Plot of hyperfine splitting with respect to magnetic field direction for fluorine coupling in the $\cdot\text{CFHC}\text{OO}^-$ radicals in irradiated single crystals of ammonium monofluoroacetate at $-140^\circ\text{C}$ . . . . .	109

Figure		Page
19	Plot of hyperfine splitting with respect to magnetic field direction for proton coupling in the $\cdot\text{CFHCOO}^-$ radicals in irradiated single crystals of ammonium monofluoroacetate at $-140^\circ\text{C}$ . . . . .	111
20	Variation with magnetic field orientation in the $ac$ plane of the ESR hyperfine lines for the $\cdot\text{CFHCOO}^-$ and $\cdot\text{CF}_2\text{COO}^-$ radicals produced in irradiated single crystals of ammonium difluoroacetate at room temperature. . . . .	116
21	Second-derivative ESR spectra of the room-temperature radicals, $\cdot\text{CFHCOO}^-$ and $\text{CF}_2\text{COO}^-$ , produced in irradiated single crystals of ammonium difluoroacetate . . . . .	117
22a	Second-derivative ESR spectrum of the radicals produced in single crystals of ammonium difluoroacetate at room temperature . . . . .	118
22b	First-derivative ESR powder spectrum of ammonium difluoroacetate irradiated at $77^\circ\text{K}$ . . . . .	118
23	Second-derivative ESR spectrum of radicals produced in a single crystal of ammonium chlorodifluoroacetate by irradiation at $77^\circ\text{K}$ . . . . .	126

## CHAPTER I

### INTRODUCTION

It has been almost thirty years since the discovery of electron spin resonance (ESR) spectroscopy, generally attributed to Zavoisky in 1945.<sup>1</sup> In the intervening time studies in spin resonance have ranged from paramagnetic transition metals and other inorganic systems to organic radicals in solution and irradiated organic single crystals. Perhaps the most information to be gleaned from ESR can be obtained by studying single crystals. Geometric and electronic structure along with bonding and hybridization are among the types of information gathered through electron spin resonance studies. Much literature now exists in the area of ESR studies and several excellent reviews and books concerning inorganic radicals,<sup>2,3,4</sup> transition metal ions,<sup>5,6</sup> and organic systems, including radicals in solution,<sup>7,8</sup> single crystals,<sup>9,10</sup> and substances of biological interest<sup>11,12</sup> are available.

Accumulation of data and information about radicals and structures has generated interest in applications of ESR to chemical, biological and pharmacological areas. For example, a new area of research in spin labelling

has been created by McConnell<sup>13</sup> and others<sup>14</sup> which now has general application to many investigations. Studies of polymers and macromolecules have entailed the use of the spin resonance technique.<sup>15</sup> Studies of photolytic reactions, aging processes and drug detection<sup>16,17</sup> have utilized the electron spin resonance phenomenon.

With organic molecules it is usually necessary to generate the paramagnetic (free-radical) species. This can be accomplished in a number of ways. Various flow systems have been used for generating transient radicals in solution.<sup>18</sup> UV photolysis is widely used and experiments with hydrogen atoms generated in a hydrogen discharge have been successful in producing radicals.<sup>19</sup> Generally, for organic solids the most widely used method for producing unpaired spins has been irradiation. Perhaps the most convenient of these have been X-rays and  $\gamma$ -rays, but high energy electrons or neutrons are also employed. This thesis will be concerned with only those aspects applicable to organic single crystal ESR studies.

In early work,<sup>20</sup> single crystal studies were conducted on stable room-temperature radicals. However, to better understand radiation processes, a considerable amount of attention has been focused on radicals generated at low temperatures (usually 77° K and 4.2° K) which tend to be unstable, yielding secondary stable room-temperature radicals by reactions in the solid. It is

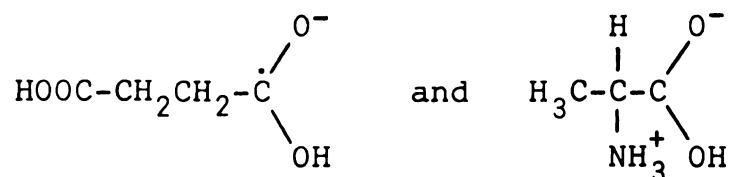
necessary, then, to understand the radiation damage processes resulting from ionizing radiations.

Initial processes are relatively well-understood. The total absorption coefficient may be given as a sum of three coefficients due to photoelectric absorption, Compton scattering and pair production.<sup>21</sup> The interaction of the absorber with photoelectrons, Compton electrons or Compton photons has become of considerable interest to the chemist.

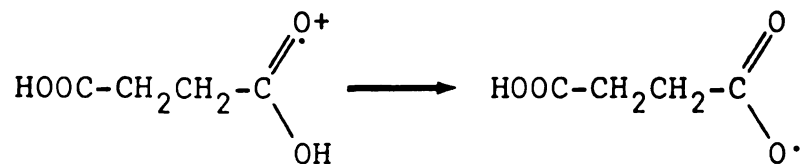
Studies seem to show that the main primary process induced by ionizing radiation is the ejection of an electron from a molecule leaving a positive hole trapped in a preferred site (molecular cation). This is followed by capture of the electron by another molecule and the formation of a molecular anion. These species should be detectable by ESR methods at low temperatures. Neutral radicals may then be created by a series of reactions from these ionic primaries until a stabilized room-temperature species is formed or, in some instances, until a diamagnetic species is formed by recombination or disproportionation. Quite often, the secondary room-temperature radicals are short-lived and to study them they are quenched by cooling and data collected at this lower temperature.

Studies of carboxylic acids and amino acids irradiated at low temperatures have produced examples of molecular

cations and anions. Typical examples of each are given by irradiation of succinic acid<sup>22-24</sup> and its salts, and by alanine,<sup>25-27</sup> which seem to be rather general; the molecular anions produced are:

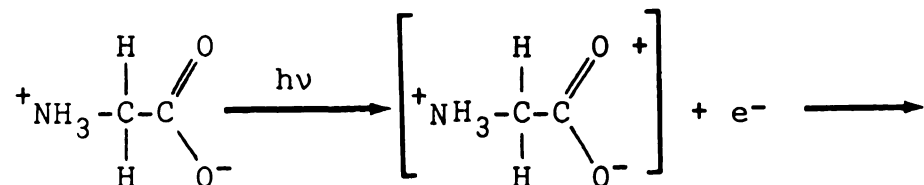


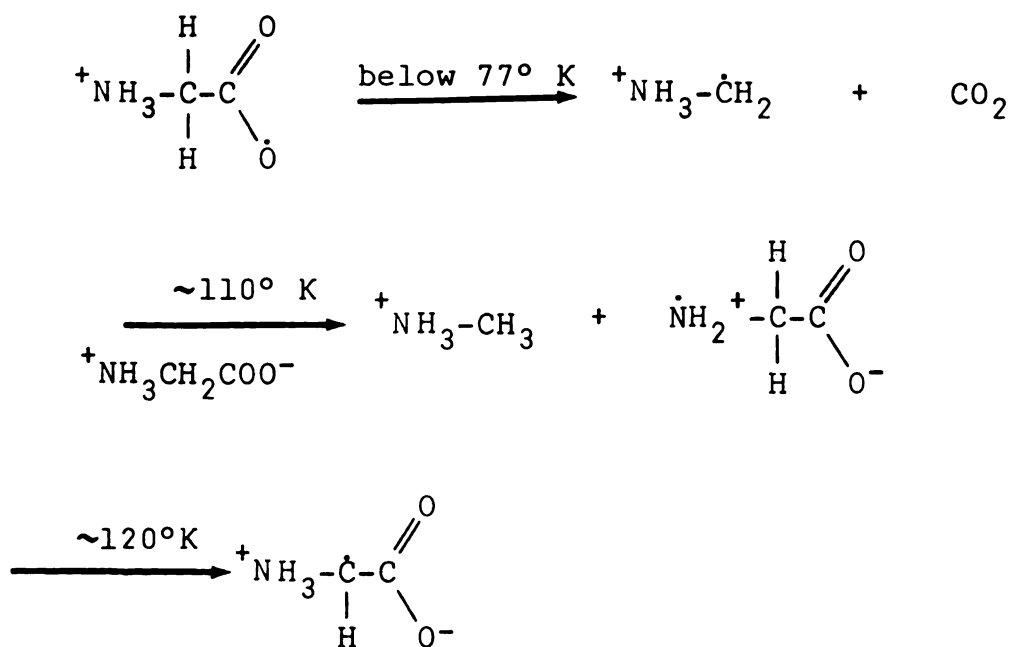
Observation of molecular cations, on the other hand, is more difficult. It appears that they react spontaneously by transfer of the acidic proton to a neighboring molecule to form the neutral species:<sup>22</sup>



There is still some confusion concerning the existence of a positive center in alanine.<sup>28</sup>

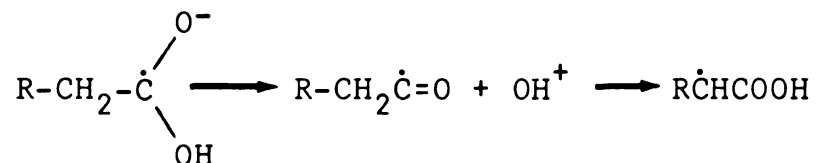
The radicals produced from these ionic primaries have been studied extensively in numerous carboxylic acids<sup>29-34</sup> and amino acids<sup>35-38</sup> in attempts to elucidate the nature of the secondary radicals. Several reaction mechanisms have been proposed. However, there is considerable ambiguity and a general reaction sequence has not been found. The following process has been proposed, for example, in glycine<sup>39</sup> using the positive primary:





(stable at room temperature)

Similar decarboxylations have been observed in radicals from malonic acid (*e.g.*  $\cdot\text{CH}_2\text{COOH}$ ),<sup>40</sup> but there is still some ambiguity in these proposed sequences. Similarly, negative primaries have been used to explain the production of secondary radicals through dissociative electron capture followed by hydrogen abstraction. Thus, in the malonic acid example:<sup>41</sup>



Again, there has been considerable discussion as to whether  $\cdot\text{CO}_2^-$  radicals play a role in these reactions.

In any event, experimental results seem to indicate that radical formation is stereospecific and is strongly

affected by the crystalline field, that is, molecular packing, orientation of surrounding molecules, hydrogen bonding and other weak interactions.

One interesting phenomenon found in irradiated organic crystals has been pairwise trapping of radicals. If two neighboring molecules, or the decomposition of a single molecule, produce radicals in close proximity to one another (approx. 5 to 10 Å) a triplet state is formed by the interaction between the two unpaired electrons. These pairs are stable only at low temperatures. In one recent study, a radical pair was believed to be formed within a single molecule, the two radicals being in different parts of the molecule.<sup>42</sup> The mechanism of pairwise trapping has been discussed.<sup>43</sup> Three possible explanations are given: 1) hot hydrogen atom liberated from a molecule reacts with a neighboring molecule; 2) ion-molecule reaction followed by charge neutralization of a cation and an electron; and 3) charge neutralization of the anionic and cationic primaries to produce a pair of radicals by charge migration in the lattice. Support of the third mechanism arises from anion and cation pairs found in maleic anhydride<sup>44</sup> and potassium hydrogen fumarate.<sup>45</sup>

Another interesting phenomenon has been stereoselectivity in the formation of the isolated radicals. It is possible to distinguish two chemically equivalent species



if their orientations in the single crystal are different. Horsfield and coworkers<sup>40</sup> have shown that two distinguishable  $\cdot\text{CH}_2\text{COOH}$  radicals are formed from malonic acid depending on which COOH group is lost. ELDOR analysis confirmed these results.<sup>46</sup> One of these two radicals is predominantly favored. Further, it has been shown by Rogers and Kispert<sup>47</sup> that water of crystallization plays a dominant role in which type of radical is preferentially formed. And, in addition, succinic acid gives two stable radicals  $\text{HOOCCH}_2\dot{\text{C}}\text{HCOOH}$  and  $\text{CH}_3\dot{\text{C}}\text{HCOOH}$ , while the disodium salt<sup>48</sup> gives the latter predominantly.

Considerable mobility appears to be possible in the solid state despite the close packing of the molecules in the crystal. For example, a hydrogen-deuterium exchange reaction was first noted by Itoh and Miyagawa<sup>49</sup> in the stable radical formed in alanine. When the normally exchangeable  $\text{NH}_3$  protons are replaced with deuterons by growing the crystals in heavy water, it was observed that the protons bonded to carbon, which are normally unexchangeable, were successively replaced by deuterons to yield  $\text{CD}_3\dot{\text{C}}\text{DCOO}^-$  radicals. Two other types of exchange reactions have recently been observed in the alanine system.<sup>50</sup> However, when a similar radical formed in  $\alpha$ -ureidopropionic acid was studied<sup>51</sup> only the  $\alpha$ -proton exchanged for a dueteron. Further evidence of crystal field effects was obtained in the case of radicals in

irradiated aspartic acid,<sup>52</sup> which exchanged protons for deuterons, but not in the similar radical found in succinic acid. And, in fact, the fumaric acid impurity found in succinic acid<sup>53</sup> was shown to selectively exchange protons for deuterons.

A number of studies have shown that internal molecular motions may take place in the solid state. For example, the methyl group in the  $\text{CH}_3\dot{\text{C}}\text{HCOO}^-$  radical found in alanine exhibits motional averaging of the protons at room temperature.<sup>54</sup> On cooling to 77° K the motion is hindered and different couplings from the three distinguishable protons are observed. Interpretation of the motion with a modified Bloch treatment proved successful and an activation energy of 3.6 kcal/mole was determined. A number of examples of hindered motion have been found in single crystal ESR studies and Table 1 is presented as a comprehensive review.

It may also be noted that motional averaging has been observed in methylene groups such as in the radical  $\cdot\text{CH}_2\text{COO}^-$  in glycine.<sup>55</sup> Hayes and coworkers<sup>58</sup> have pointed out that consideration must be made of changes with motion in the principal axes of the coupling tensors. Their analysis, based on the density matrix description, showed the spectral changes which take place in  $\cdot\text{CH}_2\text{COO}^-$  in zinc acetate. Bogan and Kispert<sup>83</sup> extended the analysis to motions in the  $\cdot\text{CF}_2\text{CONH}_2$  radical found in trifluoro-

Table 1. A summary of motional averaging effects observed for radicals in irradiated organic single crystals by ESR methods.

Radical Type	Matrix	$E_a$ (kcal/ mole)	A (sec <sup>-1</sup> )	Method*	Temp. Range (°K)	Ref.
<u>α-Protons</u>						
•CH <sub>2</sub> COO <sup>-</sup>	Glycine	N.V. <sup>†</sup>	-----	--	145-300	55, 39
	Triglycine sulfate	3.6	1.2×10 <sup>12</sup>	B	130-280	56
	Zinc acetate	5.0	7.25×10 <sup>11</sup>	B	130-300	57
	Zinc acetate	4.6	5.3×10 <sup>11</sup>	DM	130-300	58
	Zinc acetate	5.8	4.4×10 <sup>12</sup>	B	150-370	59
	Sodium acetate	3.0	N.V.	B	150-250	60
•CH <sub>2</sub> - $\overset{+}{P}$ -Ph <sub>3</sub>	Triphenylphospho- methylene	2.3	4.0×10 <sup>11</sup>	B	100-300	61
	Methylammonium alum	N.V.	-----	--	100-300	62
<u>β-Protons</u>						
-CH <sub>2</sub> - $\overset{\cdot}{C}$ -R   R	R=(-CH=CH) Oriented polyethylene	0.41	4.6×10 <sup>8</sup>	B	90-410	63
	(-COOH) Fumaric acid (in urea)	2.4	N.V.	B	77-335	64
	(-COOR') Ester- urea inclusion	~3	N.V.	B	7-300	65
	(-COO <sup>-</sup> ) Hexamethylene diammonium adipate	5	N.V.	B	150-400	66

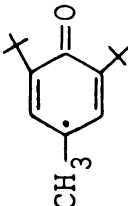
Table 1 - Continued

Radical Type	Matrix	$E_a$ (kcal/ mole)	A (sec <sup>-1</sup> )	Method*	Temp. Range (°K)	Ref.
$-\text{CH}_2-\dot{\text{C}}-\text{R}$   OH	R=(-COOH) Armonium malate monohydrate	N.V.	N.V.	-	77-300	67
$\text{HOOC}-\dot{\text{C}}-\text{COOH}$   R	R=(ethyl, n-propyl) Ethyl and n-propyl malonic acid	N.V.	N.V.	-	77-300	68
$\text{CH}_3\text{CH}_2\text{NO}_2^-$	Nitroethane, nitropropane	1.4	N.V.	QM	77-300	69
$\beta\text{-CH}_3$						
$\text{CH}_3-\dot{\text{C}}-\text{COOH}$   H	Alanine	$\sim 4(4.8)$	$\sim 10^8$	B	100-200	70
	Alanine	3.6	$10 \times 10^{12}$	B	77	54
	Alanine	N.V.	N.V.	QMT	4.2	71
$\text{CH}_3-\dot{\text{C}}-\text{NHCO}-\text{C}_6\text{H}_5$   H	Benzoylalanine	N.V.	$> 10^7$	B	77	72
$\text{CH}_3-\dot{\text{C}}-\text{COOH}$   R	R=(CH <sub>3</sub> CONH-) Acetylalanine	$\Delta E = 26^\circ\text{K}$	$15 \times 10^3$	QMT	1.2-30	73

Table 1 - Continued

Radical Type	Matrix	E <sub>a</sub> (kcal/ mole)	A (sec <sup>-1</sup> )	Method*	Temp. Range (°K)	Ref.
	(CH <sub>2</sub> ClCONH-) Chloroacetylalanine	.5	N.V.	QMT	4.2-77	74
	(-COOH) Methylmalonic acid	<.1	>10 <sup>9</sup>	QM	4.2	75
	(-COOH) Methylmalonic acid	1-2	N.V.	QMT	4-80	76
$\text{CH}_3-\dot{\text{C}}-\text{COOCH}_3$   RCH <sub>2</sub>	poly-Methylmeth- acrylate	.2	N.V.	B	6-77	77
$\text{CH}_3-\dot{\text{C}}-\text{COOH}$   CH <sub>2</sub> COOH	Itaconic acid	N.V.	N.V.	-	---	78
$\text{CH}_3-\dot{\text{C}}-\text{COO}-$   CH <sub>3</sub>	α-Aminoisobutyric acid	N.V.	10 <sup>7</sup>	(Qual)	40-77	79,80,36
	α-Aminoisobutyric acid (only l-methyl group rotating)	N.V.	N.V.	(ENDOR)	4	81
$\text{CH}_3\dot{\text{C}}\text{OO}^-$	Strontium acetate	2.3	N.V.	B	100-150	33

Table 1 - continued

Radical Type	Matrix	$E_a$ (kcal/ mole)	A (sec <sup>-1</sup> )	Method*	Temp. Range (°K)	Ref.
 4-Me-2,6-di-t-butyl- phenol		.65	N.V.	QMT	4.2	82

\* A general classification based on three ways of determining the values:

B = Standard Bloch calculation

QMT = Quantum mechanical tunnelling

DM = Density matrix calculation

<sup>†</sup>N.V. = no values were determined.

acetamide. These motions can be explained in terms of site-exchanges or restricted oscillations of large amplitude.

In some cases, motion cannot be quenched even at 4.2° K and a quantum mechanical effect has been postulated. Rapid tunnelling was predicted by Freed<sup>84</sup> theoretically and subsequently was observed in acetylalanine radicals<sup>73</sup> at liquid helium temperatures. For the methyl group, an intensity ratio of 1:3:3:1 is predicted for the motionally averaged system. However, tunnelling through a potential barrier would yield a 1:1:1:2:1:1:1 pattern as predicted by the theory. As can be seen from Table 1, a large range of activation energies has been reported.

In the past decade, considerable ESR data have been collected on fluorine-containing organic radicals. Most of the studies have centered on irradiated salts and amides of fluorinated carboxylic acids. The room-temperature systems usually involve loss of fluorine from the  $\alpha$ -carbon atom. However, irradiation at low temperatures often gives different radicals. Table 2 is a comprehensive list of fluoro-radicals found in organic single crystals.

Considerable motional averaging is also exhibited in these systems in certain cases. The  $\cdot\text{CF}_2\text{CONH}_2$  radical has been studied by a number of workers.<sup>86,87</sup> As previously mentioned, Bogan and Kispert<sup>83</sup> have applied a

Table 2. Summary of ESR results obtained for radicals trapped in irradiated single crystals of fluorine-containing organic compounds.

Compound	Irrad. Temp. (°K)	Radical	$\alpha$ -Fluorine			Other Data	Ref.
			$a_{\text{iso}}$	Tensor (Gauss)	Hyperfine		
$\text{CFH}_2\text{CONH}_2$	300	$\cdot\text{CFHCONH}_2$	56.4	189	-3.9 -16	$A(\text{H}) = -34.3$ -22.5 -11.1 $A_{\text{max}}(^{13}\text{C}) = 85$	85
$\text{CF}_3\text{CONH}_2$	300	$\cdot\text{CF}_2\text{CONH}_2$	75.0	178	24 24		86
$\text{CF}_3\text{CONH}_2$	300	$\cdot\text{CF}_2\text{CONH}_2$	72.5	180	23.5 14	$A(^{13}\text{C}) = 130$ 67.6 66.1	87
$\text{CF}_3\text{CONH}_2$	77	$\cdot\text{CF}_2\text{CONH}_2$	77.3	202	16 14	$A_{\text{max}}(^{13}\text{C}) = 147.5$	87
	300	$\cdot\text{CF}_2\text{CONH}_2$	72.7	181	23.2 14.0		
	at 77	$\cdot\text{CF}_2\text{CONH}_2$ $F_1$	75.3	202	18 6		83
		$F_2$	75.3	202	6 18		
$\text{CF}_3\text{COO}^-\text{NH}_4^+$	300	$\cdot\text{CF}_2\text{COO}^-$	72.	188	14 14		88
$\text{ClF}_2\text{CCOO}^-\text{Na}^+$	300	$\cdot\text{CF}_2\text{COO}^-$ Rad1	68.8	182.8	16.4 7.3	$A_{\text{max}}(^{13}\text{C}) = 124$	
		Rad2	69.7	182.8	15.7 10.5	124 $A(\text{HH}) = 6.4, 3.9,$ 3.4	
		Rad3	72.4	185.7	20.6 14.3	135	89



Table 2 Continued.

Compound	Irrad. Temp. (°K)	Radical	$\alpha$ -Fluorine			Other Data	Ref.
			$a_{iso}$	Tensor (Gauss)	Hyperfine		
$KOCCF_2COOK$	300	$\cdot CF_2COO^-$ Rad1	181	13	11		90
		Rad2	188	19	7		
$KOCCF_2COOK$	300	$-OOC\dot{C}FCOO^-$	84	208	27		91
$NH_2OCCF_2CONH_2$	300	$NH_2OCC\dot{C}FCONH_2$	63	200	-10		92
$NaOCCCF_2CF_2COONa$	300	$-OOC\dot{C}CF_2\dot{C}FCOO^-$	71.2	150.4	59	3.9 $A(F)_{\beta_1} = 63$ 23 19 = 35 $A(F)_{\beta_2} = 71$ 27 23 = 40	93
	cooled to 77°K	I	75	217	17	2 $A(F)_{\beta_1} = 122$ 41 41 = 68 $A(F)_{\beta_2} = 9$ -3 -2 = 1.4	94
		II	77	224	5	4 $A_{\beta_1} = 125$ 44 41 = 70 $A_{\beta_2} = 14$ -1 -2 = 3.7	
		IV	~90	202	47	21 $A_{\beta_1} = 107$ 44 25 = <59 $A_{\beta_2} = 24$ 13 7 = <15	
$CF_3CF_2CONH_2$	300	$CF_3\dot{C}FCONH_2$	74	201	12	8 $A(CF_3)_{\beta} = 36$ 17 14	95

Table 2 Continued.

Compound	Irrad. Temp. (°K)	Radical	α-Fluorine			Other Data	Ref.
			$a_{\text{iso}}$	Tensor (Gauss)	Hyperfine		
$\text{CF}_3\text{CONH}_2$	77	$\cdot\text{CF}_3$	144.6	253	92	88 $A(\text{CF}_3) = 318$ 238 257 = 271	87
$\text{CF}_3\text{COONH}_4$	77	$\text{CF}_3\text{COONH}_3(?)$	$F_1$	254	113	89 $A(\text{H}) = 14.1, 6.5, 5.7$	
				260	103	53	
					85	67	
$\text{CF}_2\text{ClCONH}_2$	300	$\cdot\text{CClFCONH}_2$	$F_3$	257	86	84	88
				142.3	257		
				50.1	168	-10.7 -6.9 $A_{\text{max}}(^{13}\text{C}) = 90.6$	
						$A(^{35}\text{Cl}) = 18 -3.2 -5.8$	96

density matrix treatment to the ESR data to analyze the motions found in the system over a temperature range of 77°-290° K. An activation energy of 0.41 kcal/mole was determined.

In addition to the  $\cdot\text{CF}_2\text{CONH}_2$  radical found in trifluoroacetamide, Rogers and Kispert<sup>87</sup> have reported the  $\cdot\text{CF}_3$  radical at 77° K. The isotropic splittings of fluorine and carbon-13 are reported to be 144.6 G and 271 G, respectively, in good agreement with those reported for the same radical formed in liquid  $\text{C}_2\text{F}_6$ .<sup>97</sup> The radical exhibits nearly cylindrical symmetry, with equivalent coupling by the three fluorine atoms indicating rotational averaging about the threefold symmetry axis. The radical exhibits nearly tetrahedral geometry. It would be of considerable interest to study the related fluorine-substituted methyl radicals,  $\cdot\text{CFH}_2$  and  $\cdot\text{CF}_2\text{H}$ , to gain more information about structure and bonding in the series. Fessenden and Schuler<sup>97</sup> have determined isotropic coupling values from rapidly tumbling  $\cdot\text{CH}_2\text{F}$  and  $\cdot\text{CF}_2\text{H}$  in fluorinated methanes (Table 3). Schrader and Karplus<sup>101</sup> have derived an equation for degree of bending in the methyl radical:

$$a_C(\theta) = a_C(0) + 1190(2\tan^2 \theta) \quad (1)$$

where  $\theta$  is the angle of bend from planarity (the angle between the CH bond and the plane normal to the symmetry

Table 3. Isotropic hyperfine coupling constants and  $g$  values for fluorinated methyl radicals.

Radical	Experimental <sup>97</sup> (solution)				Experimental <sup>87,98</sup> (single crystal)				Calculated <sup>99,100</sup>			
	$a(\text{H})$	$a(\text{F})$	$a(^{13}\text{C})$	$g$	$a(\text{H})$	$a(\text{F})$	$a(^{13}\text{C})$	$g$	$a(\text{H})$	$a(\text{F})$	$a(^{13}\text{C})$	angle $\theta$
$\cdot\text{CF}_3$	--	142.4	271.6	2.0031	--	144.6	271	2.0036	--	159.5	184.6	17.8
$\cdot\text{CF}_2\text{H}$	+22.2	84.2	148.8	2.0041	--	--	--	--	21.9	87.1	145.1	12.7
$\cdot\text{CFH}_2$	-21.1	64.3	54.8	2.0045	--	--	--	--	-7.8	71.3	92.7	5.0
$\cdot\text{CH}_3$	-23.0	--	38.5	2.0026	-22.3	--	37.7	2.0028	-22.4	--	45	0

axis). Partial substitution of fluorine indicates an increase in  $s$  character in the bond. These results are in accord with calculations by Pople<sup>99,100</sup> (Table 3).

The present study was undertaken to further understand the irradiation processes in organic, particularly fluoro-organic, single crystals. This thesis is presented in two parts. The first concerns studies of radiation damage in sodium acetate and related compounds and motional averaging of one of the resulting species, the methyl radical. The second part concerns formation of radicals in substituted fluoroacetate salts with particular emphasis on ammonium fluoroacetate and motions of the radicals produced at room temperature.

## CHAPTER II

### THEORETICAL CONSIDERATIONS

There have been a number of excellent books recently published which deal rather extensively with electron spin resonance spectroscopy. A book by Poole<sup>102</sup> deals comprehensively with the instrumentation involved. Several books such as those by Alger<sup>103</sup> and Ayscough<sup>104</sup> have thorough treatments of experimental techniques, analysis of data and results. Perhaps Abragam and Bleaney's<sup>105</sup> book is the most comprehensive on transition metals, while that by Atkins and Symons<sup>2</sup> thoroughly investigates other inorganic systems. And finally, several reviews are available which periodically survey the literature.<sup>106</sup> Two excellent books on theoretical aspects of electron spin resonance are those by Carrington and McLachlan<sup>107</sup> and by Poole and Farach.<sup>108</sup> This presentation will be a summary of the latter two sources.

#### A. The Spin Hamiltonian

For a single crystal ESR problem, the usual spin Hamiltonian for an electron spin interacting with an atom with a nuclear spin is given by:

$$\mathcal{H} = \beta \vec{S} \cdot \vec{g} \cdot \vec{H} + \sum_i \vec{S} \cdot \vec{T}_i \cdot \vec{I}_i - g_N \beta_N \vec{H} \cdot \vec{I} \quad (2)$$

The first term on the right is the electronic Zeeman term which produces the main ESR transition, the second is the hyperfine interaction term which splits the observed spectrum and the third is the nuclear Zeeman term which is often small compared to the second term and so may be neglected. The  $g$  tensor and the hyperfine coupling tensor,  $T_i$ , are second-order tensors with orientation dependent matrix elements. In degenerate perturbation theory the usual Hamiltonian

$$\mathcal{H} = \mathcal{H}_0 + \mathcal{H}', \quad (3)$$

is employed, where  $\mathcal{H}_0 = \beta \vec{S} \cdot \vec{g} \cdot \vec{H}$  is the zero-order Hamiltonian whose solution is known and the perturbation  $\mathcal{H}' = \sum_i \vec{S} \cdot \vec{T}_i \cdot \vec{I}_i$  removes the degeneracy in first order.

For organic radicals, the  $g$  factor is nearly isotropic, hence the Hamiltonian simplifies to

$$\mathcal{H} = \beta g \vec{H} \cdot \vec{S} + \vec{S} \cdot \vec{T} \cdot \vec{I}. \quad (4)$$

The hyperfine interaction tensor,  $T$ , includes an isotropic Fermi contact interaction term and an anisotropic dipolar interaction term.

In the principal axis coordinate system ( $x, y, z$ ), which must be deduced from experimental angular rotation data, the solution of the eigenvalue problem leads to the hyperfine term

$$\mathcal{H}' = AS_x I_x + BS_y I_y + CS_z I_z, \quad (5)$$

where  $A$ ,  $B$  and  $C$  include both dipolar ( $A_d$ ,  $B_d$ ,  $C_d$ ) and isotropic ( $a$ ) parts:

$$\begin{aligned} A &= A_d + a \\ B &= B_d + a \\ C &= C_d + a \end{aligned} \tag{6}$$

Now the contact hyperfine term is given explicitly as

$$a = \left( \frac{8\pi g \beta}{3\hbar} \right) g_N \beta_N \rho(r_N), \tag{7}$$

where  $\hbar$  is Planck's constant,  $g$  is the isotropic  $g$  factor,  $g_N$  is the nuclear  $g$  factor,  $\beta$  and  $\beta_N$  are the Bohr magneton and nuclear magneton, and  $\rho(r_N)$  is the electron spin density at the nucleus whose radius vector is  $r_N$ . For the spatial distribution of the electron over the  $p$  orbital wave function, the dipolar components are given by:

$$\begin{aligned} A_d &= \frac{g \beta g_N \beta_N}{\hbar} \int_{\epsilon} \rho(r) \frac{(1-3 \sin^2 \theta \cos^2 \phi)}{|r-r_N|^3} d\tau \\ B_d &= \frac{g \beta g_N \beta_N}{\hbar} \int_{\epsilon} \rho(r) \frac{(1-3 \sin^2 \theta \sin^2 \phi)}{|r-r_N|^3} d\tau \\ C_d &= \frac{g \beta g_N \beta_N}{\hbar} \int_{\epsilon} \rho(r) \frac{(1-3 \cos^2 \theta)}{|r-r_N|^3} d\tau \end{aligned} \tag{8}$$

where  $(\overrightarrow{r - r_N})$  is the vector denoted by the polar and



azimuthal coordinates  $\theta$  and  $\phi$  between the electron and the nucleus in the principal coordinate system  $(x, y, z)$  wherein  $T$  is diagonal.

Since the principal directions are not usually known at the outset, this dipolar term can be written in the non-diagonal coordinate system as:

$$T_d = \frac{g\beta g_N \beta_N}{\hbar} \begin{vmatrix} \frac{r^2 - 3x^2}{r^5} & \frac{-3xy}{r^5} & \frac{-3xz}{r^5} \\ \frac{-3xy}{r^5} & \frac{r^2 - 3y^2}{r^5} & \frac{-3yz}{r^5} \\ \frac{-3xz}{r^5} & \frac{-3yz}{r^5} & \frac{r^2 - 3z^2}{r^5} \end{vmatrix} \quad (9)$$

There exists a real unitary transformation which can transform  $T_d$  into a diagonal matrix with eigenvalues  $A_d$ ,  $B_d$  and  $C_d$  for which the trace vanishes

$$A_d + B_d + C_d = 0. \quad (10)$$

Hence the isotropic hyperfine interaction constant is given by

$$a = \frac{1}{3} (A + B + C). \quad (11)$$

One experimental difficulty in analyzing the ESR spectra is the presence of the off-diagonal elements of the  $T_d$  matrix, since the principal directions are unknown.

The Hamiltonian may be represented by a matrix in which  $S_z$  is diagonal. This hyperfine matrix has nine

terms:

$$\begin{aligned}
 \begin{bmatrix} S_x & S_y & S_z \end{bmatrix} \begin{bmatrix} T_{xx} & T_{xy} & T_{xz} \\ T_{yx} & T_{yy} & T_{yz} \\ T_{zx} & T_{zy} & T_{zz} \end{bmatrix} \begin{bmatrix} I_x \\ I_y \\ I_z \end{bmatrix} &= T_{xx}S_xI_x + T_{xy}(S_xI_y + S_yI_x) \\
 &+ T_{xz}(S_xI_z + S_zI_x) + \\
 &T_{yy}S_yI_y + T_{yz}(S_yI_z + S_zI_y) \\
 &+ T_{zz}S_zI_z. \tag{12}
 \end{aligned}$$

With the simplification  $S_x=S_y=0$ , this may be written in the much simpler form

$$\mathcal{H} = g\beta H S_z + S_z(T_{zx}I_x + T_{zy}I_y + T_{zz}I_z) \tag{13}$$

and the secular matrix becomes:

$$\begin{vmatrix} \frac{1}{2}[g\beta H + \frac{1}{2}T_{zz}] & \frac{1}{4}[T_{zx} - iT_{zy}] & 0 & 0 \\ \frac{1}{4}[T_{zx} + iT_{zy}] & \frac{1}{2}[g\beta H - \frac{1}{2}T_{zz}] & 0 & 0 \\ 0 & 0 & -\frac{1}{2}[g\beta H + \frac{1}{2}T_{zz}] & -\frac{1}{4}[T_{zx} - iT_{zy}] \\ 0 & 0 & -\frac{1}{4}[T_{zx} + iT_{zy}] & -\frac{1}{2}[g\beta H - \frac{1}{2}T_{zz}] \end{vmatrix} \tag{14}$$

from which, the eigenvalues are readily calculated as

$$E_i = \pm \left\{ \frac{1}{2}g\beta H \pm \frac{1}{4} [T_{zx}^2 + T_{zy}^2 + T_{zz}^2]^{\frac{1}{2}} \right\} \tag{15}$$

for  $i = 1, 2, 3, 4$ . Accordingly, the ESR selection rules,  $\Delta M_s = \pm 1$  and  $\Delta M_I = 0$ , give two allowed transitions with the energies

$$g\beta H \pm \frac{1}{4} \sqrt{T_{zx}^2 + T_{zy}^2 + T_{zz}^2}. \tag{16}$$

It will be necessary, then, to take a radical whose principal axes  $x, y, z$  are unknown at the outset relative to the crystal axes  $a, b, c$  and find the rotation  $R$  which transforms the principal axis system ( $xyz$ ) to the crystal axis system ( $abc$ ):

$$T_{abc} = \tilde{R} T_{x,y,z} R. \quad (17)$$

The usual procedure is to rotate a crystal in the magnetic field in three orthogonal directions, determining the elements of the  $T_d$  matrix by one of several methods, and then diagonalizing the matrix to obtain the squares of the eigenvalues. The transformation matrix then becomes the direction cosines of the principal axes  $x, y, z$  relative to the crystallographic axes  $a, b, c$ . That is,

$$R = \begin{bmatrix} \cos \theta_{ax} & \cos \theta_{ay} & \cos \theta_{az} \\ \cos \theta_{bx} & \cos \theta_{by} & \cos \theta_{bz} \\ \cos \theta_{cx} & \cos \theta_{cy} & \cos \theta_{cz} \end{bmatrix}. \quad (18)$$

In a completely analogous manner, the  $g$  factors may also be determined. The spin Hamiltonian is written (without the hyperfine term) as

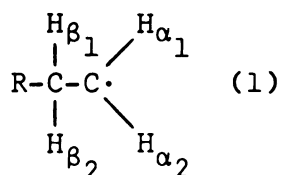
$$\mathcal{H} = \begin{bmatrix} H_x & H_y & H_z \end{bmatrix} \begin{bmatrix} g_{xx} & g_{xy} & g_{xz} \\ g_{yx} & g_{yy} & g_{yz} \\ g_{zx} & g_{zy} & g_{zz} \end{bmatrix} \begin{bmatrix} S_x \\ S_y \\ S_z \end{bmatrix}. \quad (19)$$

Again, measurements of  $g$  values for three orthogonal rotations give the elements of the  $g$  tensor in the laboratory axis system. Diagonalization of the tensor will give the principal  $g$  values and the direction cosines which transform the laboratory axes to the principal axis system.

### B. Hyperfine Interactions

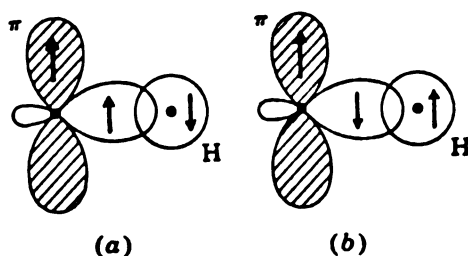
For many organic free radicals, the unpaired electron is localized on a carbon  $p_z$  orbital. Hyperfine structure arises, then, from nuclei with magnetic moments ( $^1\text{H}_{1/2}$ ,  $^{19}\text{F}_{1/2}$ ,  $^{15}\text{N}_1$ , etc.) bonded directly to that carbon (called  $\alpha$ ) or to an adjacent carbon (called  $\beta$ ). Long-range couplings extending beyond the  $\beta$  position are usually negligibly small unless brought about by delocalization of the odd electron in a  $\pi$  system as in aromatic rings.

In a qualitative manner, hyperfine coupling of protons may be accounted for in terms of valence-bond structures. The dominant structure which gives rise to anisotropic hyperfine interactions at the  $\alpha$  and  $\beta$  protons through dipole coupling may be represented as



The isotropic proton hyperfine interactions may be explained as arising from a spin polarization of the electrons in the C-H bond. That is, the spins of the two

electrons forming the C-H  $\sigma$  bond can be represented with respect to the unpaired electron in the  $2p_z$  orbital of carbon, as indicated in diagrams (a) and (b):



In the approximation of perfect pairing, both structures would be equally important. However, the exchange interaction between the  $\pi$  electron and the carbon  $\sigma$  electron slightly favors structure (a) for which the spins on carbon are parallel. If the odd electron has a spin  $\alpha$ , there is then a slight excess of  $\alpha$  spin in the carbon  $\sigma$  orbital and hence excess  $\beta$  spin in the hydrogen  $1s$  orbital, which gives rise to the isotropic proton splitting. It has been shown both experimentally<sup>109</sup> and theoretically<sup>110</sup> that the  $\alpha$ -proton coupling constant is negative while the  $\beta$ -proton coupling is positive.<sup>111,112</sup>

The anisotropic contribution to the hyperfine coupling arises from dipole-dipole interactions of the electron with the magnetic nuclei. Its magnitude may be estimated from the approximation

$$A_i \approx (g\beta g_N \beta_N) \langle (3 \cos^2 \theta - 1)/r^3 \rangle, \quad (20)$$

where  $\theta$  is the angle between the electron-nucleus vector

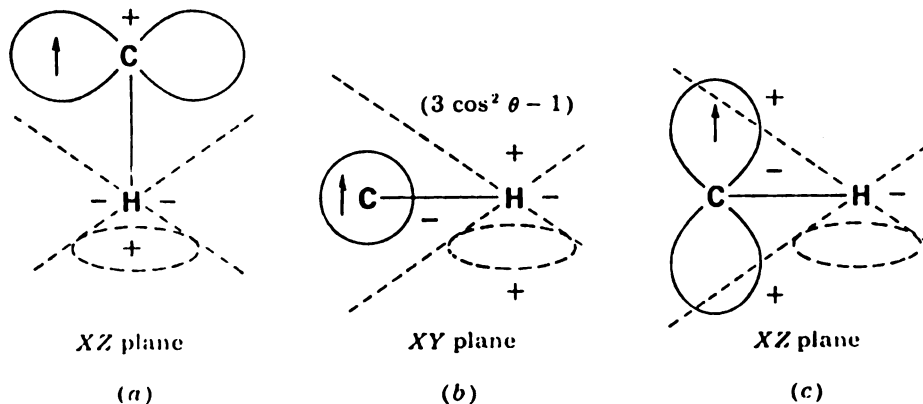
and the magnetic field direction; for protons

$$A_i = 28 \left( \frac{3 \cos^2 \theta - 1}{r^3} \right) G \quad (21)$$

where  $r$  is in angstroms.

For an unpaired electron in a  $p_z$  orbital which is perpendicular to the C-H bond (*i.e.*, a  $p_\pi$  orbital), the principal directions are along the C-H bond, parallel to the  $p_\pi$  orbital and perpendicular to both the  $p_\pi$  orbital and the C-H bond.

The  $(3 \cos^2 \theta - 1)$  term leads to a dependence of the sign of the coupling on direction. The positive regions may be designated by cones as shown below for the external field oriented along each principal direction.



Hence, for  $\vec{H}$  along the bond direction (a), the  $p_z$  orbital is in the positive region of the cone and the anisotropic hyperfine component is positive. For  $\vec{H}$  along the  $p_z$  orbital direction (c), the  $p_z$  orbital is in both positive and negative regions of the cone so the coupling is small. And when the magnetic field is along the principal

direction (b), the  $p_z$  orbital is in the negative region, so the anisotropic hyperfine component is negative.

Typical  $\alpha$ -proton coupling constants are:<sup>69</sup>

$$A_d = -10 \text{ G (along } \perp \text{ to C-H and in plane)} \quad A = -30 \text{ G}$$

$$B_d = +10 \text{ G (along C-H)} \quad B = -10 \text{ G}$$

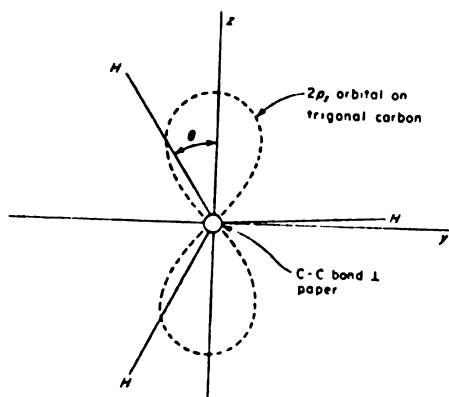
$$C_d = 0 \text{ G (along p-orbital)} \quad C = -20 \text{ G}$$

$$\text{and } a_{iso} = -20.$$

The isotropic interaction for  $\beta$  protons is comparable to that for  $\alpha$  protons, except that it is positive. For the general case of an electron in the  $p_z$  orbital on  $C_\alpha$ , and the  $C_\beta$ - $H_\beta$  bond at an arbitrary angle, the contact hyperfine interaction will vary according to the equation<sup>69</sup>

$$a = B_0 + B_2 \cos^2 \theta,$$

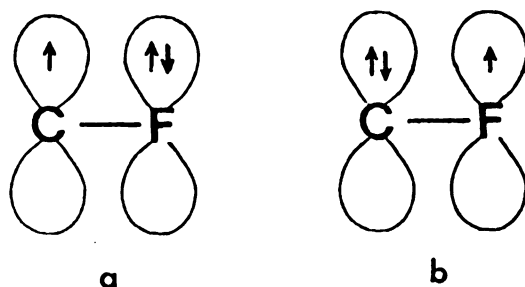
where  $\theta$  is the angle between the projection of the C- $H_\beta$  bond on a plane perpendicular to the  $C_\alpha$ - $C_\beta$  bond and the direction of the  $p_\pi$  orbital in that plane:



Typically,  $B_0$  and  $B_2$  have values approximately 2 G and 40 G, respectively. On the other hand, the dipolar interaction is only about one-eighth as large as for an  $\alpha$  proton because of the increased distance  $\vec{r}$ .

It might be thought that fluorine hyperfine couplings would be similar to those of hydrogen, since the spins are the same and the magnitudes of the magnetic moments are similar. However, due to the mixing of the fluorine  $2p$  orbital with that of the unpaired spin, the actual hyperfine couplings are entirely different. Both the isotropic and anisotropic couplings of  $\alpha$  fluorines are much larger than those of  $\alpha$  hydrogens. Also, the principal directions of the hyperfine tensor components are different.

The predominant contribution to the anisotropic fluorine coupling arises from spin density in the fluorine  $2p_\pi$  orbital. The origin of this spin density is attributed to the contribution from the excited spin configuration (b) to the ground state (a):



The interaction between the  $C_{2p_\pi}$  spin density and the fluorine nucleus gives only a minor contribution and causes the slight observed deviation from axial symmetry.



The large isotropic coupling is due to spin density in the fluorine  $1s$  and  $2s$  orbitals which arises from spin polarization. Only small amounts of spin density in the  $1s$  and  $2s$  orbitals give large isotropic couplings since a pure  $1s$  fluorine coupling is 321,000 gauss and a pure  $2s$  coupling is 16,400 gauss.<sup>20,104</sup> The radicals with fluorine substituents show near cylindrical symmetry for the fluorine couplings and the unique direction is taken parallel to the  $2p_{\pi}$  orbital of fluorine.

The anisotropic hyperfine tensor for carbon-13 nuclei depends mainly on the unpaired electron density in the  $2p$  atomic orbital of the carbon atom and the isotropic part is a measure of the  $C_{1s}$  and  $C_{2s}$  character of the odd electron.

If the unpaired electron was entirely localized in a  $2p_z$  orbital on carbon, the dipolar tensor would be axially symmetric. Since the electron is located in the positive region of the expression  $(3 \cos^2 \theta - 1)$ , the sign of the coupling is positive. Usually, there are small deviations from axial symmetry due to some small unpaired electron density being delocalized onto neighboring atoms.

### CHAPTER III

#### EXPERIMENTAL ASPECTS

##### A. Sample Preparation

Most of the single crystals in this study were grown from saturated ethanol-water solutions. Anhydrous sodium acetate was the notable exception. Commercial anhydrous sodium acetate (Matheson, Coleman and Bell) was placed in an oven at 120° C for at least eight hours.<sup>113</sup> The anhydrous salt was then transferred in a desiccator to a dry box where it was dissolved in absolute ethanol and returned to a desiccator for crystal growing. Thin platelets of the salt were obtained. Care had to be taken in handling the crystals since they were deliquescent.

The anhydrous salt was also used to grow crystals of the deuterated trihydrate ( $\text{CH}_3\text{COONa} \cdot 3\text{D}_2\text{O}$ ) by dissolving it in a solution of  $\text{D}_2\text{O}$  (K & K Laboratories, Inc.) and deuterioethanol,  $\text{CH}_3\text{CH}_2\text{OD}$  (Diaprep, Inc.).

The  $\text{d}_3$ -sodium acetate ( $\text{CD}_3\text{COONa} \cdot 3\text{D}_2\text{O}$ ) was prepared by neutralizing  $\text{d}_4$ -acetic acid (Diaprep, Inc.) with  $\text{NaOD}$  (made by dissolving  $\text{NaOH}$  in  $\text{D}_2\text{O}$ ) to a phenolphthalein endpoint and growing the crystals from  $\text{D}_2\text{O}$  solution.

The sodium and ammonium salts of the monofluoro, difluoro and chlorodifluoro acetates were prepared by neutralizing  $\text{CFH}_2\text{COOH}$  and  $\text{CF}_2\text{HCOOH}$  (Columbia Organic Chemical Co.)

and  $\text{CF}_2\text{ClCOOH}$  (PCR, Inc.) with ammonium hydroxide or sodium hydroxide, respectively. Crystals of the monofluoroacetate,  $\text{CFH}_2\text{COOND}_4$ , and the trifluoroacetate,  $\text{CF}_3\text{COOND}_4$ , were prepared by neutralization of the acid with  $\text{ND}_4\text{OD}$  (26% in  $\text{D}_2\text{O}$ , Diaprep, Inc.) followed by slow evaporation.

#### B. Crystal Morphology

The single crystals were observed with a polarizing microscope to determine extinctions.<sup>114</sup> Using the crystal morphology and extinction axes, preliminary crystal alignments were made for observation in the ESR Spectrometer. In some cases the radical could be aligned using the maximum or minimum splitting features of the spectra as displayed on the oscilloscope mode of the spectrometer.

As far as is known, only the crystal morphology of sodium acetate trihydrate has been studied. Groth<sup>115</sup> lists the crystal as monoclinic with eight molecules per unit cell and  $\beta = 112.1^\circ$  and  $\text{C2/m}$  space group.

#### C. Sample Handling

One of the difficult experimental techniques in ESR is the accurate alignment of single crystals in the magnetic field. Ideally, one would like to mount a sample and collect data for rotations about three mutually orthogonal axes. Space requirements in the cavity and irradiation techniques combine to make this rather difficult. Research workers in this laboratory have

experimented with and modified procedures to arrive at a fairly routine and relatively good technique for obtaining the desired data.

Various irradiation sources were used. These included a  $\gamma$ -ray source which delivered a dose rate of  $2 \times 10^6$  rad/hr., a 1 MeV G. E. Resonant Transformer which produced accelerated electrons, a General Electric XRD-1 Model X-ray unit operating at 20/50 kV and 12.5 ma, and a G. E. mercury arc BH-6 capillary uv lamp operating at 900 watts power. In addition, several samples were irradiated using the University of Michigan Ford Reactor neutron source in the hope of producing different radicals. In all cases, however, these irradiation sources yielded essentially the same radicals. Since the  $\gamma$ -ray source proved to be the most convenient, the technique will be described more fully.

Samples were either placed in a one-dram vial or mounted with glue on a flattened copper wire attached to a glass rod. They were then either left at room temperature or placed in a liquid nitrogen filled Dewar and centered in the  $\gamma$ -cell. Irradiations were carried out for 2-6 hours.

Several methods for mounting crystals in the spectrometer were used. For room-temperature systems, the crystals were mounted on a Teflon sample holder as previously described.<sup>114</sup> In the case of low-temperature

studies two methods were generally used. In one, the sample was placed between the prongs of a brass clip which had been glued to a quartz rod. Mounting and aligning was done under liquid nitrogen conditions as previously thoroughly described.<sup>116</sup> This method afforded the use of the same crystal for more than one rotation study; however, alignment accuracy was slightly reduced. In the second method, the crystal was aligned at room temperature on a flattened copper wire attached to a glass tube. The crystals were then glued (PlioBond Cement, Goodyear Tire and Rubber Company) to the copper wire and irradiated. Signals from the glue proved not to be a significant problem. This method usually did not allow use of a crystal for more than one alignment. However accurate crystal alignments could be made at room temperature with the aid of the polarizing microscope.

These rods were then mounted in a specially designed Dewar (previously described by Watson)<sup>116</sup> and rotated in the magnetic field using a pointer and protractor. Alternatively, a Varian variable-temperature Dewar was used. In most instances, the crystals were rotated in the cavity. However, provisions have been made for rotating the magnet about the crystal and this method was used in the case of the Q-band experiments.

Irradiated sodium acetate crystals were allowed to warm to 198° K for five minutes by placing the samples

in a test tube immersed in a dry ice-ethanol bath; they were then returned to liquid nitrogen temperatures in order to maintain radical concentration. When these experiments were completed, the crystals were warmed to room temperature for five minutes and returned to liquid nitrogen for further studies.

#### D. Instrumentation

Various Varian components comprised the ESR Spectrometer systems. Preliminary spectra were recorded on an E-4 Varian X-band system using a Fieldial calibration. The bulk of the experimental work was then carried out on a Varian V-4502 X-band system with a 100 kHz field modulation control unit, Mark II Fieldial regulation and a 12-inch magnet. Both first- and second-derivative displays of the absorption were used. Spectra were monitored on an oscilloscope display and recorded on a Moseley 7000A or a Hewlett Packard 7005B X-Y recorder. The field was calibrated with the NMR signal from water using a marginal oscillator which, with a Monsanto counter, gave the field value in frequency units. The microwave frequency was determined by a calibrated TS-148/UP U.S. Navy Spectrum Analyzer. Frequent checks of the field and frequency measurements were made using the normal ESR standards of pitch, DPPH (diphenyl picrylhydrazine) and Fremy's Salt (peroxylamine disulphonate). A Varian

V-4533 rotating cavity or a Varian V-4531 multipurpose cavity was used along with the Varian V-4540 variable temperature accessory.

Spectra were also recorded on a Varian V-4503 spectrometer system operating at Q-band frequencies (12,500 gauss and 35 GHz). There was no calibration system available for this range, so the field and frequency as indicated on the spectrometer were used, with a significant loss in accuracy. Information was also gleaned from a Varian E-700 ENDOR accessory operating in conjunction with the X-band spectrometer in the range 3-48 MHz and using the Varian special large-access cylindrical cavity modified to deliver 1 kilowatt of peak rf power at the sample.

#### E. Studies Below 77° K

A considerable effort was made setting-up, modifying and devising new experimental techniques for studies at liquid helium temperatures.

The first system to be used was an Air Products and Chemicals, Inc. AC2-110 Cryo-Tip refrigerator with a Ventron Magnion cylindrical sample cavity. After a considerable time adapting this Cryo-Tip to the ESR system, including modification of the cavity, the feasibility of using hydrogen gas from the point of view of safety precluded the use of this equipment.

The second system, which proved to be the easiest

to operate, involved what will be called the "flow-method". A liquid helium transfer tube was designed and modified from a version of that used in Dr. Richard Sands' laboratory at the University of Michigan. It consists of a double-walled stainless steel tube wrapped with Mylar film and provided with a port for evacuating the outer chamber. The tube was designed for insertion in a thirty-liter liquid helium Dewar. The boil-off gas, produced by heating a resistor immersed in the liquid, was allowed to pass through the transfer tube and into a specially designed quartz Dewar as shown in Figure 1. Evacuation of the Dewar was necessary before each run since the warmed helium gas was shown to be permeable to the quartz. The sample was then inserted from above and the temperature was regulated by the rate of helium boil-off. With an efficient transfer, it was possible to force liquid to the tip of the transfer tube and hence approach  $4.2^{\circ}$  K at the sample. Temperatures were recorded with a 0.07% iron-doped gold-copper thermocouple. This method resulted in large expenditures of liquid helium but proved to be very stable.

The third system to be used was an Andonian Associates variable-temperature Throttle-System Dewar (Model MHD/0-17/7M). This consisted of (Figure 2) a three-liter modular liquid helium Dewar with liquid nitrogen shield, a tail section with Suprasil quartz inner and outer tubing, a



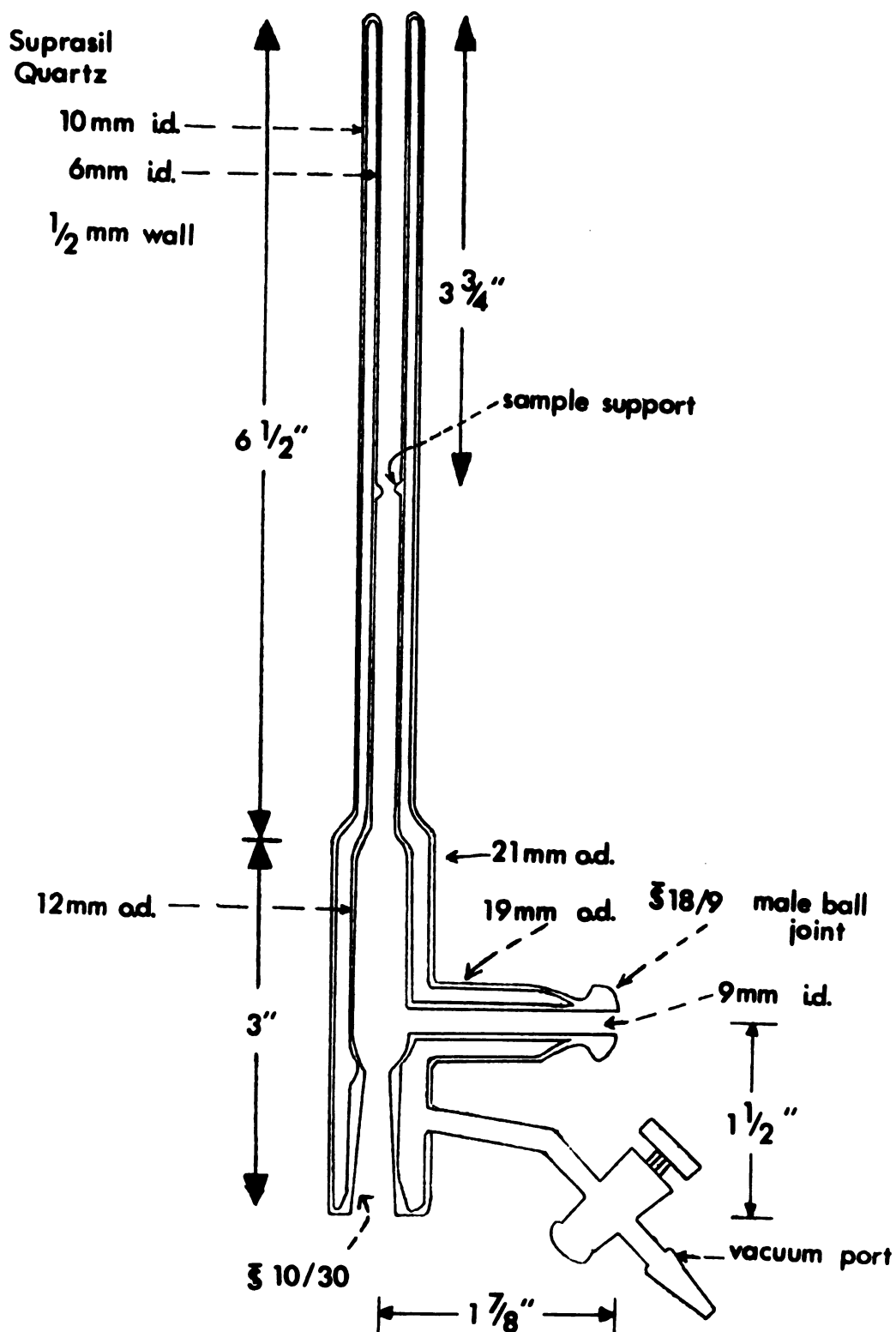


Figure 1. Liquid helium quartz Dewar for "flow-method" studies below 77°K. Dewar is designed to insert in Varian V-4531 variable temperature cavity.

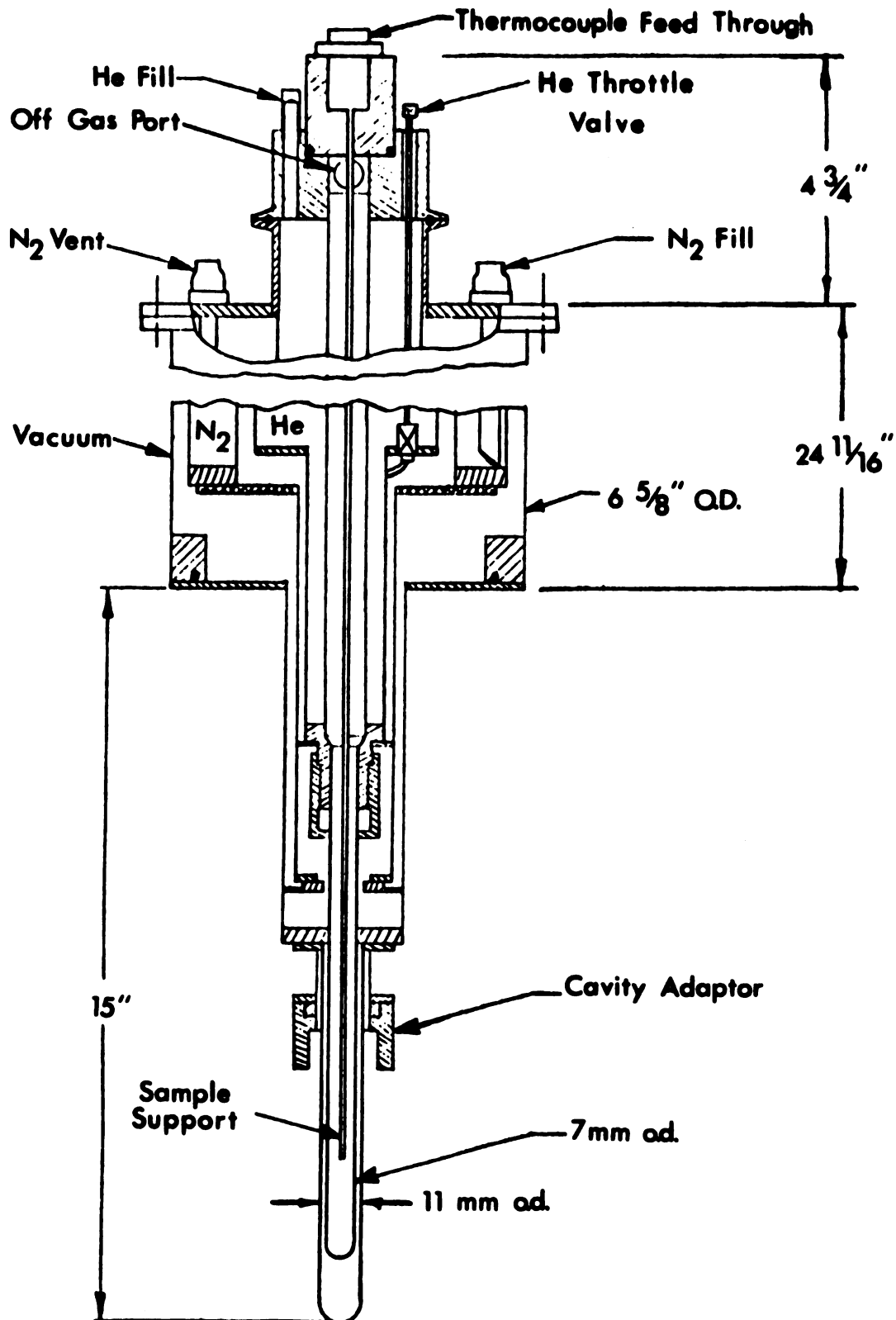


Figure 2. Schematic diagram of the Andonian Associates variable-temperature throttle-system Dewar (Model MHD/0-17/7M).

liquid helium throttling system and a removable sample positioner and support tube with heat reflecting baffles. With this system, after the vacuum jacket is cryo-pumped, three liters of liquid helium are introduced into the body of the liquid-nitrogen cooled Dewar. A throttling valve then allows passage of liquid helium through a stainless steel capillary to the sample port and an intimate flow of evaporating helium around the sample allows for cooling. Control of the valve is used for varying the flow of helium and, under full throttling conditions, liquid can actually be introduced at the sample. Since evaporating helium passes up through the sample port and out the top, the sample support may be removed for changing samples without seriously disturbing the system. This Dewar had to be modified with a beryllium window to allow for irradiation from the bottom and a mounting collar was designed to allow for rotation of the sample in the cavity.

Temperatures of  $4.5^{\circ}$  K were recorded with the iron-doped gold-copper thermocouple. This thermocouple had the advantage of greater sensitivity in the temperature range  $4-60^{\circ}$  K (greater than  $10 \mu\text{V}/^{\circ}\text{K}$ ). The thermocouple was calibrated at several temperatures and the accuracy of temperature measurements was estimated as about  $\pm 0.25^{\circ}$  K.

#### F. Analysis of Data

Generally, a single crystal was rotated about three

mutually perpendicular axes in the magnetic field of the spectrometer. A judicious choice of axes can make analysis of data easier. The rotations were carried out over  $180^\circ$  in steps of 5 or 10 angular degrees. In some instances smaller steps were taken depending upon the complexity of the spectra. A plot of rotations in degrees versus absolute line positions in gauss gives an isofrequency plot from which the nuclear coupling scheme can usually be deduced. The couplings are then determined and a tensor is set up and diagonalized to find the principal values and direction cosines.

Several diagonalization routines are available for computer analysis of the data. These were used interchangeably to assure consistency of results. One such method, developed from programs written by W. G. Waller<sup>117</sup> of this laboratory, will be described. The coupling values were determined as a function of orientation for the three rotations in the magnetic field. These values were then submitted in a FITCURV routine<sup>117</sup> to produce a least-squares fit of the data to the equation:

$$\alpha + \beta \cos 2 \theta + \gamma \sin 2 \theta. \quad ^{118} \quad (22)$$

A plot of this curve and the  $\alpha\beta\gamma$  parameters were the output of the program. These nine parameters were then submitted in a diagonalization program the output of which gave the principal values and direction cosines of the

tensor. In order to confirm these results, a third program, PLOT11, was used to give a calculated curve for comparison with the experimental values.

Certain constants and conversion factors have been used in this work. They are given here for units of gauss, which will be designated by G throughout this thesis.

$$g = \frac{(0.714489) (\nu_e \text{ MHz})}{H_o \text{ (gauss)}}$$

$$H \text{ (gauss)} = (2.348682 \times 10^2) (\nu_p \text{ MHz})$$

where  $\nu_e$  is the klystron frequency and  $\nu_p$  is the proton oscillator frequency.

In addition, the standard field markers used as a check against the spectrum analyzer and NMR probe are given:

DPPH:  $g = 2.0036$

Pitch:  $g = 2.0028$

Freymy's salt:  $g = 2.00550$

$$a_N = 13.0 \pm 0.1 \text{ G}$$

## CHAPTER IV

### IRRADIATED SODIUM ACETATES

#### A. CH<sub>3</sub>COONa·3D<sub>2</sub>O

In order to proceed with the study of motional effects in the spectra of methyl radical, it was necessary to become familiar with the spectra of the radicals produced on irradiation of sodium acetate. Rogers and Kispert<sup>98</sup> had previously reported irradiation studies at 77° K of the trihydrate salt. It was decided to study this system in the form of the deuterated trihydrate salt.

1. Analysis of Spectra at 77° K. The ESR spectra of CH<sub>3</sub>COONa·3D<sub>2</sub>O irradiated and observed at 77° K gave an intense quartet with approximate intensity ratios 1:3:3:1. In addition, small satellite lines on either side of each line of the quartet appeared. These satellites have been observed before<sup>119</sup> and were associated with "spin-flip" transitions occurring at the usual NMR spacing,  $H_{\text{NMR}} = \hbar\omega/g_N\beta_N$  gauss, symmetrically placed on both sides of each of the main lines of the quartet.<sup>120</sup> They arise from simultaneous changes in the spin state of a neighboring nucleus and that of the electron induced by weak dipole-dipole coupling between the magnetic moments of the electron and the nucleus. Even deuteration did not completely remove these lines, indicating either

long-range coupling with protons associated with the diamagnetic molecules or exchange of D and H induced by radiation. Further, increased microwave power had the effect of saturating the main quartet while not affecting these spin-flip transitions (Figure 3a).

Spectra from rotation of the crystal about three orthogonal axes indicated a slight anisotropy in the  $c^*$  direction, with the smallest coupling of 21.5 G occurring when the magnetic field is along this axis. Site splitting could be observed when the magnetic field approached this unique  $c^*$  direction. Rotation in one plane produced essentially no change in the coupling, indicating a cylindrically symmetric system.

The radical has been shown to be the  $\cdot\text{CH}_3$  radical by the carbon-13 studies of Rogers and Kispert.<sup>98</sup> The radical has a unique axis and shows two slightly skewed orientations (Figure 3b). It was therefore concluded that the methyl radical produced in  $\text{CH}_3\text{COONa}\cdot 3\text{D}_2\text{O}$  is a planar  $\pi$ -electron radical reorienting rapidly about its threefold axis with a rate greater than the anisotropic hyperfine interaction between the electron and proton which is about  $10^8 \text{ sec}^{-1}$ . Principal values and direction cosines for this radical are given in Table 4.

The methyl radical has been of considerable interest both experimentally and theoretically. Table 5 provides a convenient summary of the experimental ESR results

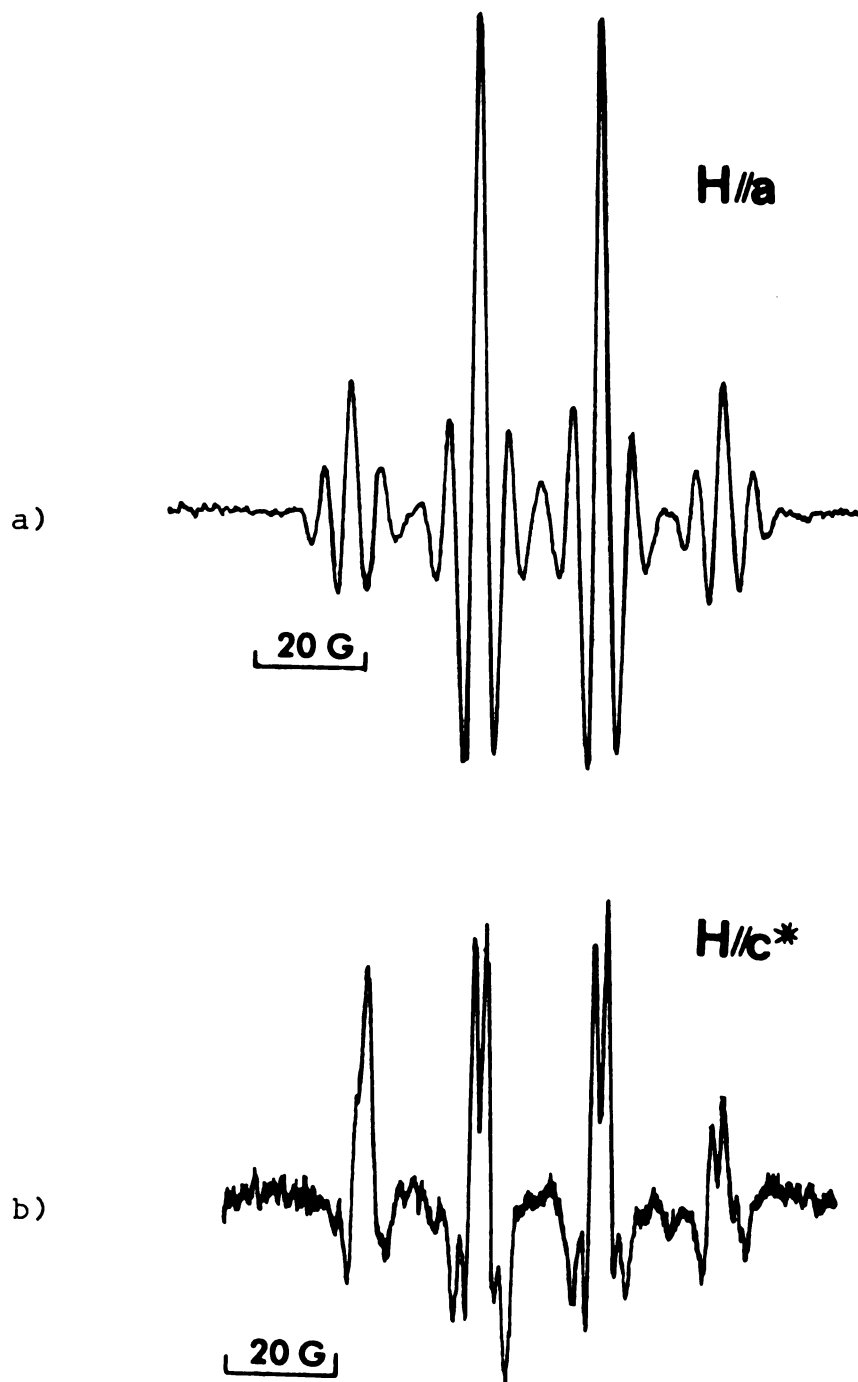


Figure 3. Second-derivative ESR spectra of  $\cdot\text{CH}_3$  radical in  $\gamma$ -irradiated single crystals of  $\text{CH}_3\text{COONa}\cdot 3\text{D}_2\text{O}$  at  $77^\circ\text{ K}$ . Spectrum (a) shows a relative increase in the "spin flip" transitions as a result of the saturation of the methyl lines at higher microwave power. Spectrum (b) shows site splitting when the magnetic field is parallel to the  $c^*$  direction.



Table 4. ESR parameters for radicals produced in  $\gamma$ -irradiated single crystals of  $\text{CH}_3\text{COONa}\cdot 3\text{D}_2\text{O}$ .

Radical	Temp.	Principal Values (Gauss)	Direction Cosines <sup>†</sup>		
			a	b	c*
$\cdot\text{CH}_3$	77° K	$A(\text{H}) = -22.4$	0.383	-0.924	0.004
		-22.4	0.922	-0.382	-0.061
		-21.5	0.058	0.019	0.998
		$a_{\text{iso}} = -22.1$			
$\cdot\text{CH}_2\text{COO}^-$	198° K	$A(\text{H}_1) = -10.8$	0.679	-0.679	0.278
		-31.0	0.543	0.720	0.432
		-21.1	-0.494	-0.143	0.858
		$a_{\text{iso}} = -21.0$			
		$A(\text{H}_2) = -12.4$	0.827	0.333	0.453
		-33.6	-0.237	0.937	-0.256
		-20.1	-0.510	-0.104	0.854
		$a_{\text{iso}} = -22.0$			
$\cdot\text{CO}_2^-$	300° K	$g = 2.0034$	0.412	-0.283	0.866
		2.0012	-0.678	0.540	0.499
		1.0974	-0.609	-0.792	0.030
		$g_{\text{iso}} = 2.0007$			

<sup>†</sup>Direction cosines with respect to the crystallographic a, b, c\* axes.

Table 5. Summary of ESR results reported for methyl radical.

Source	$a(H)^*$	$a(D)$	$a(^{13}C)$	Comments	Ref.
$CH_4$ at 96° K } Kr at 85° K }	23.04	3.58	28.3, 36.0		121
$CH_3I$ at 77° K	25. ±2		41. ±3		122
Methane } $CH_3I$ in Ar } 4.2° K $H_2$	22.97 23.06 23.21			1:2.2:2.2:1	123
Flow system -42° C	22.71	3.495			124
$CH_4$ { at 4.2° K Xe }	23.3 22.94			Unusual intensity 1:1:1:1	125
$CH_4$ at 20° K	27				126
$CH_3I$ on Vycor glass at 77° K	23.4			2.6 G from $^{11}B$	127
$CH_3I$ on glass from 77°-400°	23.0-22.0		30.-40.		128
$CH_3I$ UV at 77° K } $CH_3I$ UV at R.T. }	23.2 22.7	3.5	38.5		129
Flow system 0-60° C	22.7-22.6				130

Table 5 continued

Source	$a(\text{H})^*$	$a(\text{D})$	$a(^{13}\text{C})$	Comments	Ref.
$\text{CH}_3\text{COOH}$ in flow system at 25° C	22.6				131
Zinc acetate	23 ±1 22.14			Single crystal Single crystal	59 57
Sodium acetate · 3H <sub>2</sub> O	21.8 22.5 22.5	22.3	82.7 15.5 15.0	Single crystal	98
			37.7		
Sodium acetate · 3H <sub>2</sub> O	21.3 22.4 22.5	22.1	82.7 21.5 13.8	Single crystal Na coupling	132
			39.3		

\*Values reported in units of gauss.

reported on methyl radical. When available, deuteromethyl and carbon-13 data are also reported. In addition, Schrader and Karplus<sup>101</sup> and Davidson *et al.*<sup>133</sup> have reported theoretical studies on methyl radical. In most cases, the radical appears to be undergoing a free tumbling motion in the matrices. This may be due to the relatively small size of  $\cdot\text{CH}_3$ , to the inertness of the matrix used, or to the method employed to generate the radical. Consequently the proton and carbon-13 couplings show isotropic behavior. In some instances the methyl radical showed changes in coupling with temperature (Table 5). Studies of methyl radical formed by UV photolysis of  $\text{CH}_3\text{I}$  on porous Vycor glass at 77° K indicated an interaction of 2.6 gauss believed to arise from interaction of  $\cdot\text{CH}_3$  with boron-11 nuclei found in the glass.<sup>127</sup>

Janecka, Vyas and Fujimoto<sup>132</sup> have presented evidence for a superhyperfine interaction of sodium with the methyl radical in carbon-13 substituted  $\text{CH}_3\text{COONa}\cdot 3\text{D}_2\text{O}$ . In our studies we have not been able to detect this interaction.

2. Analysis of Spectra at 198° K. The crystal was allowed to warm to dry ice-ethanol temperature for approximately five minutes, then returned to liquid nitrogen temperature to prevent rapid decay of the radical. For most orientations, the ESR spectra showed a doublet of

doublets of approximately equal intensities. This quartet was complicated by the appearance of another set of quartets with a slightly different  $g$  value, indicating a second site of the radical. When the two couplings of the doublet of doublets became coincidentally equal, a triplet resulted with relative intensities approximately 1:2:1 (Figure 4). The coupling scheme was typical of that of two  $\alpha$ -protons and, hence, the radical was assigned to the  $\cdot\text{CH}_2\text{COO}^-$  species. Since the complete analysis of the spectra of this radical in sodium acetate had not been done, the necessary data were collected for rotations about three orthogonal axes. The coupling values were submitted in a computer least-squares fitting routine and the  $\alpha$ ,  $\beta$ ,  $\gamma$  parameters which resulted (Equation 22) were diagonalized according to the method previously described. Typical  $\alpha$ -proton principal values were obtained and are given in Table 4.

During the course of this investigation a report by Fujimoto and Janecka<sup>60</sup> appeared on the study of radicals produced in this same matrix along with data for the carbon-13 substituted radical. In addition to the  $\cdot\text{CH}_2\text{COO}^-$  radical produced at 198° K and observed at 77° K, they noted motional averaging effects on warming the crystal. It is curious that their information on the  $\alpha$ -proton couplings and  $g$  values show that the HCH angle is 107°. This is unusually small for an  $sp^2$ -hybrid (expected 120°) and,

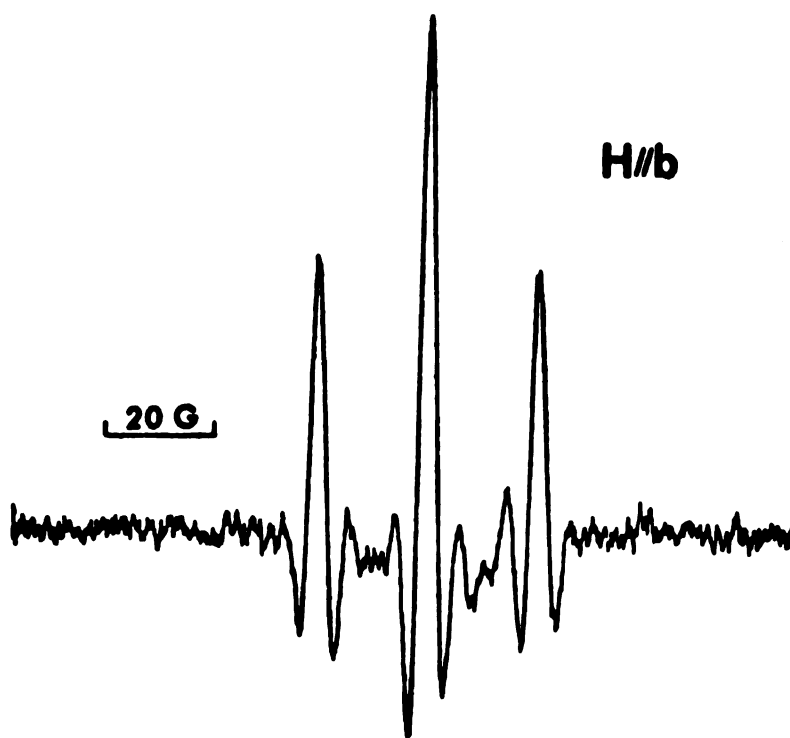
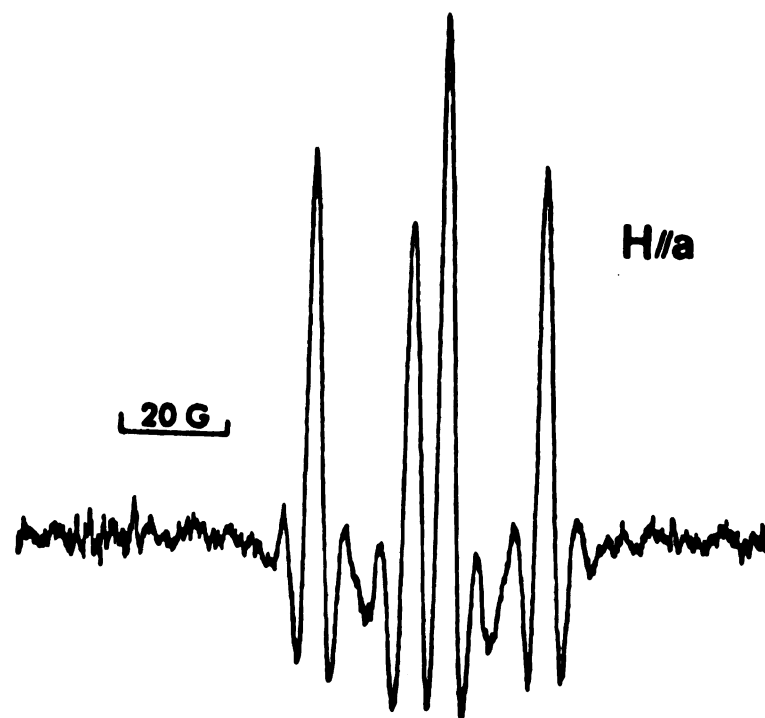


Figure 4. Second-derivative ESR spectra for two orientations of the magnetic field with respect to the  $\cdot\text{CH}_2\text{COO}^-$  radical produced in irradiated  $\text{CH}_3\text{COONa}\cdot 3\text{D}_2\text{O}$  single crystals which have been warmed to  $\sim 198^\circ\text{ K}$  for five minutes.

further, their intermediate proton principal values, along with the smallest  $g$  value, do not correspond to a planar radical. However, the present study of this same radical shows a planar structure with an HCH angle of  $116^\circ$ . These values were determined on the basis of the direction cosines for the minimum proton principal values which are known to be directed along the C-H bonds.<sup>40</sup>

A study of the literature shows a number of matrices which give the  $\cdot\text{CH}_2\text{COO}^-$  radical and the data are presented in Table 6. Comparison of the data shows the HCH angle to be on the order of  $115$ - $120^\circ$  for all the radicals, including many which undergo motional averaging. It will be further noted that the  $g$  value data are inconsistent. This is not surprising since no consistent standard of measurement has been utilized in ESR spectroscopy as, say, the use of TMS in NMR. In malonic acid, it was shown<sup>40</sup> that the smallest  $g$  value should lie perpendicular to the plane of the radical with the other two being in the plane of the radical and nearly equal. Most of the results are consistent with this interpretation.

3. Analysis of Room-Temperature Spectra. Finally, the crystal was allowed to warm to room temperature for approximately five minutes and again returned to the liquid nitrogen bath for observation of the spectra of the radical. Radical concentrations decayed if the crystal was kept at room temperature for more than

Table 6. Summary of ESR results reported for  $\cdot\text{CH}_2\text{COO}^-$  radical found in single-crystal.

Compound	$\angle\text{HCH}$	Splitting values* (gauss)	g values		Other data	Ref.
			C-C bond	$\perp$ plane		
Malonic acid	116 $\pm$ 5	H <sub>1</sub> 32.5    H <sub>2</sub> 32.8	10.7    10.7	2.0034    2.0020		40
(R.T.)						
sol'n		$a=21.2$			2.00323 (sol'n)	134
Glycine 165°K		31.0	19.2    10.5	2.0038    2.0025		135
273°K		H <sub>1</sub> =H <sub>2</sub> 24.6	20.0    17.1		A( <sup>13</sup> C) 78.9 6.8 47.5	39,55
Glycine·HCl	116	H <sub>1</sub> 33.2    H <sub>2</sub> 32.8	21.0    10.7			136
110°K			21.4    9.3			
Triglycine sulfate	116 $\pm$ 5	H <sub>1</sub> 32.9    H <sub>2</sub> 32.6	21.3    10.8			56
77°K			21.7    9.8			
R.T. (Rotating)		H <sub>1</sub> =H <sub>2</sub> 25.1	19.6    16.7	1.9999    1.9994		
Sarcosine HCl	121 $\pm$ 5	H <sub>1</sub> 31.5    H <sub>2</sub> 32.6	21.0    13.7	2.0040    2.0029		72
R.T.			21.0    9.7			
Zinc acetate	116.9 $\pm$ .3	H <sub>1</sub> 32.9    H <sub>2</sub> 33.1	21.3    21.1	2.00353    2.00242		57
133°K			9.4			



Table 6 Continued

Compound	$\angle$ HCH	Splitting values* (gauss)	g values		Other data	Ref.
			C-C bond	$\perp$ plane		
Zinc acetate 77°K	118.3	H <sub>1</sub> 33.3	2.0031	2.0024	2.0013	59
		H <sub>2</sub> 33.4				
Strontium acetate	118.6	H <sub>1</sub> 32.5	2.0031	2.0024	2.0013	33
		H <sub>2</sub> 32.7				
(2 Radicals)		H <sub>1</sub> 31.6	2.0031	2.0024	2.0013	55
		H <sub>2</sub> 32.4				
233°K	120.8	H <sub>1</sub> 33.3	2.0031	2.0024	2.0013	60
		H <sub>2</sub> 32.8				
Sodium acetate · 3D <sub>2</sub> O	107°	H <sub>1</sub> 33.3	2.0031	2.0024	2.0019	60
		H <sub>2</sub> 32.8				
77°K		H <sub>1</sub> =H <sub>2</sub> 26.1				
R.T.						

\* Signs of the couplings are assumed negative.

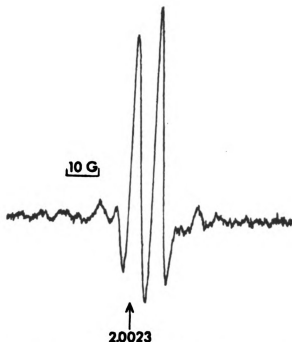


Figure 5a. Second-derivative ESR spectrum of  $\cdot\text{CO}_2^-$  radical produced in irradiated single crystals of  $\text{CH}_3\text{COONa}\cdot 3\text{D}_2\text{O}$  at room temperature. The two lines indicate two magnetically distinguishable sites of the radical.

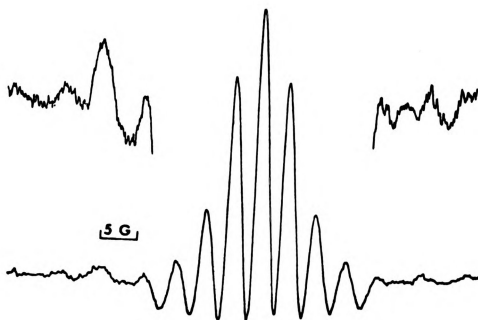


Figure 5b. Second-derivative ESR spectrum of  $\cdot\text{CD}_3$  radical produced in irradiated single crystals of  $\text{CD}_3\text{COONa}\cdot 3\text{D}_2\text{O}$  at  $77^\circ\text{K}$ .

several hours. Spectra observed at liquid nitrogen temperature for this room-temperature radical showed a singlet for certain orientations, which split into two singlets for most of the orientations in the three orthogonal planes (Figure 5a). A determination of the  $g$  values gave principal elements of 1.9974, 2.0012 and 2.0034. These values are similar to those reported for a  $\cdot\text{CO}_2^-$  sigma-type radical which has been studied by several workers in irradiated sodium formate.<sup>137,138</sup>

The  $\cdot\text{CO}_2^-$  radical has been shown<sup>137</sup> to be a sigma radical with the unpaired electron localized in an  $sp$  hybrid-type orbital directed along the  $C_{2v}$  symmetry axis. The radical retains the bent configuration with an angle of  $128^\circ$ .

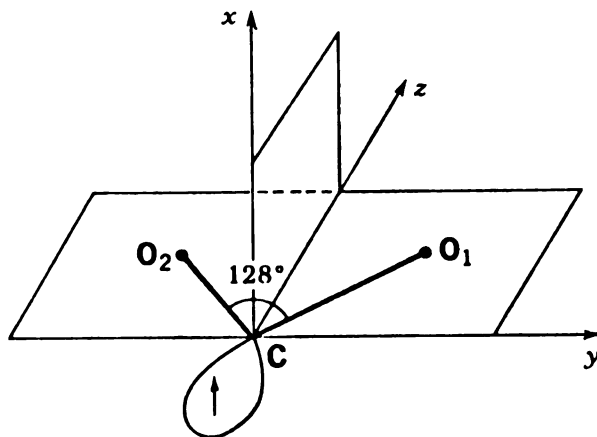


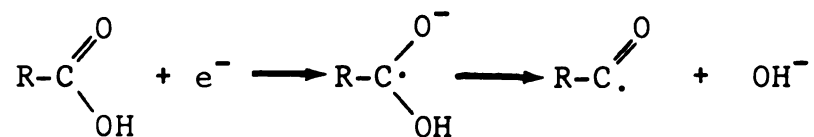
Fig. 6. Structure of the  $\cdot\text{CO}_2^-$  radical.

The unusual feature of this particular radical is the low isotropic  $g$  value, with the smallest value determined

both theoretically<sup>107</sup> and from carbon-13 data<sup>137</sup> to be along the y axis (Figure 6). Also, from carbon-13 data it has been shown that the large isotropic part of the coupling is due to unpaired spin density in the carbon 2s orbital.

The intermediate  $g$  value is directed along the z axis in the plane of the radical. Further, the anisotropic part of the coupling which is nearly cylindrical about the z axis derives mainly from the carbon  $2p_z$  electron density.

It is interesting to note that several other studies of  $\cdot\text{CO}_2^-$  in irradiated sodium formates,<sup>139</sup> in sodium hydrogen oxalate,<sup>140</sup> in calcite,<sup>141,142</sup> in sodium deposits in dry ice<sup>143</sup> and in potassium bicarbonate<sup>144</sup> are in good agreement with the above analysis. On the other hand, spectra of irradiated carboxylic acids (*e.g.*, succinic<sup>145</sup>) thought to produce  $\cdot\text{CO}_2^-$  radicals were shown rather conclusively<sup>41,146</sup> to actually result from a carbonyl-type radical  $\text{R}\dot{\text{C}}=\text{O}$ . This radical, with  $g$  values similar to carboxyl radical, is postulated to be produced by C-O bond scission of negative primary ions:



The  $g$  and  $A(^{13}\text{C})$  tensors reported by Fujimoto and Janecka,<sup>60</sup> in  $\cdot^{13}\text{CO}_2^-$  produced from  $\text{CH}_3^{13}\text{COONa} \cdot 3\text{D}_2\text{O}$  did not

have the same principal axes as would be expected. In addition, the near cylindrical symmetry of  $A(^{13}\text{C})$  found in other studies is not present. Nevertheless, they do not report any coupling from  $^{13}\text{C}$  in radicals produced from irradiation of  $^{13}\text{CH}_3\text{COONa}$  as would be expected if the carbonyl radical were produced, so their radical must be  $\cdot^{13}\text{CO}_2^-$ .

4. Analysis of reaction scheme. Formation of  $\cdot\text{CH}_3$  on irradiation of sodium acetate must result from a rupture of the C-C bond. This bond breakage at low temperatures is not unusual. Upon warming, the  $\cdot\text{CH}_3$  radical apparently abstracts a proton from a neighboring molecule to give  $\cdot\text{CH}_2\text{COO}^-$ . Again, this is not surprising since most studies of methyl radicals indicate that it is an unstable species at higher temperatures. Deuterium labelling studies of similar radicals produced in irradiated zinc acetate<sup>57</sup> support this mechanism. However, it is difficult to postulate a mechanism for formation of  $\cdot\text{CO}_2^-$  from the  $\pi$ -electron radical  $\cdot\text{CH}_2\text{COO}^-$ . Although some carboxyl radicals may be present at lower temperatures they are more easily saturated and so may not be observed. Nevertheless the simultaneous increase in  $\cdot\text{CO}_2^-$  and decrease in  $\cdot\text{CH}_2\text{COO}^-$  concentration on warming must certainly indicate a radical reaction of some kind.

B.  $\text{CD}_3\text{COONa} \cdot 3\text{D}_2\text{O}$

In addition to the  $\cdot\text{CH}_3$  radical it was desirable to produce  $\cdot\text{CD}_3$  radicals for study at low temperatures so single crystals of the perdeuterated acetate were irradiated and the spectra studied at 77° K. The seven-line spectrum observed was typical of a rotating trideuteromethyl radical species with the predicted intensity ratios of approximately 1:3:6:7:6:3:1 (Figure 5b). The splittings ranged in value from 3.24 to 3.60 gauss which are about 15% of the corresponding proton values. Since the ratio of magnetic moments is  $(0.85738/2.79270) = 0.3070$  and the spins are  $I = 1$  and  $I = 1/2$ , respectively, the ratio of splittings should be 0.1535. Rotation of the crystal in the magnetic field produced small anisotropy of the order of 0.4 gauss. In addition, lines from another radical were observed on either side of the septet. This radical could not be identified but the ESR spectrum showed considerable anisotropy. Upon gradual warming, the central septet collapsed and the outer lines from this unidentified species increased. The splitting, which is 40 gauss between peaks and 13 gauss between nearest lines, appears too large to arise from the expected  $\cdot\text{CD}_2\text{COO}^-$  radical. The possibility of a proton impurity cannot be ruled out since radical reactions which favor one isotopic species have appeared in several other instances.<sup>147</sup>

### C. ENDOR Studies

After the data for the ESR studies of irradiation damage in  $\text{CH}_3\text{COONa} \cdot 3\text{D}_2\text{O}$  single crystals had been collected, two papers appeared in the literature on similar studies.<sup>60,132</sup> In one, Janecka, Vyas and Fujimoto<sup>132</sup> indicated that there was a coupling of the methyl radical to a neighboring sodium atom at 77° K, as observed for the  $\cdot\text{CO}_2^-$  radical of sodium formate.<sup>137</sup> In the present investigation such a sodium coupling was not observed. One might expect to see such a sodium splitting in the  $\cdot\text{CD}_3$  spectrum since the deuterium coupling is of the order of that reported for sodium (3 gauss). No such coupling was observed.

In order to resolve the problem of whether sodium coupling was present in the ESR spectrum of  $\cdot\text{CH}_3$ , it was decided to do an ENDOR experiment for evidence of sodium hyperfine interaction. Double resonance has the inherent advantage of being capable of detecting very small couplings which may be unobservable in the ESR spectrum because they are of the order of linewidths.

Sodium has a nuclear spin of 3/2, hence four electron resonance lines are expected. Since sodium may also have a quadrupole coupling, there are six possible ENDOR transitions, three above and three below  $\nu_{\text{Na}} = 3.66 \text{ MHz}$  (the frequency of free sodium at 9.2 GHz and 3200 gauss). The range of the Varian ENDOR system is approximately 3 to 48 MHz, therefore only the high-field lines would be

observable. In sodium ENDOR measurements done on the  $\cdot\text{CO}_2^-$  radical found in irradiated sodium formate,<sup>148</sup> these high-field lines were reported to be more intense. However, only a transition in the ESR which connects one of the energy levels in the ENDOR transition will be observed. Thus, if the  $M = \pm 3/2$  lines are saturated only one high-field line would be expected. The sodium ESR hyperfine splitting for  $\cdot\text{CH}_3$  was not resolved therefore it was not possible to determine which of the sodium transitions was saturated in the ENDOR experiment. A signal was detected in the ENDOR at 5.80 MHz corresponding to a sodium splitting of 4.28 MHz, or 1.53 gauss. However,  $\nu_D$  for deuterium would be expected at 2.13 MHz, and consequently a deuterium coupling of approximately 2.6 gauss would also account for the ENDOR line observed. Therefore deuterium cannot be ruled out as an alternative.

No additional hyperfine coupling which might be attributable to sodium was observed in the case of the room temperature  $\cdot\text{CO}_2^-$  radical by Janecka *et al.* or in this work. There remains, then, some doubt whether there is a sodium coupling. Since the compound studied is a deuterio-substituted species, care must be taken in interpreting the spectra due to possible deuterium exchange reactions.<sup>149</sup>

#### D. Anhydrous Sodium Acetate

It was of interest to observe the results of



irradiated crystals of the anhydrous salt. Rogers and Kispert<sup>47</sup> have shown that production of methyl radicals depends on water of hydration in a number of acetate salts. That is, the greater the number of waters of crystallization in the salt, the greater the probability of methyl radical production and the higher the concentration of methyl radicals formed at 77° K.

Vorlander and Nolte<sup>113</sup> observed back in 1914 a remarkable difference in the anhydrous salts formed from dehydration at 120° C and above 200° C, the former being probably rhombic and the latter probably monoclinic. They noted, "it may be assumed that within the molecule there exist differences in the intensity of the energy between individual parts of the molecule or, especially, as a result of these intramolecular differences, there may likewise be variable extramolecular intensity differences between like molecules."

1. The Doublet ESR Spectrum. The crystal structure of anhydrous sodium acetate has not been determined. However, the crystals grow in very thin plates in the shape of a parallelogram with extinctions occurring along the diagonal of the parallelogram. These two extinction axes, designated *b* and *c*, were used for rotations in the magnetic field along with the axis perpendicular to the plates. Samples irradiated and observed at 77° K gave

unusually symmetric ESR patterns. For rotations about  $b$  and  $c$ , essentially identical coupling curves were observed. Most orientations gave a doublet of doublets with typical  $\alpha$ -proton couplings; these became triplets for  $\vec{H}$  parallel to  $0^\circ$  and  $90^\circ$ . From these spectra the radical was assigned the structure  $\cdot\text{CH}_2\text{COO}^-$ . The third orientation,  $a$ , gave a triplet of nearly isotropic coupling. Since the measured coupling was approximately 20 gauss, which is a typical intermediate principal value for an  $\alpha$ -proton, it was concluded that the  $bc$  plane was the plane containing the C-C bond and the bisector of the HCH angle. Simulated spectra were obtained using a computer program<sup>118</sup> and assuming that there are two  $\alpha$  protons with -10, -20, and -30 gauss principal splitting values. These confirmed that there would be equivalent coupling from the two protons for all orientations in this  $bc$  plane, with values ranging from 17.5 gauss to 20 gauss. The experimental tensor was then diagonalized and gave the principal values and direction cosines listed in Table 7.

It will be noted here again that the HCH angle is  $115.5^\circ$  from direction cosine data (Table 6). In contrast to the radical found in the  $\text{CH}_3\text{COONa} \cdot 3\text{D}_2\text{O}$ , this system shows considerably more symmetry, with only one site being observed for all orientations. A crystal structure analysis at this point would be required for further comparisons.

Table 7. Principal hyperfine splitting values and direction cosines for the  $\cdot\text{CH}_2\text{COO}^-$  radical produced at 77° K in irradiated single crystals of anhydrous sodium acetate.

$A(\text{H})$ (gauss)	Direction Cosines*		
$A(\text{H}_1) = -12.9$	.564	-.545	.620
-33.0	.403	.837	.370
<u>-21.0</u>	-.721	.041	.692
$a_{\text{iso}} = -22.3$			
$A(\text{H}_2) = -13.6$	.567	.520	.639
-33.2	-.365	.854	-.371
<u>-20.8</u>	-.740	-.022	.674
$a_{\text{iso}} = -22.5$			
$\angle\text{HCH} = 115.5^\circ$			

\* With respect to the laboratory axis system specified in the text.

2. The Triplet ESR Spectrum. In addition to the lines from the above radical, an inequivalent set of lines appeared on either side of the main quartet for certain orientations, with a maximum splitting of 150 G along the axes of rotation. The couplings for the lines on the low-field side are one-half the coupling of the main spectrum, while the lines on the high-field side show couplings of approximately one-fourth those of the main spectrum (Figure 7a). For most orientations, the lines were incompletely resolved and the intensities very quickly were reduced to the level of base-line noise. Such signals are typical of a radical pair. However, the unusual result is that the components of the pair are apparently different species. To verify these results, a powder spectrum was taken (Figure 7b). The two signals at either side of the main spectrum correspond to a splitting of approximately 162.8 gauss. In addition, the half-field transition at  $g = 4$  was observed (Figure 7c) as a very weak signal.

When two radicals are produced about 5-10 Å apart, a triplet state interaction between the two electrons results. Characteristics of the triplet state spectrum are the occurrence of the  $\Delta M_S = 1$  transition and of a weak half-field signal at  $g = 4$  due to the  $\Delta M_S = 2$  "forbidden transition". This transition becomes "allowed" by mixing of the  $M_S = 0$  and  $M_S = \pm 1$  levels in a second-

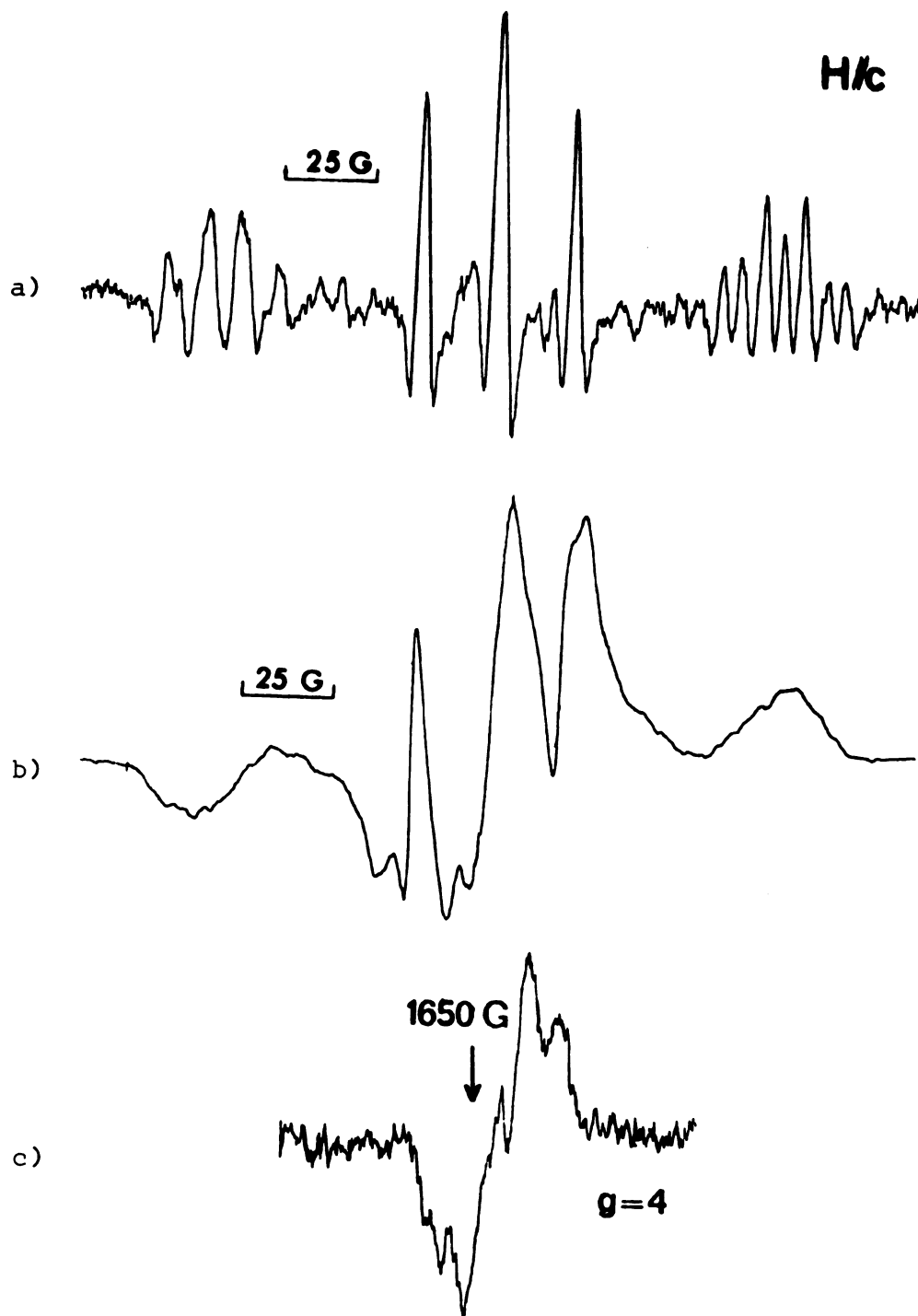


Figure 7. ESR spectra of radicals produced in irradiated anhydrous sodium acetate at 77° K. a) Single crystal second-derivative spectrum showing  $\cdot\text{CH}_2\text{COO}^-$  main radical with dissimilar coupling from the radical pair. b) First derivative powder spectrum. c) Low-field ( $\sim 1650$  G) transition for radical pair,  $g=4$ , with 1000-fold increase in gain.

order perturbation treatment. The electronic spin moment in the triplet state is that of two coupled electrons ( $S = 1$ ) and only one-half of this moment, on the average, effectively interacts with the nuclei; hence the hyperfine separations are approximately one-half those of the main singlet.<sup>150</sup>

The spin Hamiltonian for such a pair is given by:

$$\mathcal{H} = \beta \vec{H} \cdot \vec{g} \cdot (\vec{S}_1 + \vec{S}_2) + J \vec{S}_1 \cdot \vec{S}_2 + \vec{S}_1 \cdot \vec{D} \cdot \vec{S}_2 \quad (23)$$

where  $D$  is the traceless dipole-dipole coupling tensor and  $J$  is the exchange coupling. Since the distance between the two unpaired electrons is so large, a point-dipole approximation is fairly good, resulting in zero-field splitting constants with  $|E| \sim 0$  and  $D$ , therefore, axially symmetric. Hence, the vector  $\vec{R}$  between the electrons is parallel to  $D_{zz}$  and

$$D = \frac{3g\beta}{2R^3} (1 - 3\cos^2\theta) \quad (24)$$

or, rearranging,

$$R = 3.06/D, \quad (25)$$

where  $D$  is in gauss and  $R$  is in angstroms.

From these equations, the distance of  $5.77\text{\AA}$  was determined to be the maximum distance between the pairs in anhydrous sodium acetate. This is in good agreement with values found in pairs previously studied. Iwasaki<sup>151</sup>

has presented a table of data for radical pairs in terms of two modes of formation. His table (Table 8) is presented here and expanded to include more recent work for comparison. The radical obtained in this study cannot be identified from the spectra obtained, but appears to be a dissimilar pair (that is, a pair in which there are two different kinds of radicals interacting). Only one other study has shown this kind of behavior.<sup>158</sup>

Box has shown<sup>161</sup> that no pairs exist in dimethylglyoxime at 4.2° K and only form on warming to 77° K. This strongly supports the idea that pairs are not random formations of two closely-spaced molecules but must result from some radical reaction. A mechanism has been suggested<sup>161</sup> whereby a cation loses a proton to a neighboring molecule to form a radical. Electrons then migrate and combine with the protonated species with the evolution of H<sub>2</sub> and production of a second radical in the vicinity of the first to form the pair. Upon further warming above 77° K, the pairs diffuse apart by intermolecular hydrogen transfer to give the final discrete radicals.

Anhydrous sodium acetate would be an interesting system to test this reaction sequence. It would be necessary, however, to study the irradiation damage process at lower temperatures. One further observation should be noted-that in most of the pairs previously studied, formation occurred where a protonated species such as -OH or

Table 8. ESR studies of radical pairs found in irradiated single crystals.

## A. Pairs formed from two adjacent molecules

Compound	Temp. (°K)	Paired Radical*	Distance (Å)	Ref.
Dimethylglyoxime	(77°K)	$\text{HON}(\text{CH}_3)\text{C}-\text{C}(\text{CH}_3)\text{NO}\cdot$	5.4	152
			5.6	153
Glyoxime	(77°K)	$\text{HONCH}-\text{CHNO}\cdot$	<4.8	153
			<6.9	
Methylglyoxime	(77°K)	$\text{HONCH}-\text{C}(\text{CH}_3)\text{NO}\cdot$	<5.2	153
			<7.9	
p-Chlorobenzaldoxime	(77°K)	$\text{Cl}-\text{C}_6\text{H}_4-\text{CHNO}\cdot$ syn- anti-	6.1	154
			5.0	
$\text{Na}\left\{\begin{array}{l} \text{Oximinopropionate} \\ \text{K} \end{array}\right\}$	(77°K)	$-\text{OOC}(\text{CH}_3)\text{NO}\cdot$	7.2	155
Hydroquinone-acetonitrile clathrate	(77°K)	$\text{HO}-\text{C}_6\text{H}_4-\text{O}\cdot$	5.1	156
Oxalic acid	(77°K)	$\text{HOOC}-\text{COO}\cdot$ dihyd. anhyd.	6.33	157
			9.93	
Monofluoroacetamide	(77°K)	$\left\{ \begin{array}{l} \cdot\text{CH}_2\text{CONH}_2 \\ \cdot\text{CHFCNH}_2 \end{array} \right\}$ dissimilar pair	7.03	158



Table 8 Continued

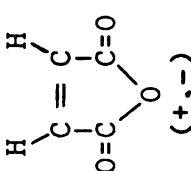
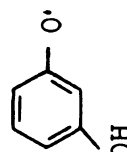
Compound	Temp. (°K)	Paired Radical*	Distance (Å)	Ref.
Hydroxyurea	(5°, 30°, 77°K)	NH <sub>2</sub> CONHO·	6.38 ≤5.3	159
Carbazine	(77°K)	NH <sub>2</sub> NHCONHNH or NHNHCONHNH (biradical)	4.37	42
Potassium hydrogen malonate	(4.2°K)	<sup>+</sup> K <sup>-</sup> OOCĊHCOOH	5.6	160 161
Maleic anhydride	(77°K)	 (+, -)	5.39	44
Potassium hydrogen fumarate	(77°K)	(KOOCCCH=CHCOOH) <sup>+</sup> , -	6.46	45
n-Hydrocarbons and polymers	(77°K) (77°K)	Adjacent Allyl carbons	5.75	151 43 162
Resorcinol	(77°K)		5.2 7.25	163

Table 8 Continued

## B. Pairs formed by the decomposition of a single molecule

Compound	Temp. (°K)	Paired Radical*	Distance (Å)	Ref.
Methane	(4.2°K)	H·    ·CH <sub>3</sub>	6.76	150
Azobis-isobutyronitrile	(77°K)	·C(CH <sub>3</sub> ) <sub>2</sub> CN	6	164
Tetraphenylhydrazine	(77°K)	·N(C <sub>6</sub> H <sub>5</sub> ) <sub>2</sub>	5.9 3-4	165
Diphenylcarbonate and others	(77°K)	·O-C <sub>6</sub> H <sub>5</sub>	5.9 ~5.8	166
Potassium persulfate	(R.T.)	·OOSO <sub>3</sub> <sup>-</sup>	15.8	167
Dibenzoyl peroxide in dibenzoyl disulfide	(4.2°K)	C <sub>6</sub> H <sub>5</sub> ·    photolysis C <sub>6</sub> H <sub>5</sub> COO·    x-rays	6.5 3.6	161

\* In some cases more than one pair was observed.

-NH was available. In anhydrous sodium acetate, no protons of this type exist.

One further experiment with anhydrous sodium acetate indicated that under controlled warming conditions the  $\cdot\text{CO}_2^-$  radical did not appear to be produced. A detailed crystal structure analysis is needed, but certainly it can be concluded that the crystal packing is strongly influencing radical formation in these acetate systems.

#### E. Methyl Radical Below 77° K.

Several authors<sup>125,128,130</sup> have reported unusual ESR line intensities for methyl radical at low temperatures. Normally, a 1:3:3:1 quartet would be expected from equivalent coupling of three protons with the unpaired electron. Jackel and Gordy<sup>125</sup> observed an unusual 1:1:1:1 quartet for the radical found in inert matrices such as xenon at 4.2° K. They ascribed this phenomenon to separations in the low-level rotational energies as predicted by McConnell.<sup>168</sup> The over-all wave function for the three equivalent hydrogens in the lowest rotational state is required by symmetry to be a symmetric function. Each function must correspond to a separate hyperfine component and each would have equal weight. Hence, the predicted intensities should be 1:1:1:1. As the temperature is raised, higher rotational states are populated and the intensities approach the expected 1:3:3:1 quartet. McConnell<sup>168</sup> points out that if there is a barrier to

the rotation in some matrices, then the normal quartet will be observed; this appears to be the case for most matrices other than xenon which have been used (Table 5).

It was of interest to study the ESR spectra of the methyl radical found in sodium acetate trihydrate down to temperatures below 77° K. If the radical did experience restricted motion, perhaps the type of motion could be determined and the barrier to rotation calculated.

There were a number of experimental difficulties encountered. Since the radical was unstable in the acetate matrix above liquid nitrogen temperatures, it was difficult to transfer the crystals after irradiation at liquid nitrogen temperature without introducing slight warming and resultant interference from the spectrum of the  $\cdot\text{CH}_2\text{COO}^-$  radical so formed. In experiments with the Andonian Dewar system it was found that the crystals irradiated at 77° K could not be inserted into the helium cold finger without some warming difficulty. Hence the helium "flow method" was used to collect data. The  $\cdot\text{CH}_2\text{COO}^-$  radical may even exist at 77° K but may not be observable due to differences in saturation properties, the methyl radical being less susceptible to power saturation. Evidence from these liquid helium ESR experiments indicates that  $\cdot\text{CH}_2\text{COO}^-$  is indeed present at 77° K and appears to undergo further motional changes at lower temperatures.

The second problem encountered was power saturation from the incident microwaves at the cavity. At temperatures approaching  $4.2^{\circ}$  K the crystal relaxation mechanisms prevent the rapid decay of electrons to the lower energy state and, hence, a situation is created whereby the electron levels become equally populated with resultant loss of signal. Spectra were recorded with some degree of success for both the  $\cdot\text{CH}_3$  and  $\cdot\text{CD}_3$  radicals using the low-power arm of the microwave bridge. The spectra are shown in Figures 8a, b, and c.

It will be noted that the spectra above  $30^{\circ}$  K show some interference from a second radical, presumably  $\cdot\text{CH}_2\text{COO}^-$ . Nevertheless, it was possible to record spectra of methyl radicals at temperatures down to  $4.5^{\circ}$  K. Several features may be observed. In all studies, the separation between the two outer lines of the quartet did not change with change in temperature. At approximately  $30^{\circ}$  K significant changes in peak intensities occurred such that the inner lines were reduced to a ratio of less than one with respect to the outer lines. The  $\cdot\text{CD}_3$  spectra were also observed to undergo a similar change in intensity ratios. The temperature at which the intensity ratios for  $\cdot\text{CH}_3$  becomes approximately 1:1:1:1 ( $30^{\circ}$  K) is considerably higher than that calculated by Gordy<sup>125</sup> on the basis of rotational level energies. At lower temperatures, these inner lines appear to be split into additional

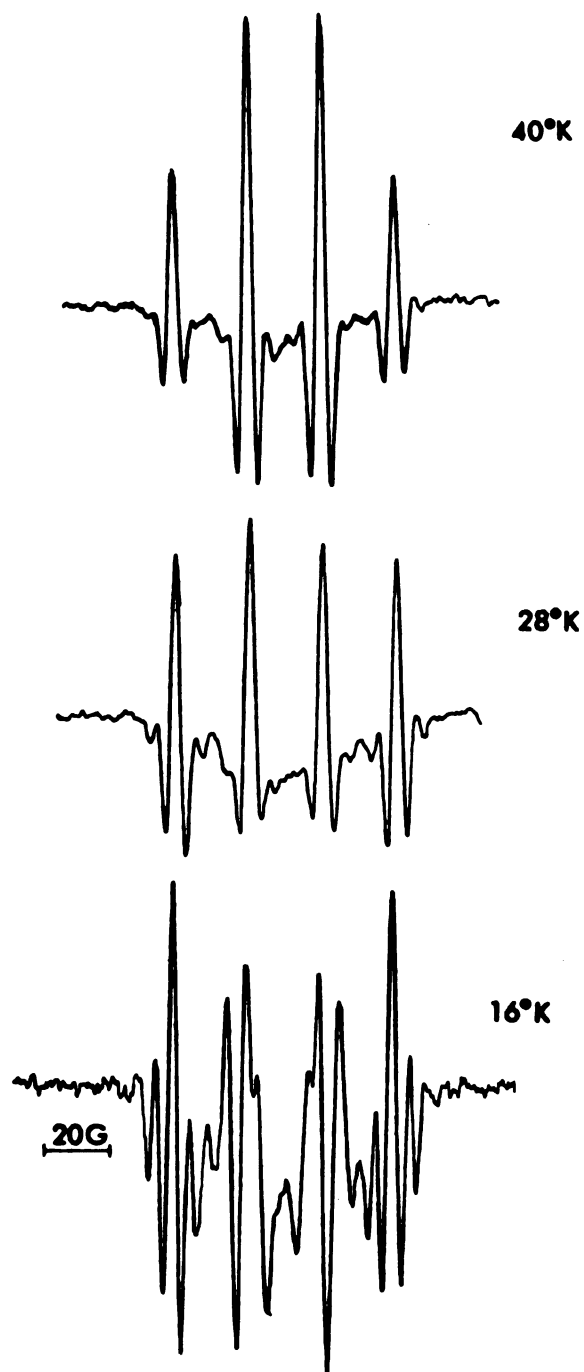


Figure 8a. Second-derivative ESR spectra for  $\cdot\text{CH}_3$  radical at temperatures below  $77^\circ\text{K}$ .

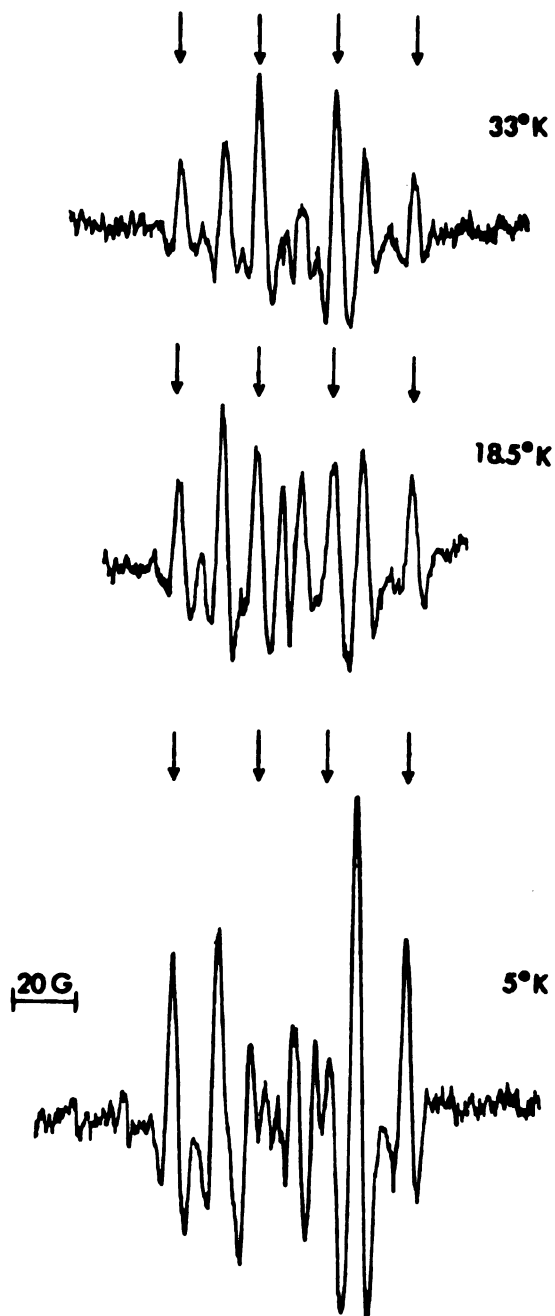


Figure 8b. Second-derivative ESR spectra for  $\cdot\text{CH}_3$  radicals (arrows) at temperatures below 77° K. Extra lines at 33° K indicate the presence of a second species, probably  $\cdot\text{CH}_2\text{COO}^-$ .

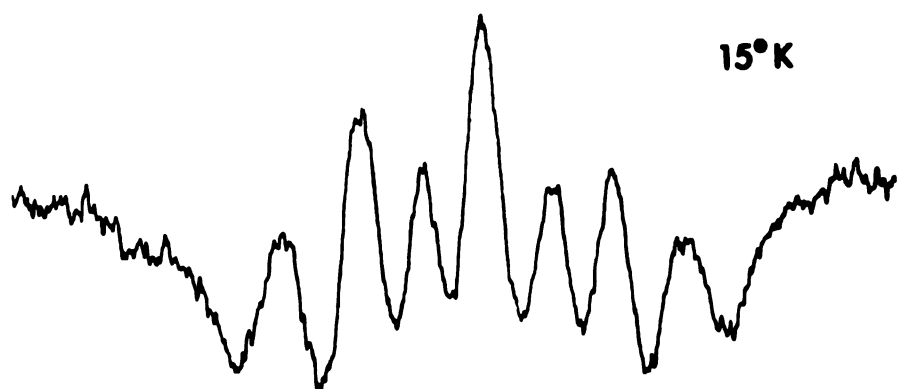
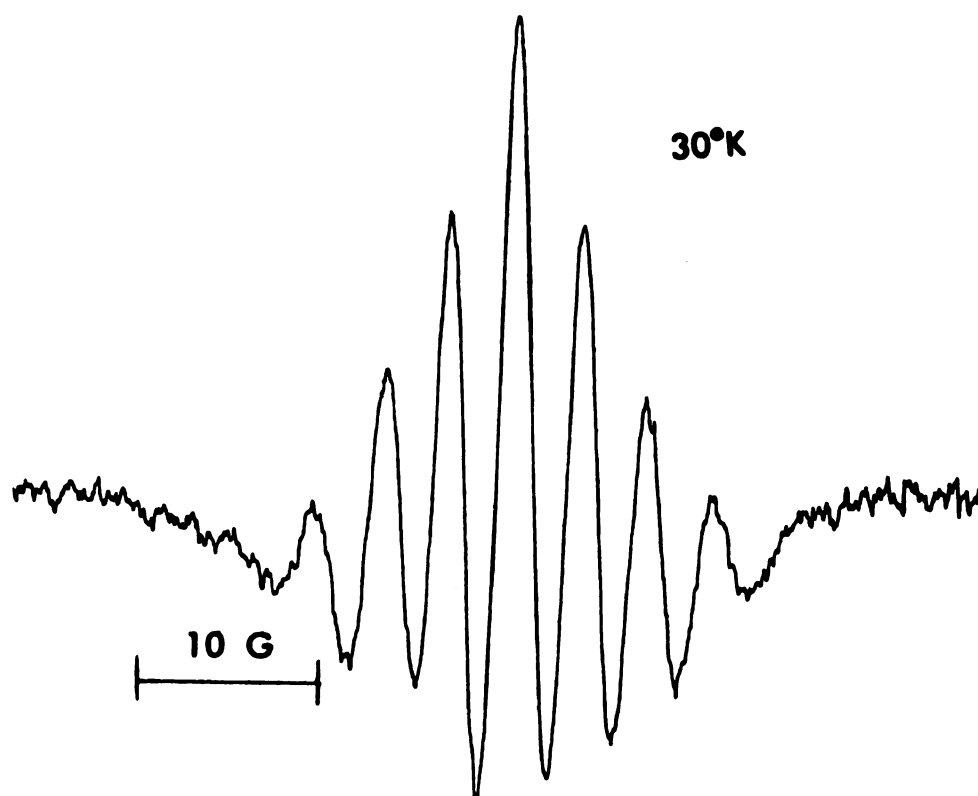


Figure 8c. Second-derivative ESR spectra for  $\cdot\text{CD}_3$  radical at temperatures below  $77^\circ\text{K}$ .



components. However, there is considerable interference from lines due to the other radical present. It can be concluded that no classical Brownian-type motion is taking place since there are no line-broadening regions as observed for other methyl-type rotations.<sup>70</sup>

Results obtained in this work appear to be comparable to those attributed to quantum mechanical tunnelling through a barrier as observed (Table 1) in several other systems.<sup>54,71,73,74</sup> In particular, the spectra observed by Clough et al.<sup>76</sup> for methyl malonic acid show some similarities to the spectra of Figure 8a. No further analysis of the spectra can be reported.

It can be concluded that the methyl radical in sodium acetate trihydrate exhibits unusual motional behavior below liquid nitrogen temperatures. Further work must be done, such as irradiating the samples in the cavity to eliminate warming problems and improving the spectrometer to reduce power saturation problems, before detailed analysis of the motional behavior can be made.

## CHAPTER V

### IRRADIATED FLUOROACETATES

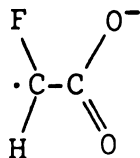
An attempt was made to prepare and study the ESR spectra of the radicals  $\cdot\text{CFH}_2$  and  $\cdot\text{CF}_2\text{H}$ . By analogy with the results reported above for methyl radical in irradiated  $\text{CH}_3\text{COONa} \cdot 3\text{H}_2\text{O}$  the salts  $\text{CFH}_2\text{COONa}$  and  $\text{CF}_2\text{HCOONa}$  were irradiated. Unfortunately, any low temperature handling of the crystals resulted in shattering, making analysis of the ESR spectra impossible. Consequently, the ammonium salts of the corresponding fluoro-substituted compounds were irradiated and the results of these studies are reported here.

Only the crystal structure of ammonium trifluoroacetate has been determined. Cruikshank, Jones and Walker<sup>169</sup> have found this salt to be monoclinic with space group  $P2_1/a$ , four molecules per unit cell and  $\beta = 100^\circ$ . The structures of the monofluoro- and difluoro-salts are not known. Extinction axes for both salts were parallel to the diagonals of the flat face. Two of the axes of rotation were chosen parallel to these diagonals with the third axis being the mutually orthogonal direction. In all systems studied, the  $c$  direction will correspond to maximum fluorine splitting and the  $a$  direction

to the minimum fluorine splitting.

#### A. Ammonium Monofluoroacetate

1. Analysis of Room Temperature Spectra. Irradiation at room temperature of ammonium monofluoroacetate produced an ESR spectrum consisting of a doublet of doublets. Typical second-derivative ESR spectra of the single crystal are shown in Figure 9. The splitting for the smaller doublet was approximately 20 gauss with an anisotropy of  $\pm 10$  gauss. The larger doublet showed typical  $\alpha$ -fluorine anisotropy with a maximum splitting of about 185 gauss and a minimum splitting close to zero. The radical was therefore assigned the structure



Although a similar radical,  $\cdot\text{CHFCNH}_2$ , had been previously studied in the amide,  $\text{CF}_2\text{HCONH}_2$ , by Cook, Rowlands and Whiffen<sup>85</sup> it was decided to carry out the present study for a number of reasons. The number of single-crystal investigations of fluoro-organic radicals has been relatively small. Most of the radicals found have had more than one fluorine atom and carbon-13 hyperfine splitting data have not been reported (Table 2). In addition, the study of  $\cdot\text{CHFCNH}_2$  in monofluoroacetamide<sup>85</sup> had added difficulties; more than one magnetically equivalent site

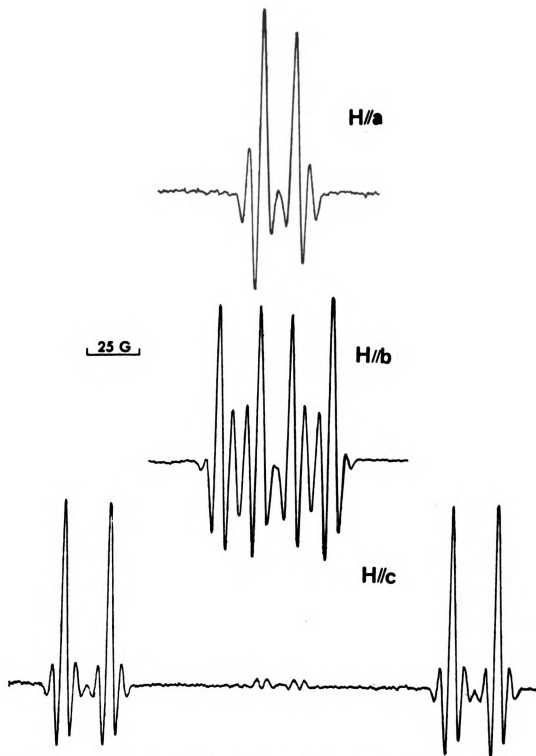


Figure 9. Second-derivative ESR spectra for  $\cdot\text{CFHCOO}^-$  radical produced in irradiated single crystals of ammonium monofluoroacetate at room temperature.

was seen and long-range coupling from the nitrogen, typical of the amides, was observed. Also they did not report  $g$  values for this radical.

The radical  $\cdot\text{CFHCOO}^-$  was well suited for study. As observed from the isofrequency plots in the following Figure 10(a-c), two planes of the rotation produced only one radical site while the other plane had two magnetically distinguishable sites. With the presence of an  $\alpha$  proton a careful evaluation of the radical structure and spin density distribution can be made. The system was analyzed and diagonalized tensors were obtained for the  $g$  value and for the fluorine and proton hyperfine splittings. These principal components, along with their corresponding direction cosines, are listed in Table 9. Values of the hyperfine interactions  $A(\text{H})$  and  $A(\text{F})$  for rotation of the magnetic field in the three orthogonal planes are shown in Figures 11 and 12 and the corresponding plots of the  $g$  values are shown in Figure 13.

Since the radical concentration was quite high for the room temperature radical, it was possible to increase the signal gain without much loss in sensitivity, hence the 1.1% natural abundance carbon-13 lines were detectable. In view of the fact that the directions of the maximum components of the carbon-13 and fluorine-19 hyperfine splitting tensors coincide within experimental error, the value for  $A_{zz} (^{13}\text{C})$  is obtained directly. It was not

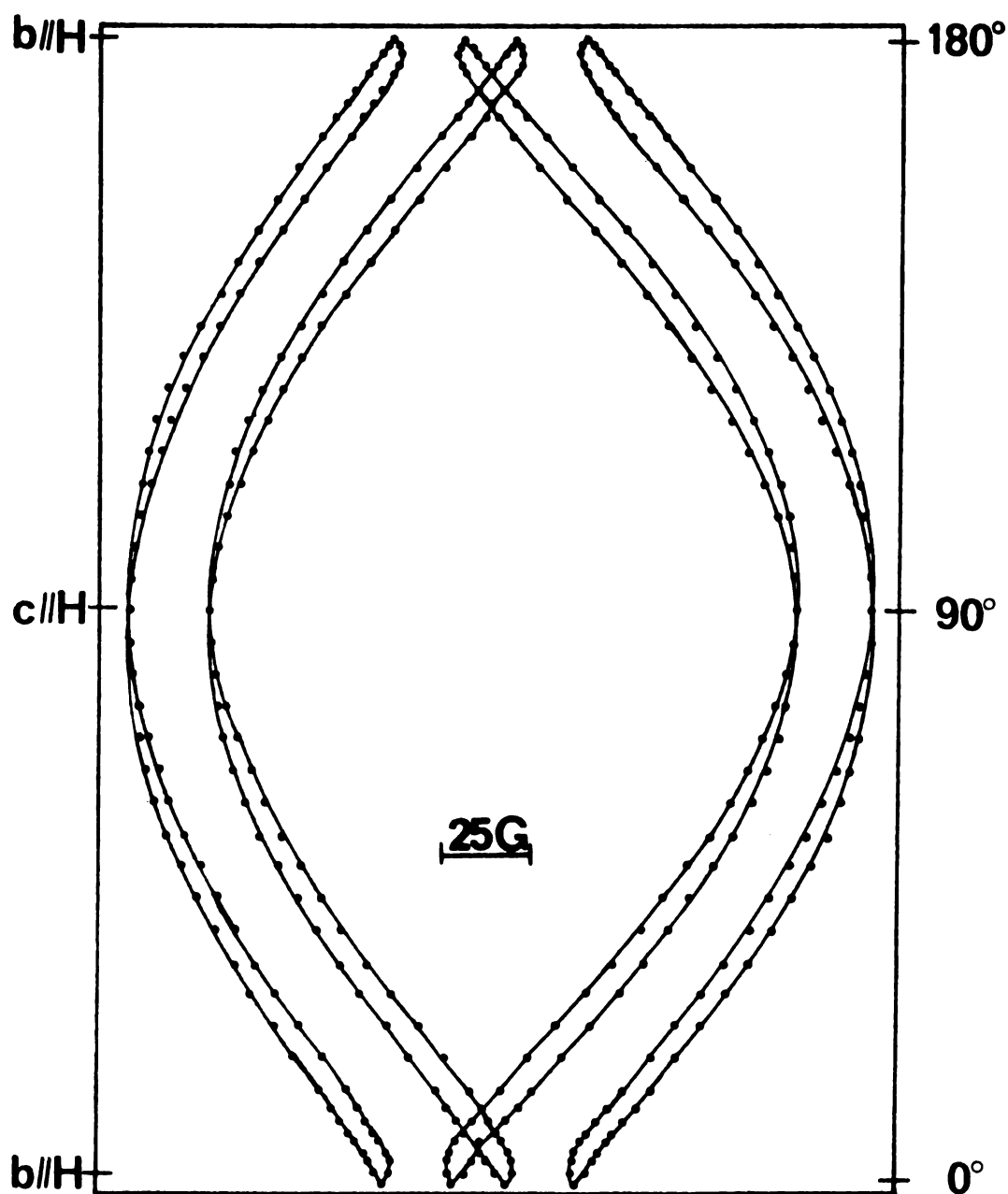


Figure 10a. Variation with magnetic field orientation of the ESR hyperfine lines in the  $bc$  plane for the  $\cdot CFHCOO^-$  radical in irradiated single crystals of ammonium monofluoroacetate at room temperature.

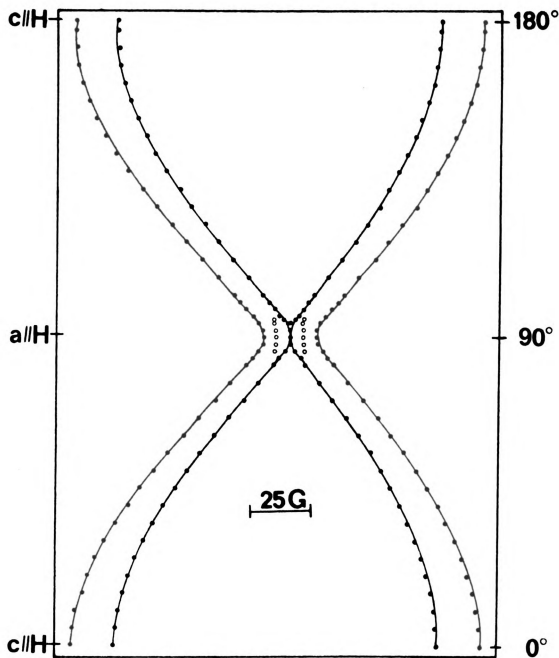


Figure 10b. Variation with magnetic field orientation of the ESR hyperfine lines in the  $ca$  plane for the  $\cdot\text{CFHCOO}^-$  radical in irradiated single crystals of ammonium monofluoroacetate at room temperature.

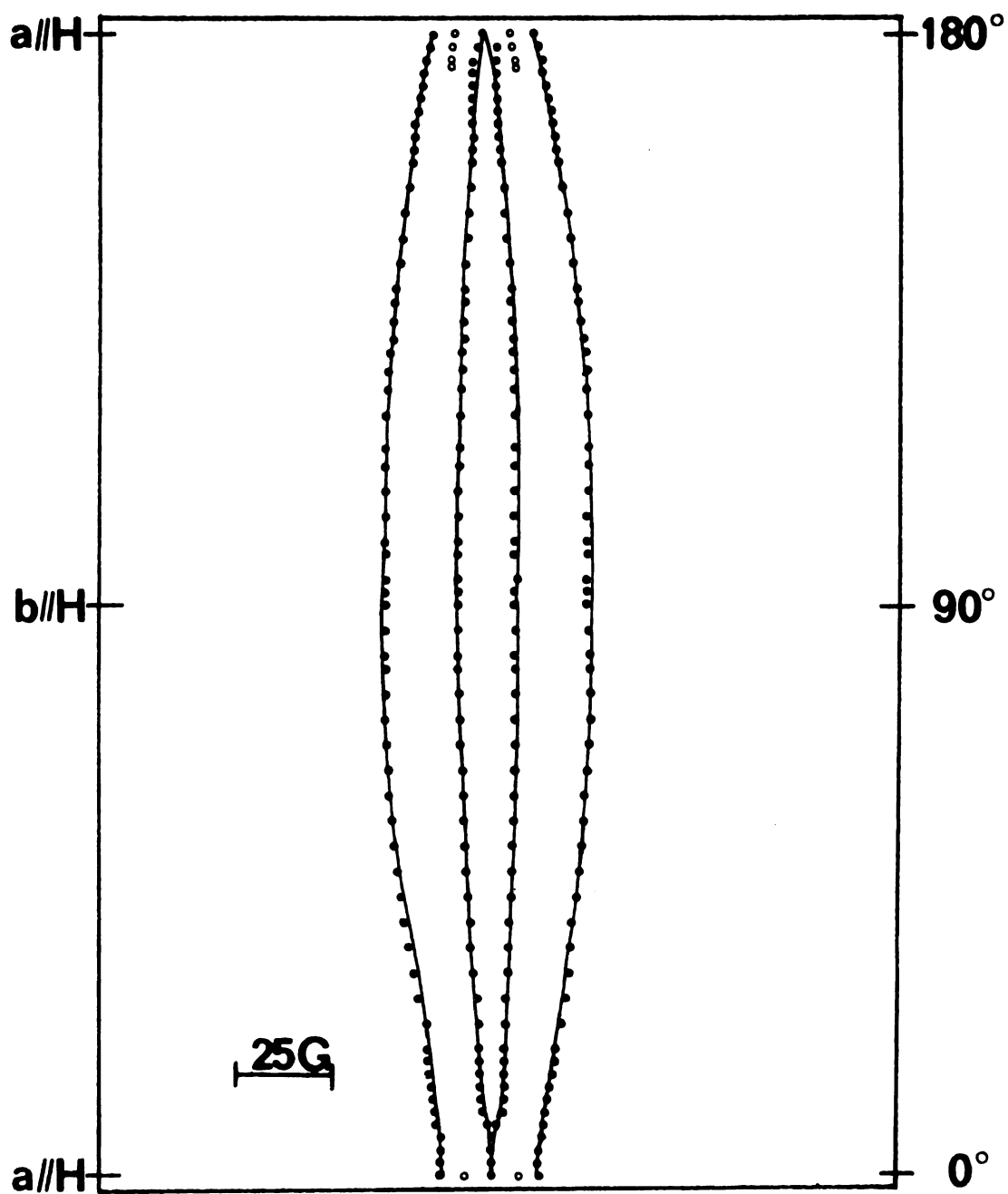


Figure 10c. Variation with magnetic field orientation of the ESR hyperfine lines in the  $ab$  plane for the  $\cdot CFHCOO^-$  radical in irradiated single crystals of ammonium monofluoroacetate at room temperature.



Table 9. Principal values and direction cosines for  $A(F)$ ,  $A(H)$ ,  $g$  and  $A(^{13}C)$  for the  $\cdot CFHCOO^-$  radical produced by room temperature irradiation of ammonium monofluoroacetate.

	Principal Elements (Gauss)	Spherical		Direction Cosines*		
		$\theta$	$\phi$	a	b	c
$A(F)$	-12.2	90	$\pm 165.7$	-0.969	$\pm 0.246$	0.000
	-17.8	90	$\pm 75.8$	0.246	$\pm 0.969$	0.000
	181.3	0	90.0	0.000	0.000	1.000
$a_{iso}$	50.4					
$A(H)$	-13.0	90.1	$\pm 3.6$	+0.998	$\pm 0.052$	-0.002
	-33.8	89.0	$\pm 93.0$	-0.052	$\pm 0.998$	+0.018
	-21.5	1.0	$\mp 80.3$	0.003	$\mp 0.018$	0.99984
$a_{iso}$	-22.8					
$g$	2.0055	90.0	$\pm 2.6$	0.999	$\pm 0.043$	0.000
	2.0051	90.0	$\pm 92.5$	-0.043	$\pm 0.999$	0.000
	2.0023	0	90.0	0.000	0.000	1.000
$g_{iso}$	2.0043					
$A(^{13}C)$	20.0	90.0	$\pm 4.4$	0.997	$\pm 0.080$	0.000
	18.6	89.1	$\pm 94.6$	-0.080	$\pm 0.997$	0.015
	85.3	0.0	$\mp 90.0$	0.000	$\mp 0.015$	1.000
$a_{iso}$	41.3					

\* With respect to the laboratory axis system specified in the text.

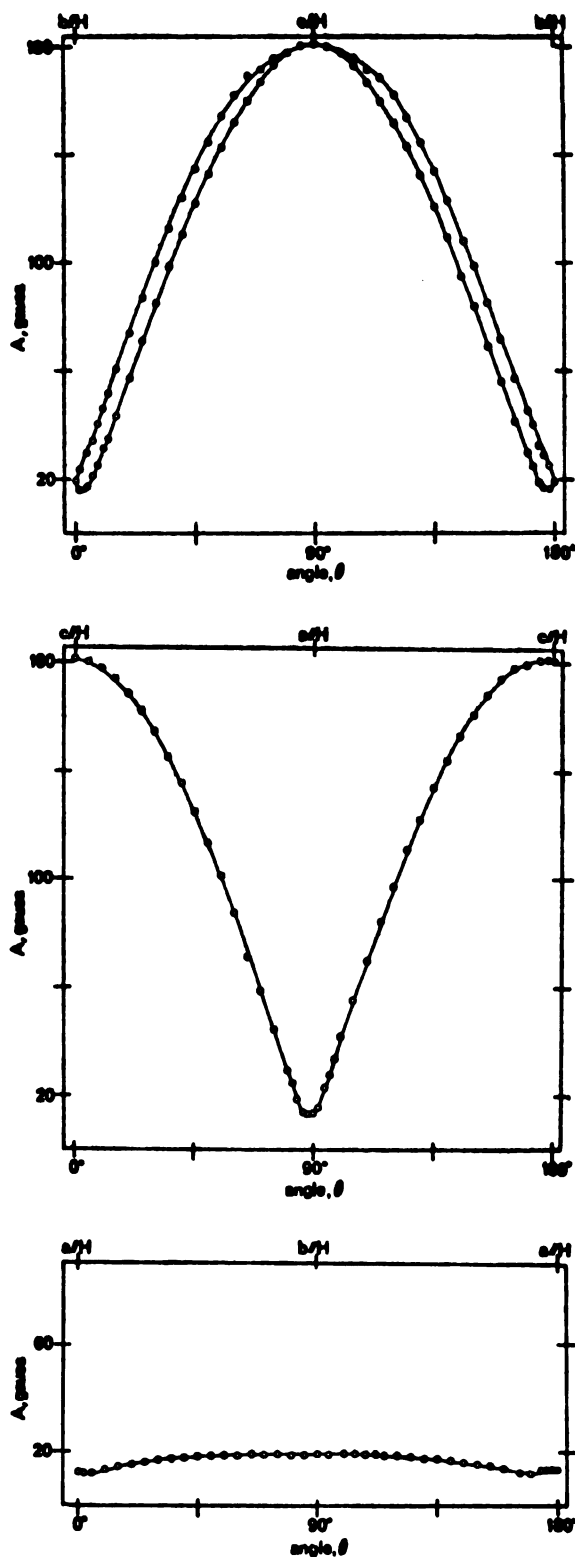


Figure 11. Plot of hyperfine splitting with respect to magnetic field direction for fluorine coupling in the  $\cdot\text{CFHCOO}^-$  radical in irradiated single crystals of ammonium monofluoroacetate at room temperature.

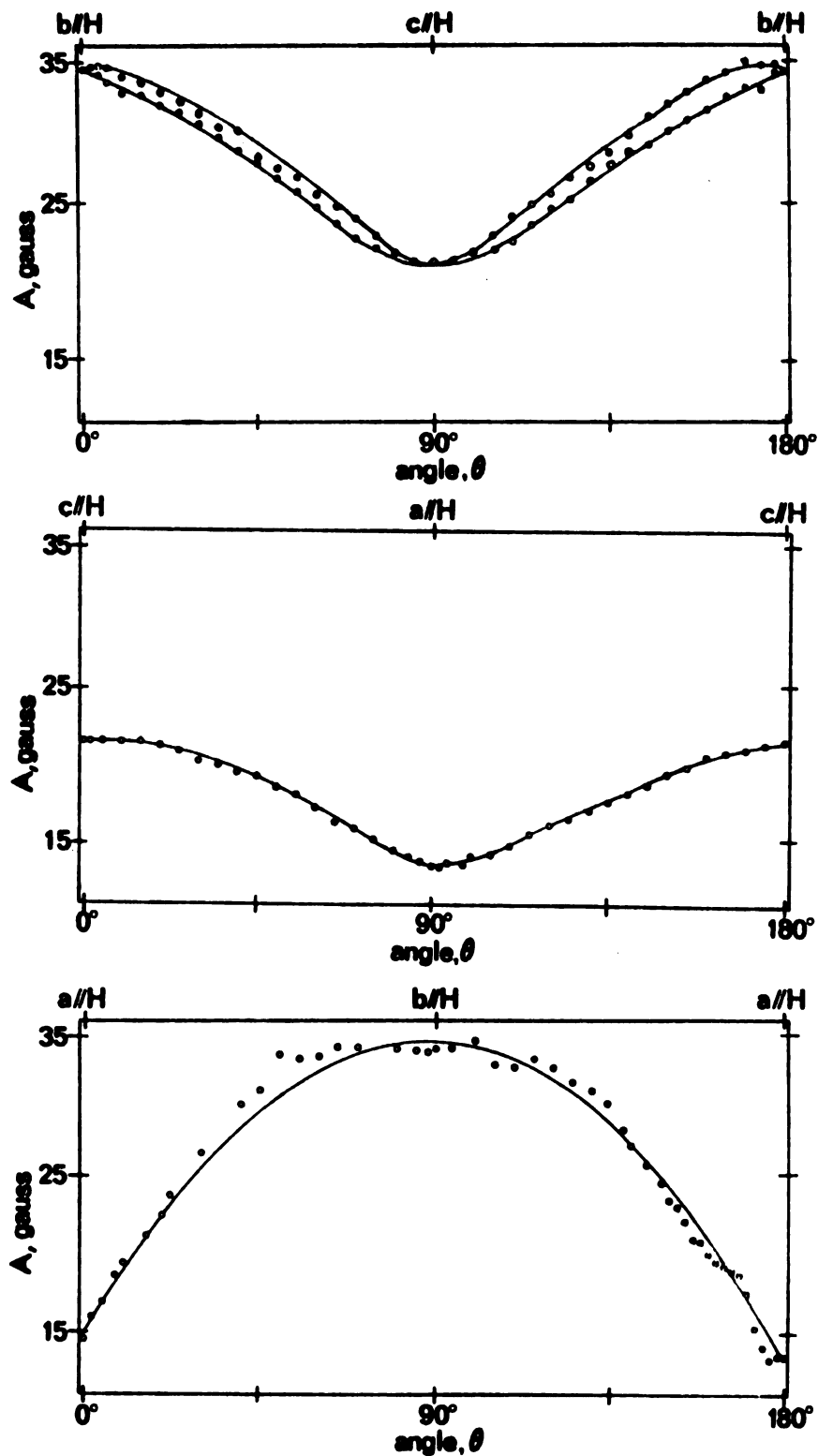


Figure 12. Plot of hyperfine splitting with respect to magnetic field direction for proton coupling in the  $\cdot\text{CFHCOO}^-$  radical in irradiated single crystals of ammonium monofluoroacetate at room temperature.

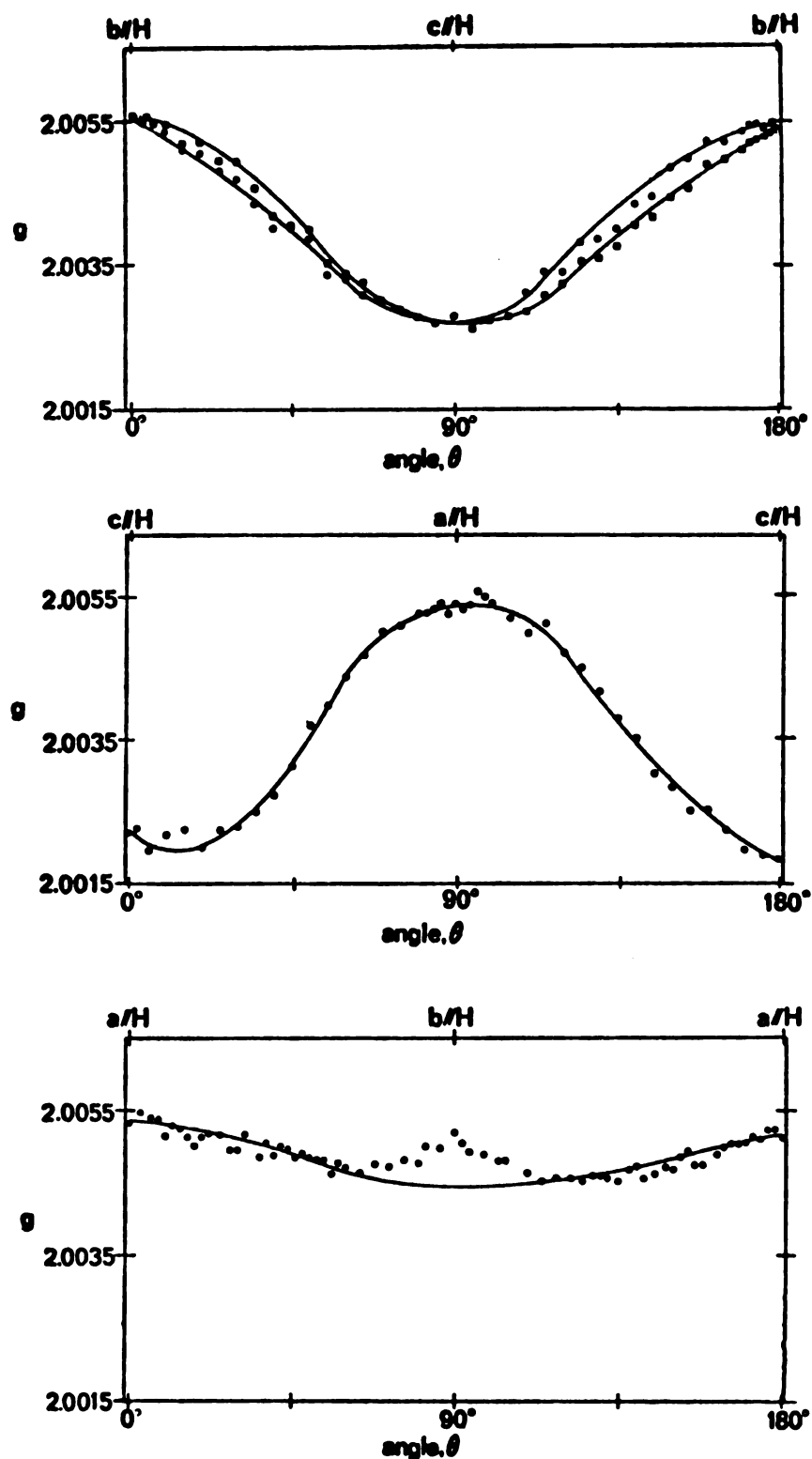


Figure 13. Plot of  $g$  values with respect to magnetic field direction for the  $\cdot\text{CFHCOO}^-$  radical in irradiated single crystals of ammonium monofluoroacetate at room temperature.

possible to observe carbon-13 coupling in the plane of the radical since the lines are not resolved as a result of the very small coupling values. However, since two rotations showed near cylindrical symmetry (Figure 14) as expected for an electron in the  $2p_{\pi}$  orbital of carbon, the use of the program COPLANR from Waller and Rogers,<sup>118</sup> as described in the experimental section, gave principal carbon-13 values which agree quite well with data available for similar radicals. The  $A(^{13}\text{C})$  principal values and direction cosines are also given in Table 9.

Relatively large "spin-flip" transitions were also observed for this radical. These transitions have been observed in other fluorine-containing radicals.<sup>94</sup> The satellites at  $\pm g_N \beta_N H$ , on either side of the normal transitions, appeared and were independent of power saturation, whereas spectra for the radical itself had to be attenuated by 20db since they tended to saturate quite readily.

Only the absolute values of the principal components of the hyperfine splitting tensors can be determined from the first-order spectra at X-band frequencies. It is generally agreed that the large fluorine coupling has a positive value. This leaves several choices for the signs of the couplings of the other two principal values. Here again, since near cylindrical symmetry would be expected, the choice becomes either both positive or both negative.

It would be extremely desirable to determine the

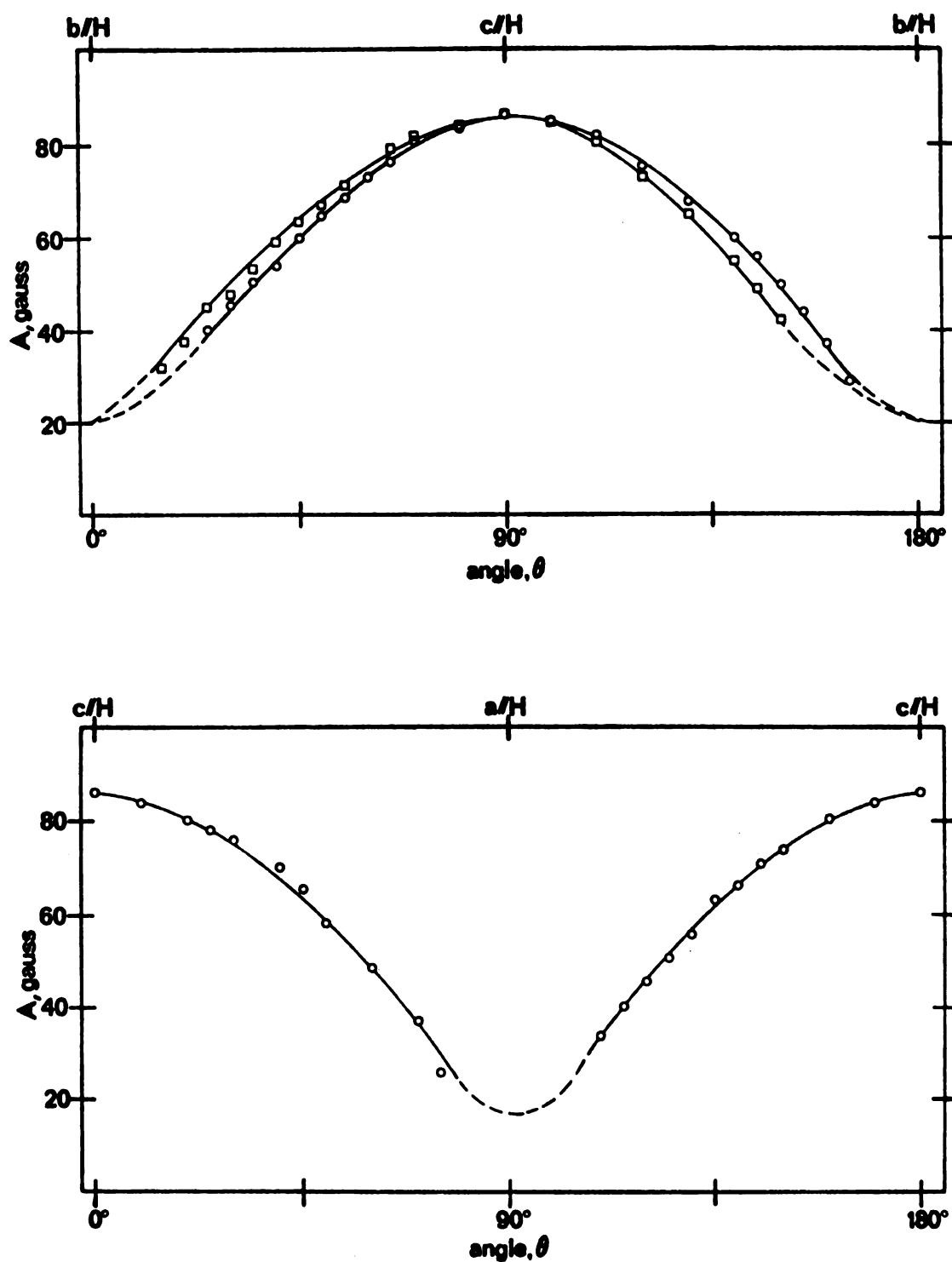


Figure 14. Plot of hyperfine splitting with respect to magnetic field direction in the  $bc$  and  $ca$  planes for carbon-13 coupling in the  $\cdot\text{CFHCOO}^-$  radical in irradiated single crystals of ammonium monofluoroacetate at room temperature.

relative signs of the principal couplings to permit analysis of the electronic structure of the radical. As can be seen from Table 2 not many signs have been determined for these radicals.

One method to resolve the problem of signs is analysis of the "forbidden" or second-order couplings. Since these become important only when the nuclear Zeeman interaction is of the same order as the nuclear hyperfine interactions they are observable only near the minima of  $A(F)$  (about 12 gauss). When spectra are taken at Q-band frequencies, the intensities of these second-order transitions become important at larger values of  $A(F)$  (up to about 35 gauss).

Spectra were collected for rotation of the crystal in the  $ca$  plane on the Q-band spectrometer. Since no field calibration was available, other than direct readings of the "Fieldial", only the relative line positions could be accurately analyzed. A computer analysis of the spectra of the  $\cdot CFHCOO^-$  radical was made using a program called MAGNSPEC (QCPE Program 150, by Marcel Kopp) modified to run on the CDC 6500 computer. With this program, the theoretical line positions, including second-order transitions were calculated for the choices (+++) and (+--) of the principal values of  $A(F)$ .

The best agreement between calculated and experimental angular variation of the line positions with the magnetic field was determined. The best choice of signs is that

with the two small principal values negative. This is in good agreement with the results of a similar analysis made for radicals in fluoroacetamide<sup>85</sup> and difluoromalonamide.<sup>92</sup>

2. Analysis of Spectra at 77° K. Irradiation of ammonium fluoroacetate at 77° K did not produce the  $\cdot\text{CFH}_2$  radical as expected. The spectrum contained a central portion consisting of a doublet of doublets for most orientations. This collapsed to a triplet with intensity ratios approximately 1:2:1 when the magnetic field was directed along the *c* direction. The outer set of lines, of considerably less intensity, was similar to that observed in the spectrum of the room temperature radical  $\cdot\text{CFHCOO}^-$ . The central set was assigned to the  $\cdot\text{CH}_2\text{COO}^-$  radical; it was similarly found in the irradiation studies in fluoroacetamide that  $\cdot\text{CH}_2\text{CONH}_2$  was produced at 77° K.<sup>158</sup> The ratio of the area under one of the outer lines of the  $\cdot\text{CFHCOO}^-$  radical to the area under one of the outer lines of the  $\cdot\text{CH}_2\text{COO}^-$  species gives the approximate ratio of the radical concentrations as 0.25. The areas were estimated by multiplying the half-width at half-height by the height of the peak. Upon controlled warming, the lines from the  $\cdot\text{CH}_2\text{COO}^-$  radical decayed while those from  $\cdot\text{CFHCOO}^-$  increased. There seems to be no complete correlation of the decay of the  $\cdot\text{CH}_2\text{COO}^-$  species with concomitant increase in the  $\cdot\text{CFHCOO}^-$  species. Hence, the decomposition of the  $\cdot\text{CH}_2\text{COO}^-$  radical



can either lead to a diamagnetic species or to a  $\cdot\text{CFHC}\text{O}\text{O}^-$  radical by abstracting a fluorine atom of a neighboring molecule, with no simple rate being observable. Finally, at room temperature the only radical present in substantial amounts is the fluoro species. Trace amounts of the other species always remain and even when samples were irradiated at room temperature slight traces of the  $\cdot\text{CH}_2\text{C}\text{O}\text{O}^-$  species were noted.

As with monofluoroacetamide<sup>158</sup> where only the protonated radical was present at low temperatures, a stereoselective irradiation process is taking place. One would expect to find twice as much of the fluoro radical if the loss of hydrogen and fluorine atoms were equally probable. However, the spectra observed established that there must be a large preference for C-F bond breaking over C-H bond breaking at lower temperatures.

3. Variable Temperature Studies. Another feature of the irradiation of ammonium monofluoroacetate was an important change in the ESR spectra on warming from 77° K to 300° K. Various changes have been noted in other fluorine-containing radicals,<sup>94</sup> but were not, apparently, observable for the radical in irradiated monofluoroacetamide.<sup>83</sup> The room-temperature radical  $\cdot\text{CFHC}\text{O}\text{O}^-$  was therefore selectively cooled and warmed to study this change in coupling with temperature.

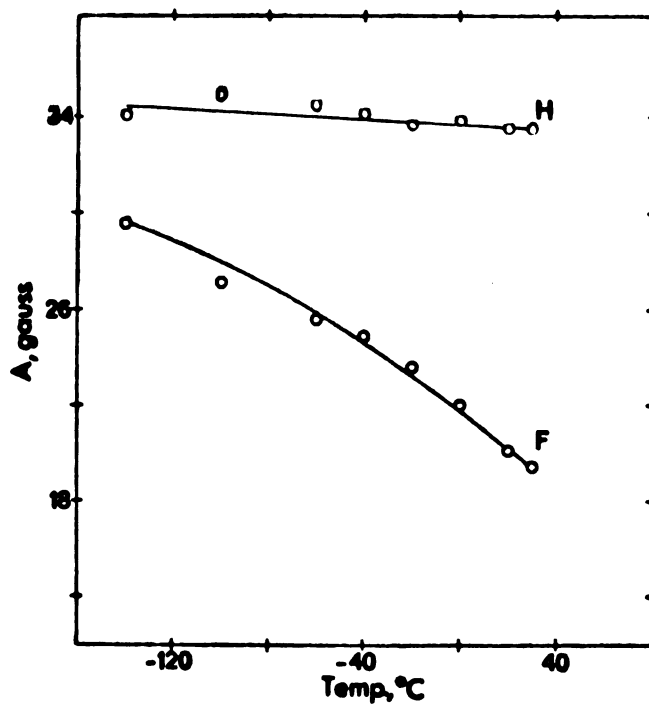
Two recent publications indicate that there is a restricted rotation or torsional oscillation about the C-C bond in  $\cdot\text{CH}_2\text{COO}^-$  radicals found in zinc acetate<sup>58</sup> single crystals and in  $\cdot\text{CF}_2\text{COO}^-$  radicals found in trifluoroacetamide<sup>83</sup> single crystals. With these studies in mind, the ESR spectra of the monofluoro radical were observed on selective warming to 100°C (where decomposition of the crystal occurred). Crystals were also cooled to -140° C which is the most convenient stable low temperature available with the Varian variable-temperature unit; further cooling did not significantly change the spectra. These changes are shown for selected orientations of the crystal in the magnetic field in Figure 15a-i.

Several features should be noted in the spectra (Figure 16). Changes in coupling did not produce any change from the four lines of equal intensity to a triplet with 1:2:1 intensity ratios as was observed in the two previously cited cases.<sup>58,83</sup> The only significant change is in the fluorine coupling, while the proton splitting changes only about one gauss for any of the orientations studied. Further, no changes were observed for either the  $g$  values or the maximum carbon-13 coupling such as had been noted for the  $\cdot\text{CF}_2\text{CONH}_2$  radical studied by Bogan and Kispert.<sup>83</sup>

In order to determine whether the radical was undergoing any motional changes with change in temperature, the room-temperature radical was studied also at -140° C.



a)



b)

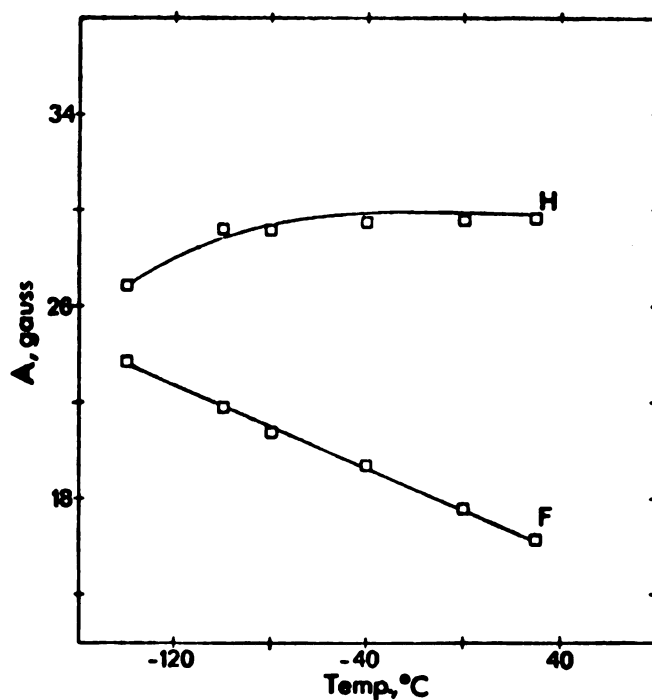
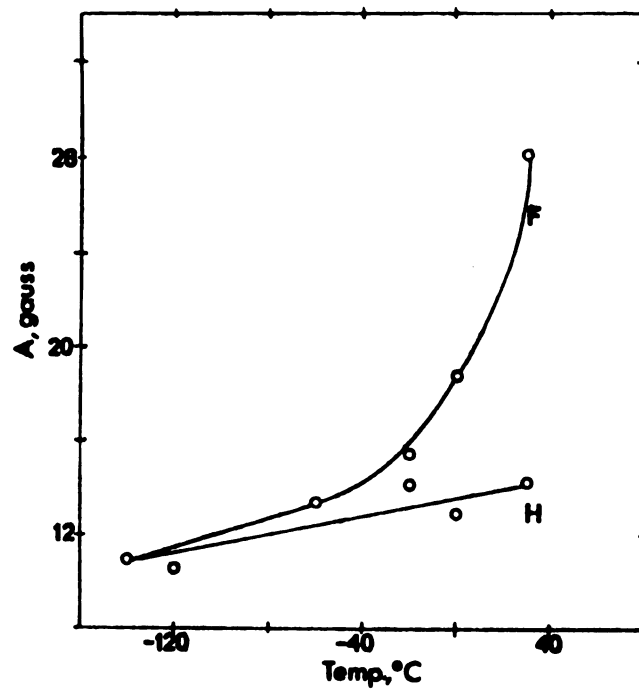


Figure 15(a-i). Variation with temperature of the fluorine (F) and proton (H) hyperfine splittings for the  $\cdot\text{CFHCOO}^-$  radical. a) The magnetic field is parallel to the  $b$  direction. b) The magnetic field is directed  $45^{\circ}$  from  $b$  in the  $bc$  plane.

c)



d)

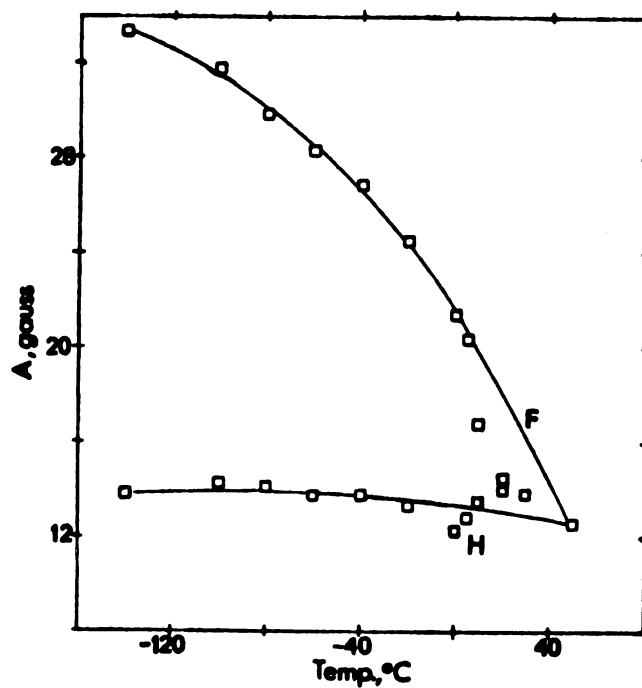
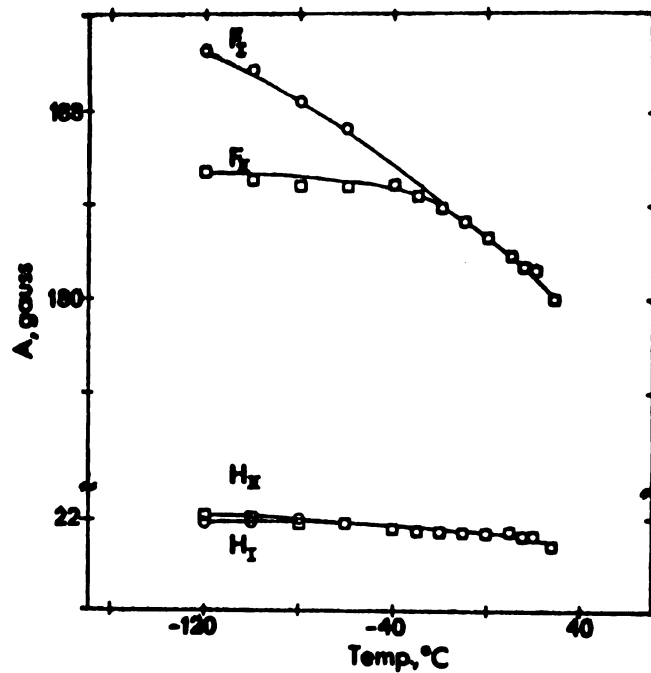


Figure 15 continued - c) The magnetic field is directed  $11^\circ$  from  $a$  in the  $ca$  plane. d) The magnetic field is parallel to the  $a$  direction.

e)



f)

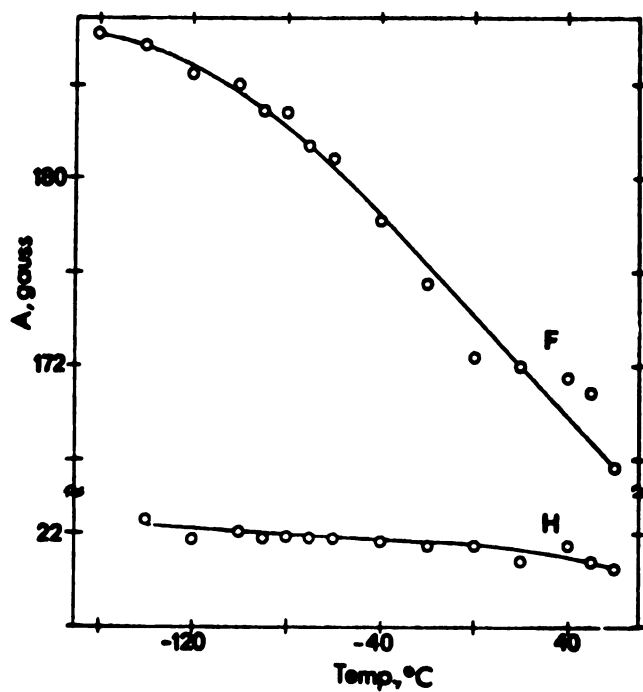
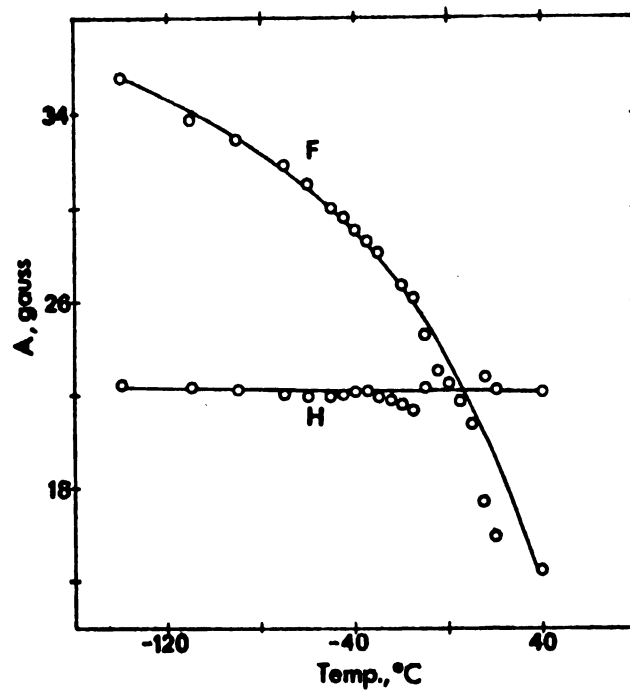


Figure 15 continued e) The magnetic field is parallel to the  $c$  direction. Subscripts I and II represent the two different radicals. f) The magnetic field is directed 25° from  $c$  in the  $ca$  plane.

g)



h)

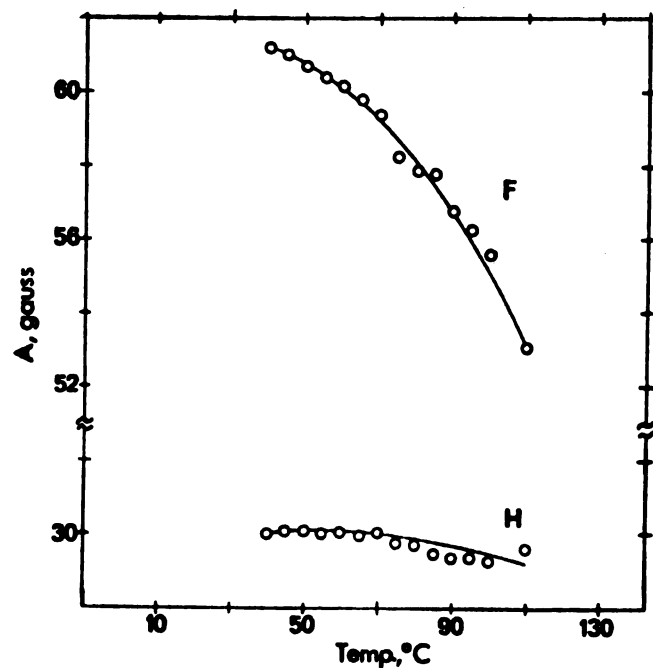


Figure 15 continued g) The magnetic field is directed  $25^{\circ}$  from  $a$  in the  $ab$  plane. h) The magnetic field is directed  $20^{\circ}$  from  $b$  in the  $bc$  plane. These fluorine and proton splittings are shown at higher temperatures.





i)

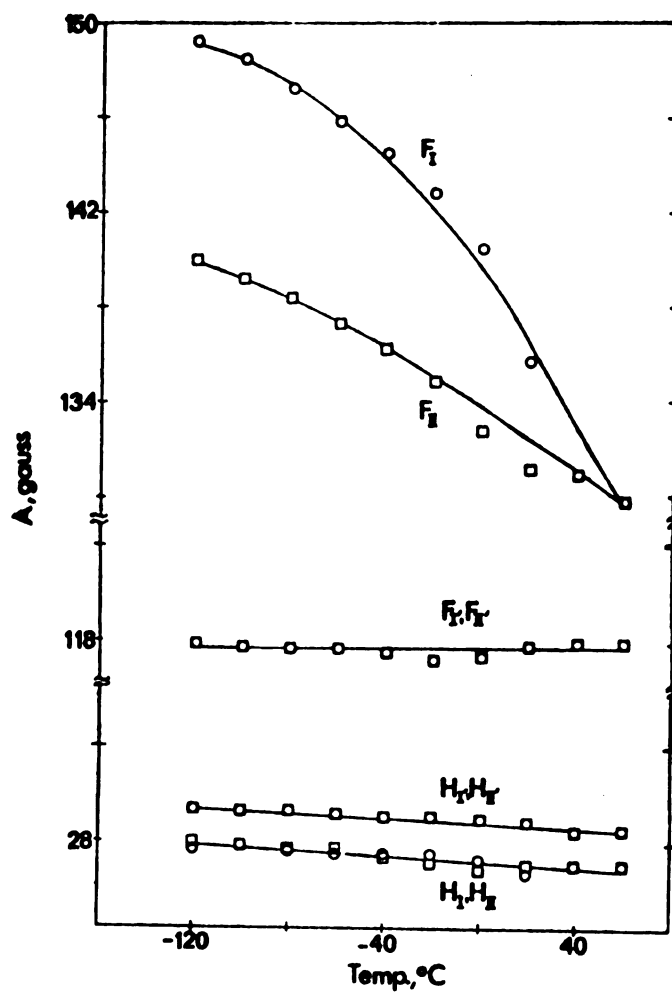


Figure 15 continued i) The magnetic field is directed  $45^\circ$  from  $b$  in the  $bc$  plane. Subscripts I and II represent the two different radicals; subscripts I' and II' represent the two magnetically inequivalent sites of Radicals I and II respectively.

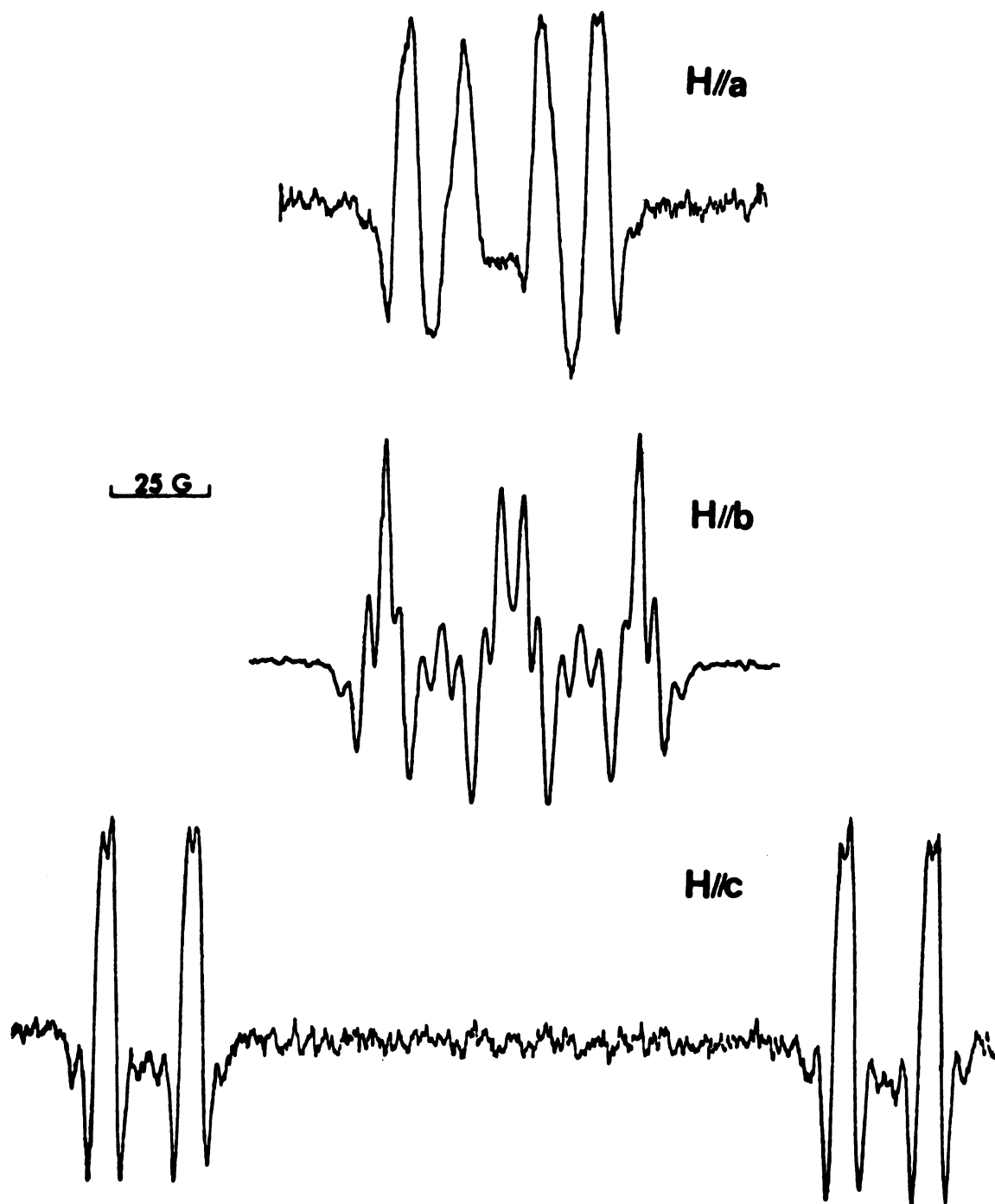


Figure 16. Second-derivative ESR spectra for  $\cdot\text{CFHCOO}^-$  radical produced in single crystals of ammonium monofluoroacetate irradiated at room temperature and observed at  $-140^\circ\text{C}$ .

Rotations were made about the three orthogonal axes previously selected. Alignment of the crystal was done at room temperature; to confirm the rotation angles the crystals were periodically warmed to room temperature and spectra taken for comparison with those previously obtained. Room temperature spectra taken with the magnetic field in the  $bc$  plane show only a single radical in two magnetically inequivalent sites, while at  $-140^{\circ}$  C two radicals each with two magnetically distinct sites appear to be present. Also, the magnitudes of the fluorine couplings, for all orientations, were significantly larger than those at room temperature.

Isofrequency plots (Figure 17a,b,c) show that for rotation in the  $ca$  plane, both the maximum and minimum couplings have increased and are shifted approximately  $10^{\circ}$  from the corresponding magnetic field directions found for the room temperature radical. A comparison of the behavior of the minimum fluorine splitting on warming is shown in Figure 15c and d. When the magnetic field direction is  $11^{\circ}$  from  $a$  in the  $ca$  plane (Figure 15c), it is seen that the fluorine splitting increases with increasing temperature. On the other hand, it is seen that the fluorine splitting decreases with increasing temperature so that at room temperature, the minimum fluorine splitting now occurs for the magnetic field direction parallel to the  $a$  axis (Figure 15d).

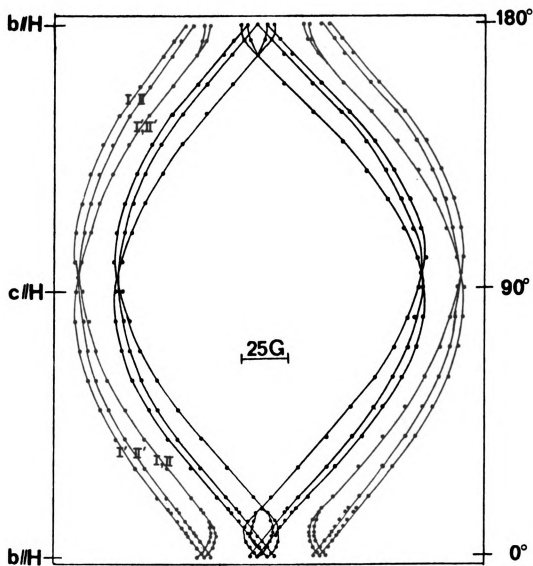


Figure 17a. Variation with magnetic field orientation of the ESR hyperfine lines in the  $bc$  plane for the  $\cdot\text{CFHCOO}^-$  radical in irradiated ammonium monofluoroacetate at  $-140^\circ\text{ C}$ . Radicals  $I$  and  $II$  have two magnetically inequivalent sites and lines for the second sites are labeled  $I'$ ,  $II'$ .

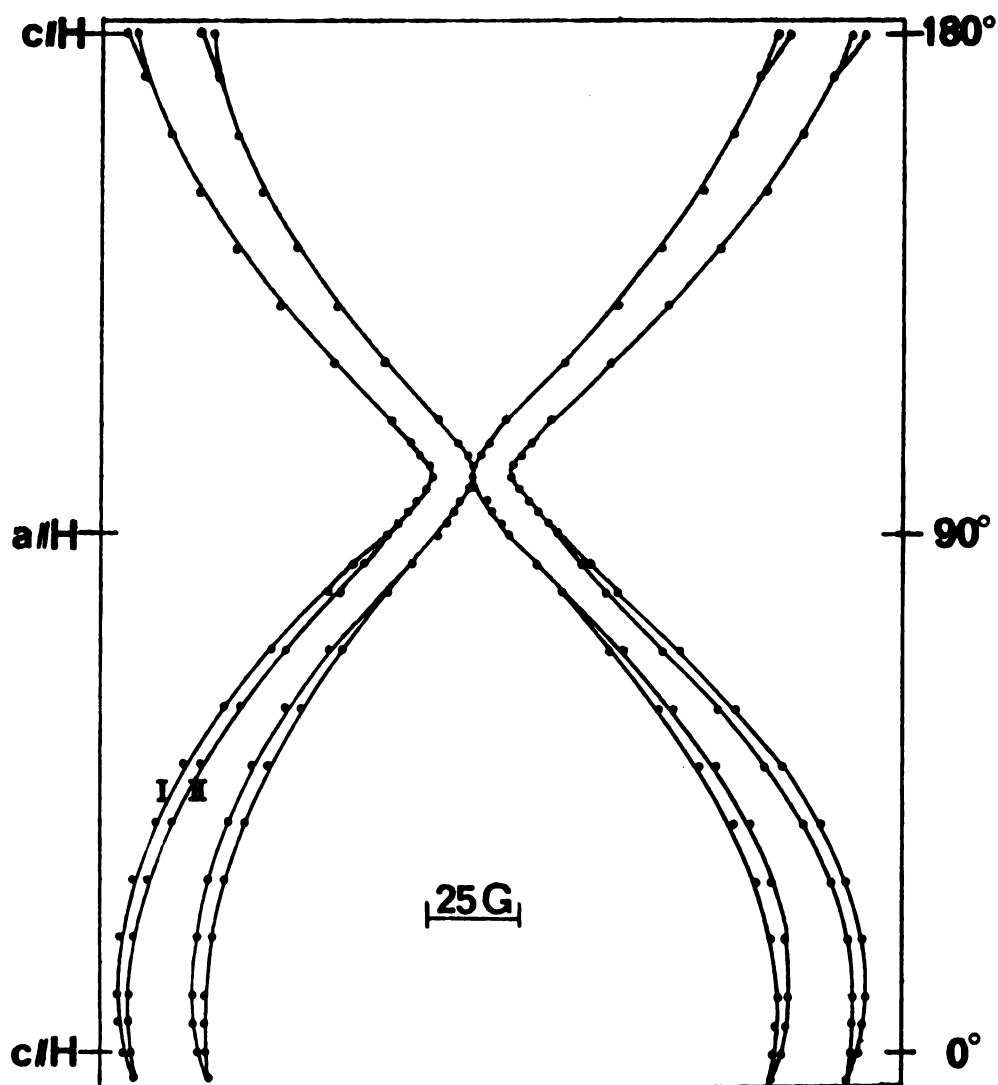


Figure 17b. Variation with magnetic field orientation of the ESR hyperfine lines in the  $ca$  plane for the  $\cdot\text{CFHCOO}^-$  radical in irradiated ammonium monofluoroacetate at  $-140^\circ\text{C}$ . Radicals I and II have two magnetically inequivalent sites.



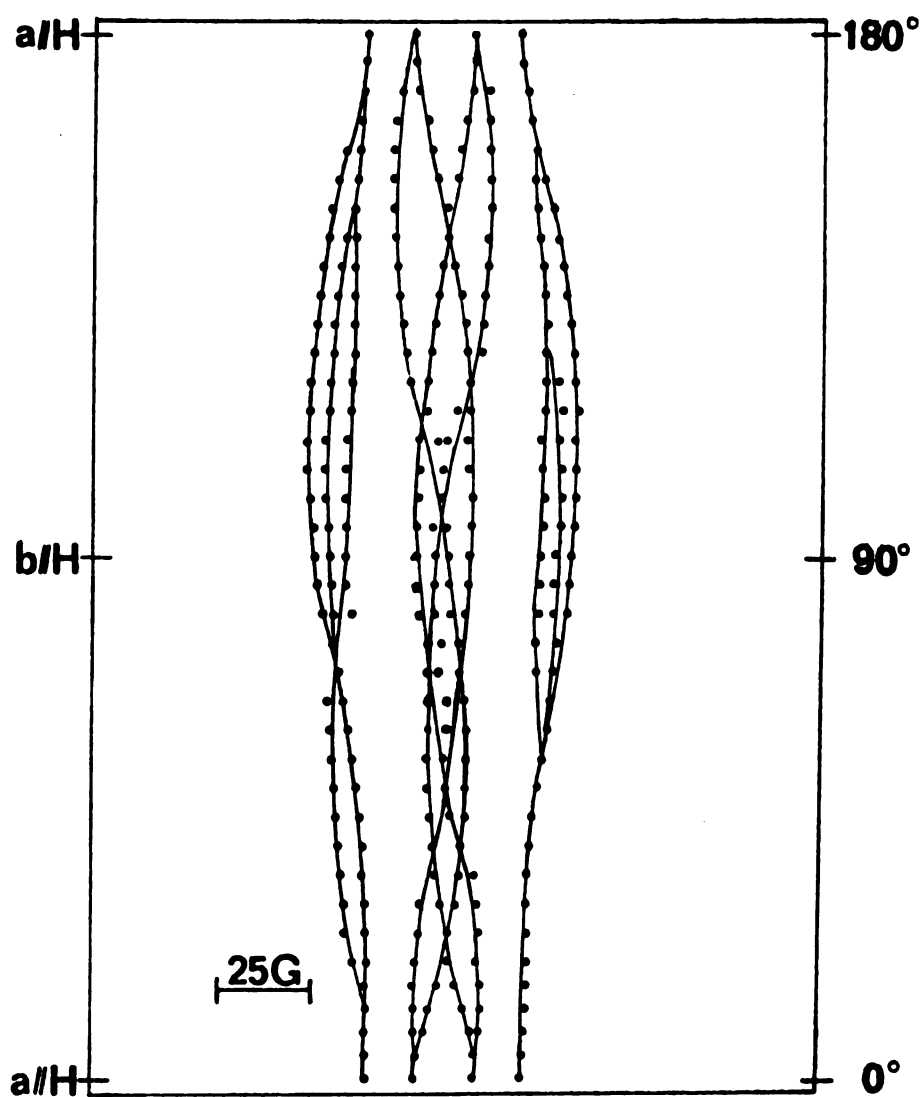


Figure 17c. Variation with magnetic field orientation of the ESR hyperfine lines in the  $ab$  plane for the  $\cdot CFHCOO^-$  radical in irradiated ammonium monofluoroacetate at  $-140^\circ C$ .

Further, observation of the isofrequency plot for the *ca* plane (Figure 17b) indicates two sets of spectra which appear to arise from two radicals unrelated by any crystal symmetry operation. This would indicate that there are two radicals present (Radical I and Radical II) with different crystal environments. The isofrequency plot for the *bc* plane (Figure 17a) shows this same behavior but each radical is now in two magnetically inequivalent sites related by a mirror plane of symmetry; this indicates a site splitting for each radical based on the crystal symmetry. The diagonalized tensors at  $-140^{\circ}$  C gave the principal values and direction cosines listed in Table 10. Two sets of principal values resulted from a diagonalization of the data based on measurements from each of the two sets of lines. A computer calculation of the angular variation of the coupling with respect to the magnetic field, as discussed previously, showed that each of the two sets of principal values and direction cosines were related to another set only by a change in the signs of the direction cosines in column b of Table 10. A plot of the fluorine hyperfine coupling with respect to orientation in the magnetic field for the three mutually orthogonal planes (Figure 18) clearly shows the presence of two radicals (I and II) and the corresponding set of magnetically inequivalent sites (I' and II'). A plot of the proton hyperfine coupling with respect to orientation in the magnetic field is shown





Table 10. Principal values and direction cosines for A(F) and A(H) for the two  $\cdot\text{CFHCOO}^-$  radicals produced at room temperature and observed at  $-140^\circ\text{C}$  by irradiation of ammonium monofluoroacetate.

Principal Elements (Gauss)		Spherical $\theta$ $\phi$		Direction Cosines <sup>*</sup> a b c		
Radical I						
A(F)	-10.5	97.0 ± 1.9		0.992	±0.020	-0.122
	-28.0	98.8 ± 92.2		-0.038	±0.987	-0.153
	193.9	11.2 ± 52.9		0.117	±0.157	0.981
$a_{\text{iso}}$	51.8					
A(H)	-11.7	106.3 ∓ 11.0		0.942	∓0.183	-0.281
	-34.9	88.6 ± 78.6		0.198	±0.980	0.024
	-21.9	16.5 ∓ 17.0		0.271	∓0.078	0.959
$a_{\text{iso}}$	-22.8					
Radical II						
A(F)	-13.2	99.1 ± 3.9		0.985	±0.060	-0.159
	-21.2	98.7 ± 94.9		-0.084	±0.985	-0.152
	188.1	12.6 ± 47.2		0.148	±0.163	0.976
$a_{\text{iso}}$	51.2					
A(H)	-12.4	100.4 ∓ 8.0		0.974	∓0.136	-0.180
	-35.2	81.0 ± 80.4		0.165	±0.974	0.157
	-21.4	13.8 ∓ 49.9		0.154	∓0.182	0.971
$a_{\text{iso}}$	-23.0					

\* With respect to the laboratory axis system specified in the text.

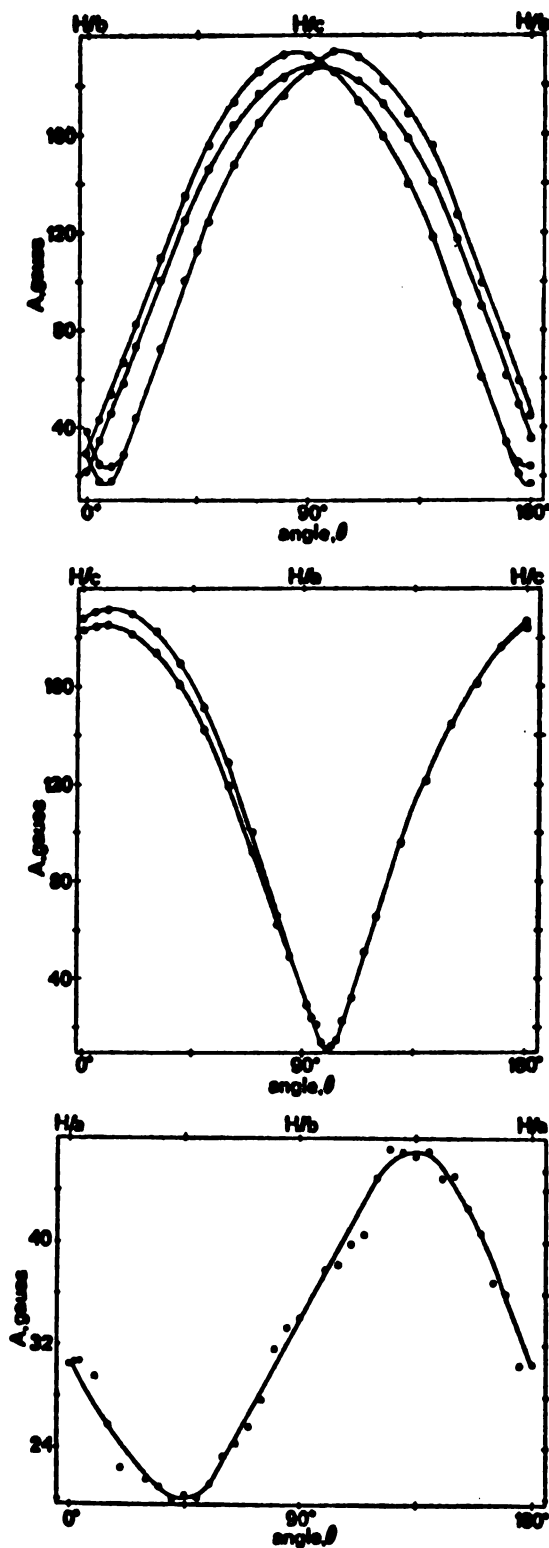


Figure 18. Plot of hyperfine splitting with respect to magnetic field direction for fluorine coupling in the  $\cdot\text{CFHCOO}^-$  radicals in irradiated single crystals of ammonium monofluoroacetate at  $-140^\circ\text{C}$ .



in Figure 19.

Because the range of couplings is small in the *ab* plane, the "in-plane" splittings are not as accurately determined as they were for the room temperature radical (Figure 17c). Nevertheless, the "in-plane" splittings observed for rotations in the *ca* and *bc* planes (Figure 18) agree well, for example, with the principal *A* values obtained by diagonalization of the *A*(*F*) tensor utilizing all the data. That is, for the rotation in the *ca* plane, a maximum value of 191.6 G and a minimum value of 10.5 G are measured for Radical I. These are close to the values predicted from the *A*(*F*) tensor (Table 10) for rotation in a plane containing the maximum and minimum principal directions. The relative signs of the principal *A*(*F*) values could not be determined from the spectra at -140°C but are presumably the same as those found at room temperature.

Several observations can be made concerning the two sets of principal values at -140°C and the set at room temperature (Table 9). If the signs of the two smaller couplings at -140° C are assumed to be negative, as in the room temperature case, then only very small changes in the isotropic coupling are observed. Consequently, no important structural changes in the radical appear to occur. However, the observed decrease in anisotropic coupling with increase in temperature suggests that the radical is undergoing some motion (oscillation) such that the principal *A*(*F*) values



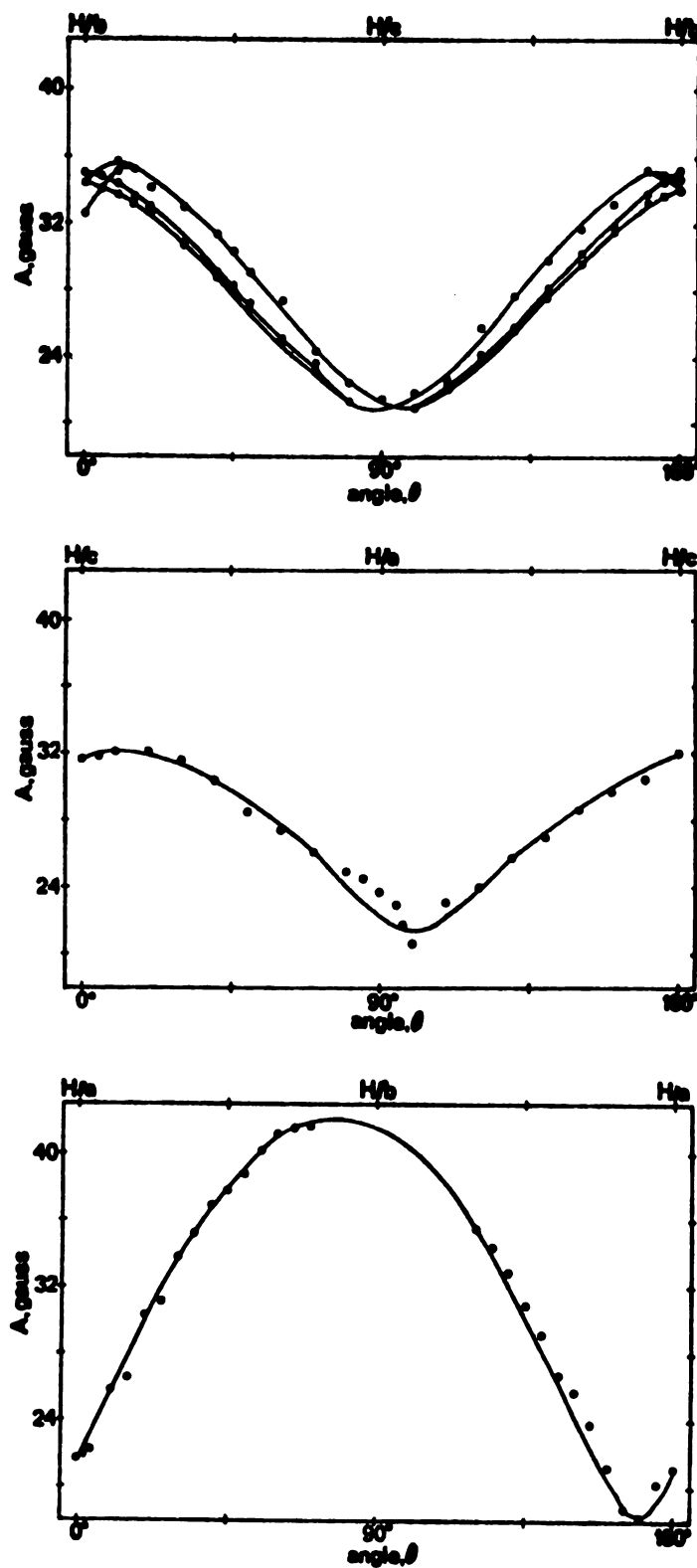


Figure 19. Plot of hyperfine splitting with respect to magnetic field direction for proton coupling in the  $\cdot\text{CFHCOO}^-$  radicals in irradiated single crystals of ammonium monofluoroacetate at  $-140^\circ\text{C}$ .





at  $-140^{\circ}$  C are partially averaged at room temperature. The motion cannot be a rotation since that would result in a cylindrically symmetric hyperfine tensor. An oscillation about the C-C bond direction would decrease  $A_{zz}(F)$  and  $A_{yy}(F)$  would move toward less negative values as observed for both radicals. The  $A_{xx}(F)$  value should also become less negative, which is found in the case of Radical II, but in Radical I it becomes more negative by 1.7 G. Also  $A_{xx}(H)$  and  $A_{yy}(H)$  should move toward one another with increase in temperature and  $A_{zz}(H)$  remain more or less unchanged; this is the observed behavior for both radicals. In view of the fact that the largest probable errors are those for the "in-plane" fluorine splitting values, the agreement with the behavior expected for an oscillation about the C-C bond is reasonably good.

The changes in ESR spectra resulting from motions of a radical may be computed using a modified Bloch theory.<sup>170</sup> Hayes and coworkers<sup>58</sup> showed that the Bloch theory was not adequate to account for the spectral changes with temperature for  $\cdot\text{CH}_2\text{COO}^-$  in a single crystal of zinc acetate, since it does not take into account effects of spin exchange. That is, in a single crystal, hindered internal motion may lead to an exchange in spins between sites having hyperfine fields which must be averaged both in magnitude and in direction. Consequently, they found it necessary to resort to the more complete density matrix



theory.

The density matrix formalism has been well-developed for many years.<sup>8,171</sup> This method provides a nearly exact treatment for calculating spectral changes with motion. Recently, computational methods have been developed<sup>172</sup> which make the calculations more feasible. This approach to magnetic resonance problems has been expanded by Binsch<sup>173</sup> and subsequently was modified by Hayes and coworkers<sup>58</sup> to treat the problem of motional averaging in  $\cdot\text{CH}_2\text{COO}^-$  in zinc acetate. Bogan and Kispert<sup>83</sup> followed these same methods but chose to define their tensors along the effective magnetic field rather than along the crystal directions. The results, however, were analogous.

It was of interest to test this method on the  $\cdot\text{CFHC00}^-$  radical. The density matrix program of Hayes *et al.*<sup>58</sup> was modified to run on the CDC 6500 computer. Calculations for  $\cdot\text{CFHC00}^-$  showed that the resultant computed spectra did not fit the experimental spectra satisfactorily. The motion does not seem to be well described by the torsional oscillation model. This is not too surprising since the density matrix calculation predicts an averaging of the inner lines of the spectrum along with a change in the coupling of the outer lines. Experimentally, no averaging of the inner lines is observed.

It appears that more complex changes are occurring on cooling than it is possible at present to include in



the density matrix formalism. In particular, the single radical observed at room temperature is replaced between 25°C and -30° C (Figures 15e and 15i) by two radicals with different orientations and different  $A(F)$  and  $A(H)$  tensors. This change could result from a change in crystal structure of the matrix to a lower symmetry space group. On warming the principal components of  $A(F)$  and  $A(H)$  for each radical change in the manner predicted for a small oscillation about the C-C bond. However,  $A(F)$  and  $A(H)$  for Radicals I and II do not average to the room temperature tensors. The density matrix method as applied here could not include all these factors and so could not be expected to reproduce the observed spectra. Further progress would require crystallographic data over the temperature range studied.

## B. Ammonium Difluoroacetate

1. Room Temperature Radicals. Irradiation of ammonium difluoroacetate was accomplished at room temperature. Selected orientations indicated that the spectrum was considerably more complicated than that of the monofluoroacetate. No crystal structure has been reported, so alignment was made along the extinction axes using the polarizing microscope. For orientation of the magnetic field along one axis, a much simplified spectrum was obtained. There were two sets of lines with slightly different  $g$  values indicating that there were two distinct



radical species. One set, a doublet of doublets, was similar to the spectrum of the monofluoro radical and was assigned to the  $\cdot\text{CFHCOO}^-$  radical.

The triplet pattern with intensity ratios approximately 1:2:1 showed a maximum separation of about 360 gauss indicating coupling from two equivalent fluorines; this was assigned to the  $\cdot\text{CF}_2\text{COO}^-$  radical. An isofrequency plot for rotation of the magnetic field in the  $\alpha\alpha$  plane (Figure 20) shows the complexity of the spectra resulting from the presence of magnetically distinguishable sites. The spectra show that there are as many as four sites for the difluoro radical and two sites for the monofluoro radical. Hence, either the crystal structure is different from that of the monofluoroacetate and/or the radicals are oriented differently in this crystal. As the coupling of the fluorine approaches a minimum, it becomes nearly impossible to distinguish between the sites or between the radicals (Figure 21). Spectra obtained on rotating the magnetic field in the planes of the radicals were not interpretable. Nevertheless, a maximum fluorine coupling could be assigned, along with carbon-13 hyperfine splitting values, for the specific orientation which is perpendicular to the plane of both radicals and parallel to the  $p_\pi$  orbital containing the unpaired spin (Figure 22a). Again, the directions of the maximum components of the carbon-13 and fluorine-19 hyperfine splitting tensors coincide within the experimental





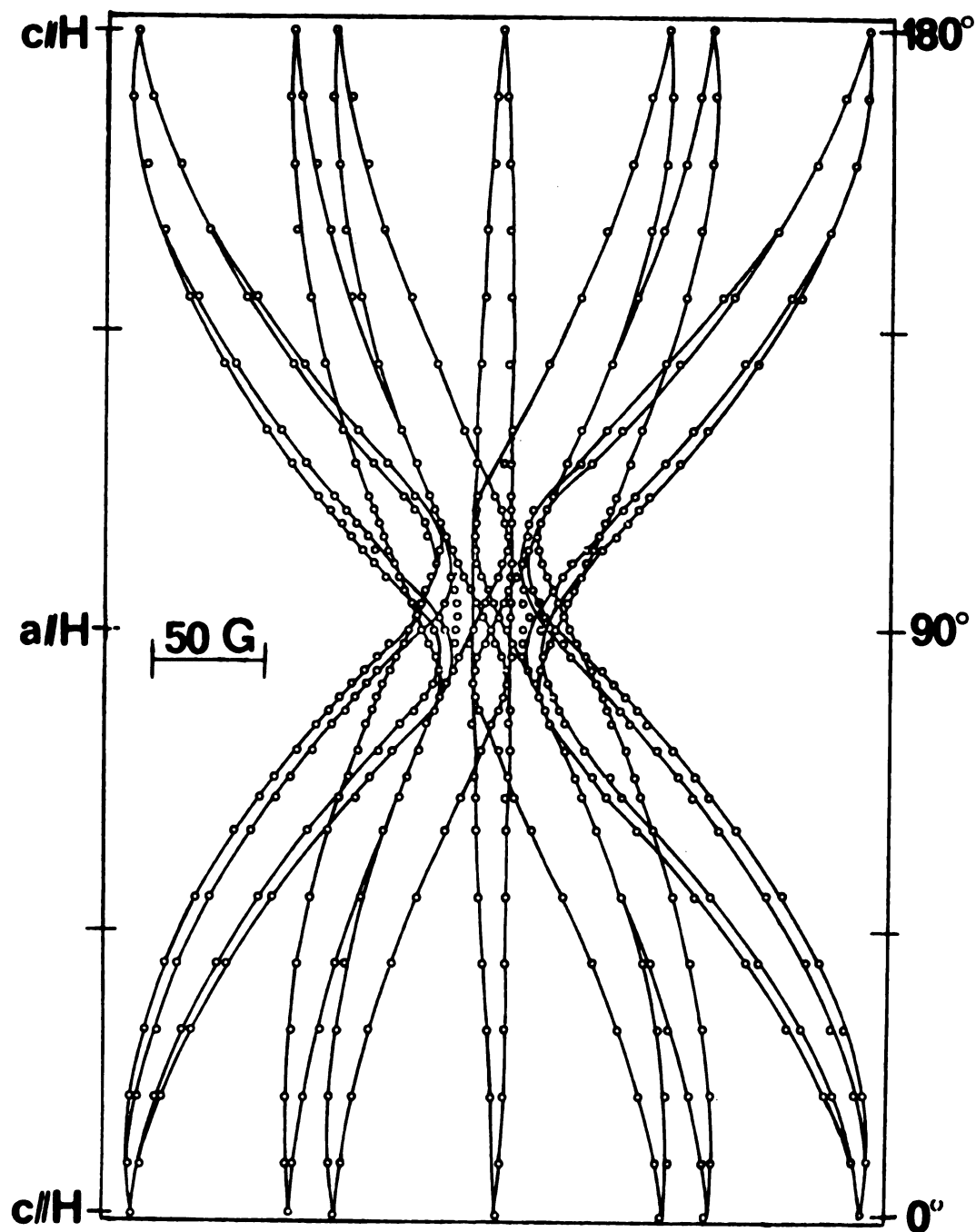


Figure 20. Variation with magnetic field orientation in the  $ac$  plane of the ESR hyperfine lines for the  $\cdot\text{CFHCOO}^-$  and  $\cdot\text{CF}_2\text{COO}^-$  radicals produced in irradiated single crystals of ammonium difluoroacetate at room temperature.

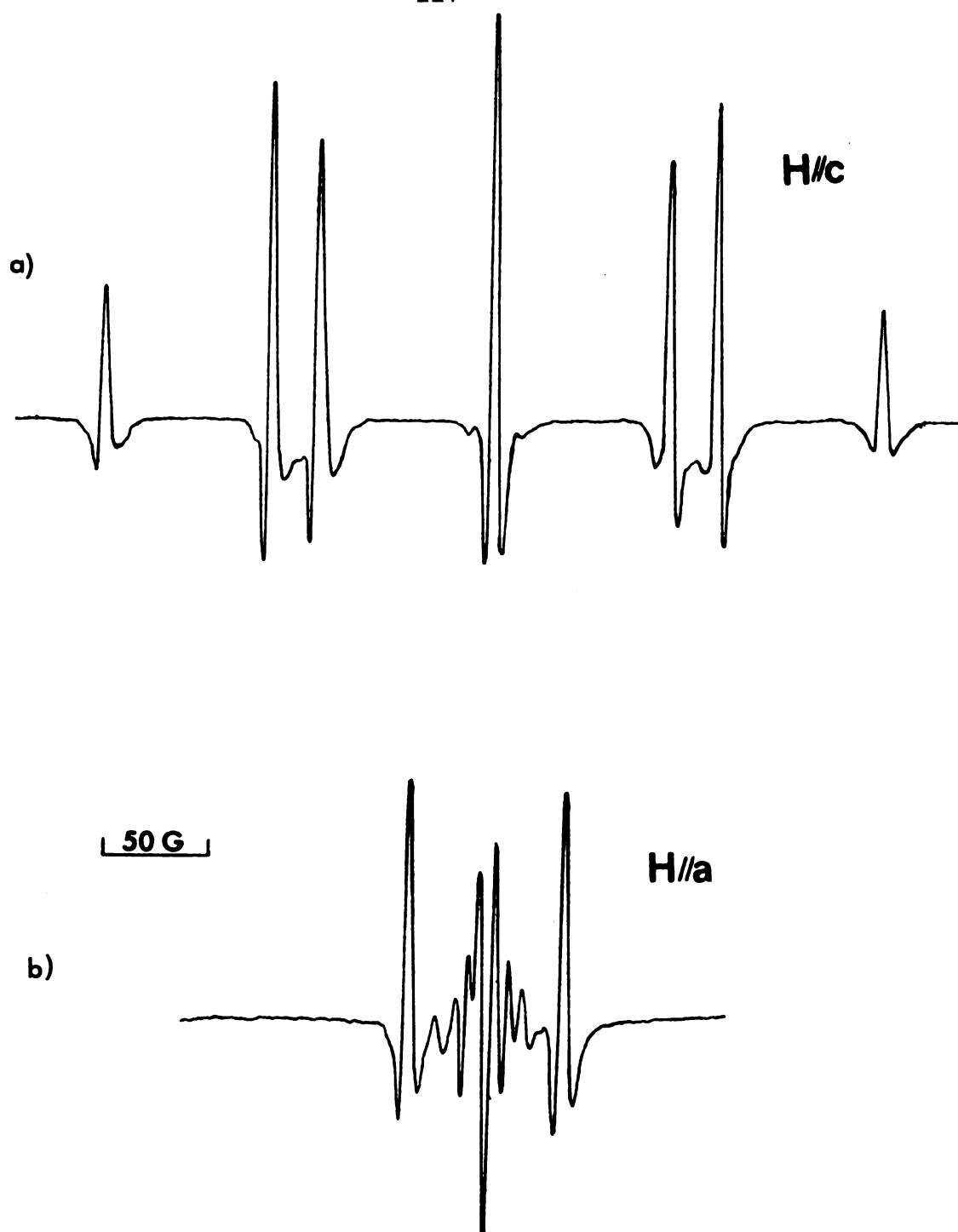


Figure 21. Second-derivative ESR spectra of the room temperature radicals,  $\cdot CFHCOO^-$  and  $\cdot CF_2COO^-$ , produced in irradiated single crystals of ammonium difluoroacetate. Spectrum (a) was obtained with the magnetic field parallel to the maximum fluorine coupling (designated the  $c$  direction). Spectrum (b) was obtained with the magnetic field  $90^\circ$  from  $c$  (designated  $a$ ).





Figure 22a. Second-derivative ESR spectrum of the radicals produced in single crystals of ammonium difluoroacetate irradiated at room temperature. The direction of the magnetic field is parallel to  $c$ . The gain has been increased by 1000 to permit observation of the  $^{13}\text{C}$  satellites since the natural abundance of  $^{13}\text{C}$  is only 1.1%.

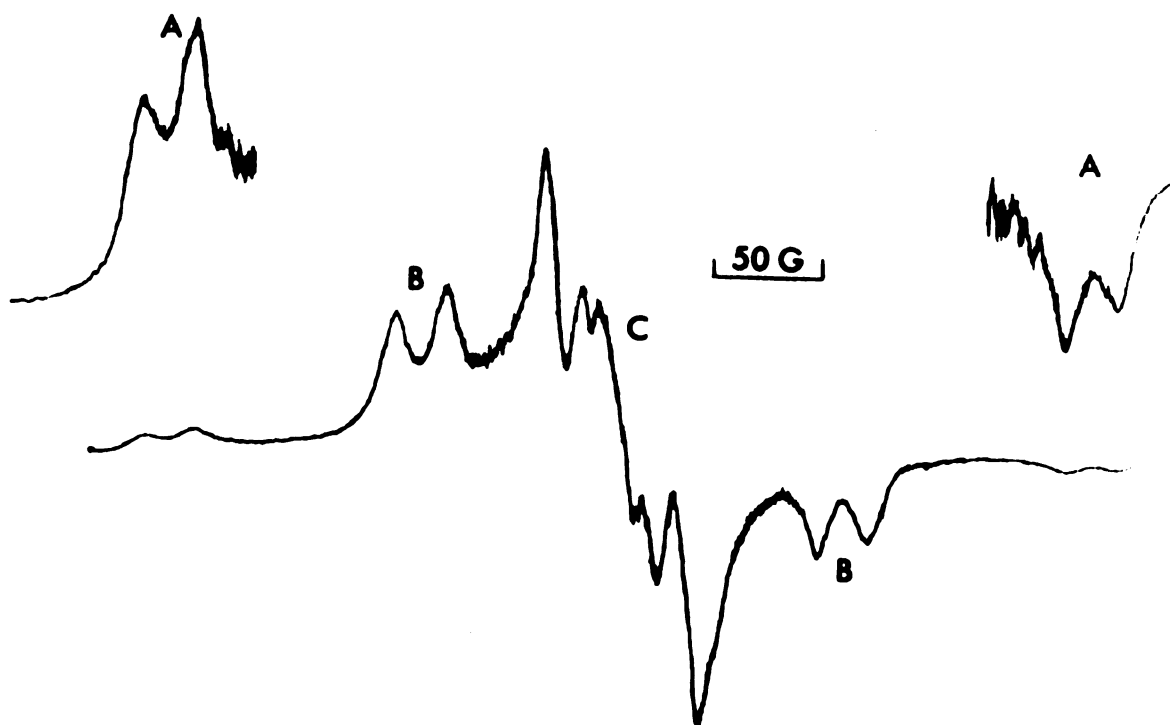
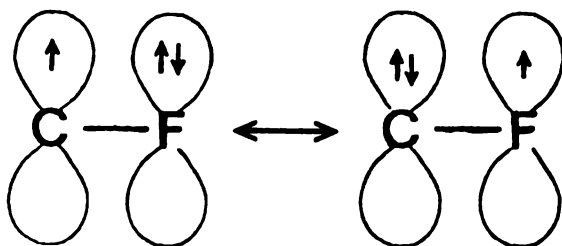


Figure 22b. First-derivative ESR powder spectrum of ammonium difluoroacetate irradiated at  $77^\circ \text{K}$ .

error and the values of  $A_{zz}({}^{19}\text{F})$  and  $A_{zz}({}^{13}\text{C})$  may be obtained directly. In this case,  $A_{zz} = 180.2$  G (E of Figure 22a) for the two fluorine atoms and  $A_{zz} = 130.5$  G (e of Figure 22a) for carbon-13 in the  $\cdot\text{CF}_2\text{COO}^-$  radical. For the  $\cdot\text{CFHCOO}^-$  radical the values are:  $A_{zz}({}^{19}\text{F}) = 185.2$  G,  $A_{zz}(\text{H}) = 21.9$  G (F of Figure 22a), and  $A_{zz}({}^{13}\text{C}) = 86.2$  G (f of Figure 22a).

2. Analysis of  $\cdot\text{CFHCOO}^-$  and  $\cdot\text{CF}_2\text{COO}^-$  Spectra. With the available data, it is possible to discuss the radical geometry and electronic structure. Since the  $\cdot\text{CFHCOO}^-$  radical is nearly axially symmetric, the primary contribution to the anisotropy must arise from electron spin density delocalized into the  $F_{2p\pi}$  orbital:



Contributions of the second structure are of the order of 12%. This estimate is based on the values (1080, -540, -540) calculated for an electron in a pure  $2p$  orbital. For the ammonium fluoroacetate radical, the anisotropic components (Table 9) are (130.9, -67.8, -62.8).

On the other hand, the departure from complete cylindrical symmetry indicates a spin polarization of the  $2p_\sigma$  orbital of the C-F bond; it has been proposed<sup>85</sup> that



this is negative and of the order of -0.003. This value is determined by a further separation of the anisotropic tensor to give:

$$\begin{vmatrix} 130.5 & & \\ & -67.8 & \\ & & -62.8 \end{vmatrix} = \begin{vmatrix} 132.2 & & \\ & -66.1 & \\ & & -66.1 \end{vmatrix} + \begin{vmatrix} -1.7 & & \\ & -1.7 & \\ & & +3.4 \end{vmatrix}.$$

The Fermi contact interaction resulting from the odd electron density in the  $F_{2s}$  orbital leads to the isotropic coupling of 50.4 G. An upper limit to the spin density in the fluorine  $2s$  orbital may then be determined from the value calculated for an electron in a pure  $2s$  orbital, (16,400 G), to be 0.0031. There is some contribution to this value from configuration interaction with the  $1s$  orbital. The analogous values for carbon-13 are given by (44.0, -21.3, -22.7) for the anisotropic part and 41.3 gauss for the isotropic part of the coupling. The  $c_{2p\pi}$  spin density calculated from these values is approximately 0.70.

Certainly one expects this value to be somewhat larger (0.83) based on the spin densities on hydrogen ( $\rho_{1s}(H) = 0.045$ ) and on fluorine ( $\rho_{2p}(F) = 0.12$ ). Using McConnell's relation<sup>110</sup> for  $\alpha$ -proton coupling,  $a_{CH} = Q\rho_{c_{2p\pi}}$ , one obtains  $\rho_{2p}(C) \cong 1.0$  using  $Q = -23$  G. This disagreement is perhaps not unexpected since the effective charge for the wave function used to determine the B parameter undoubtedly





differs from the effective charge on carbon in the fluorine-substituted radical.

The significant difference observed between  $A_{zz}(^{13}\text{C})$ , the coupling value along the  $p_\pi$  orbital direction, for  $\cdot\text{CFHCOO}^-$  and  $\cdot\text{CF}_2\text{COO}^-$  would indicate that there is a difference between the isotropic values  $a(^{13}\text{C})$  for these radicals. The three components of the  $A(^{13}\text{C})$  tensor for the  $\cdot\text{CF}_2\text{COO}^-$  radical in ammonium difluoroacetate could not be determined with certainty; however, an estimate of  $a(^{13}\text{C})$  could be made. Several tensors for these  $\pi$ -type radicals have been obtained and the anisotropic part of the coupling is observed to be nearly symmetrical with the form (2B, -B, -B) and a value of  $2B \approx 45$  G. Hence, the  $a(^{13}\text{C})$  value becomes approximately 85 gauss for  $\cdot\text{CF}_2\text{COO}^-$ . Following Fessenden and Schuler,<sup>97</sup> it is reasonable to attribute the increase in  $a(^{13}\text{C})$  with increase in fluorine substitution to increasing deviation of the radicals from planarity and consequently, an increase in the  $s$  character of the orbital. Values for  $\theta$ , the angle of bending from the plane of the radical, are computed on the basis of the formula

$$a(^{13}\text{C}) = a_o(^{13}\text{C}) + 1190(2 \tan^2 \theta), \quad (26)$$

with  $a_o(^{13}\text{C})$  taken as 38.5 gauss assuming  $\cdot\text{CH}_3$  is planar.<sup>101</sup> This formula leads to a nearly planar structure for  $\cdot\text{CFHCOO}^-$  radical while the  $\cdot\text{CF}_2\text{COO}^-$  system bends slightly, to approximately  $8^\circ$  from the plane. The odd-electron orbital

would then have 4-5% s character in the difluoro radical. Similar values were determined by Rogers and Kispert<sup>89</sup> for other fluorine containing radicals.

3. Spectra at 77° K. Identification of the radicals formed by irradiation of ammonium difluoroacetate at liquid nitrogen temperature has not been successful. Apparently the two radicals found at room temperature are present at 77° K, but at different orientations so that analysis of the spectra is difficult. In addition, though, a very weak coupling pattern was noted with a large maximum hyperfine splitting value. This radical would have to be characterized as arising from two fluorine atoms, because the coupling is greater than 360 gauss, plus a smaller doublet from an  $\alpha$  proton. Unfortunately, due to the weak intensity of the lines and to overlapping from those of the other more abundant species present no further results may be reported from the single crystal.

It is interesting to note the powder spectrum for this sample irradiated at 77° K (Figure 22b). Normally, powder spectra appear too complex to analyze.<sup>174</sup> However, in this case several observations may be made. At increased gain, a pair of doublets (A, Figure 22b) separated by about 400 G is observed. This splitting must arise from two fluorine nuclei and hence, one of the peaks in the central portion of the spectrum must form the central line (C) of a triplet

with a fluorine coupling of 211 G. The splitting for the doublet substructure present for each of the outer pairs (A) is estimated to be 22 G and so probably arises from an  $\alpha$  proton. The intermediate pair of doublets (B) with considerably greater intensity, cannot belong to the same multiplet as the triplet (A,C,A) since the splitting is different. The separation of 190 G between these lines (B, Figure 22b) suggests that they arise from an  $\alpha$  fluorine and the doublet substructure of 22.6 G is indicative of an  $\alpha$  proton. The outer-line couplings in a powder correspond to  $g_{zz}$ ,<sup>174</sup> the  $g$  value in a direction perpendicular to the plane of the radical. Consequently, a tentative assignment of the inner and more intense set (B) to the  $\cdot\text{CFHCOO}^-$  radical is made and the outer set (A,C,A) is assigned to the  $\cdot\text{CF}_2\text{H}$  radical. Since the isotropic hyperfine fluorine interaction in  $\cdot\text{CF}_2\text{H}$  (84.2 G)<sup>97</sup> is considerably larger than that in  $\cdot\text{CFHCOO}^-$  (50.4 G), it is not unreasonable to assign the values 211 G and 190 G for  $A_{zz}(\text{F})$  to  $\cdot\text{CF}_2\text{H}$  and  $\cdot\text{CFHCOO}^-$ , respectively.

### C. Ammonium Trifluoroacetate

Previous studies on irradiated ammonium trifluoroacetate<sup>88</sup> gave the  $\cdot\text{CF}_2\text{COO}^-$  radical at room temperature. However, low-temperature (77° K) irradiation yielded an unusual spectrum with three anisotropic fluorine couplings and one coupling which was assigned to a proton. The radical was reported



to be  $[\text{CF}_3\text{COOH}\cdot\text{NH}_3]^-$  on the basis of the doublet splitting since its magnitude (14.7 G) was about that expected for a long-range proton coupling. However, the isotropic fluorine coupling data indicate that the radical is probably  $\cdot\text{CF}_3$  since the splitting is comparable to that found for  $\cdot\text{CF}_3$  in trifluoroacetamide.<sup>87</sup> If it is  $\cdot\text{CF}_3$  two points may be noted, (1) the fluorine couplings are all inequivalent, indicating restricted motion, and (2) there would be no explanation for the extra doublet coupling.

With this ambiguity in mind crystals of  $\text{CF}_3\text{COOND}_4$  grown from a solution of  $\text{D}_2\text{O}$  were irradiated at 77° K. The spectra for rotations in the *ac* and *bc* planes chosen by Srygley and Gordy<sup>88</sup> were exactly comparable to their spectra. Further, on slight warming, no changes in the spectra which would indicate motional averaging were observed in the very small temperature range of stability of this radical; about 200° K,  $\cdot\text{CF}_2\text{COO}^-$  is formed. The unusual doublet structure persists even in this deuterated sample. Consequently, one can assign the doublet coupling to a long-range interaction such as that with a fluorine in the lattice. This unusual type of coupling has been reported for one of the  $\cdot\text{CF}_2\text{COO}^-$  radicals found in irradiated sodium chlorodifluoroacetate.<sup>89</sup> Here the coupling was explained as probably arising from two fluorine atoms in the lattice to give a triplet. The magnitudes of the couplings are rather similar. The assignment of  $\cdot\text{CF}_3$  as the structure of the radical is



thus reasonable.

#### D. Ammonium Chlorodifluoroacetate

The usefulness of these ammonium salts for electron spin resonance studies was further shown with the irradiation of ammonium chlorodifluoroacetate. Irradiation at 77° K indicates, from the spectrum presented in Figure 23, that the  $\cdot\text{CF}_2\text{Cl}$  radical is present. Here again, the hyperfine structure is very complex and interference from another radical species makes only tentative assignment possible. However, observations of the spectrum taken at an orientation showing maximum splitting (360 gauss) of the outer lines indicates that at least two fluorine atoms must be present. The fine structure then, on the outer lines can only be explained on the basis of superhyperfine coupling from a chlorine atom leading to the choice of  $\cdot\text{CF}_2\text{Cl}$  radical as the probable species.

On warming to room temperature, the spectrum clearly indicates that the  $\cdot\text{CF}_2\text{COO}^-$  radical is the only species remaining and there is no longer any chlorine fine structure associated with the spectrum.

#### E. Radical Formation

The large amount of information now available<sup>1,2</sup> on the formation of radicals in single crystals of fluorine-containing organic compounds enables some generalizations to be made. For the sequence  $\text{CFH}_2\text{COONH}_4$ ,  $\text{CF}_2\text{HCOONH}_4$ ,





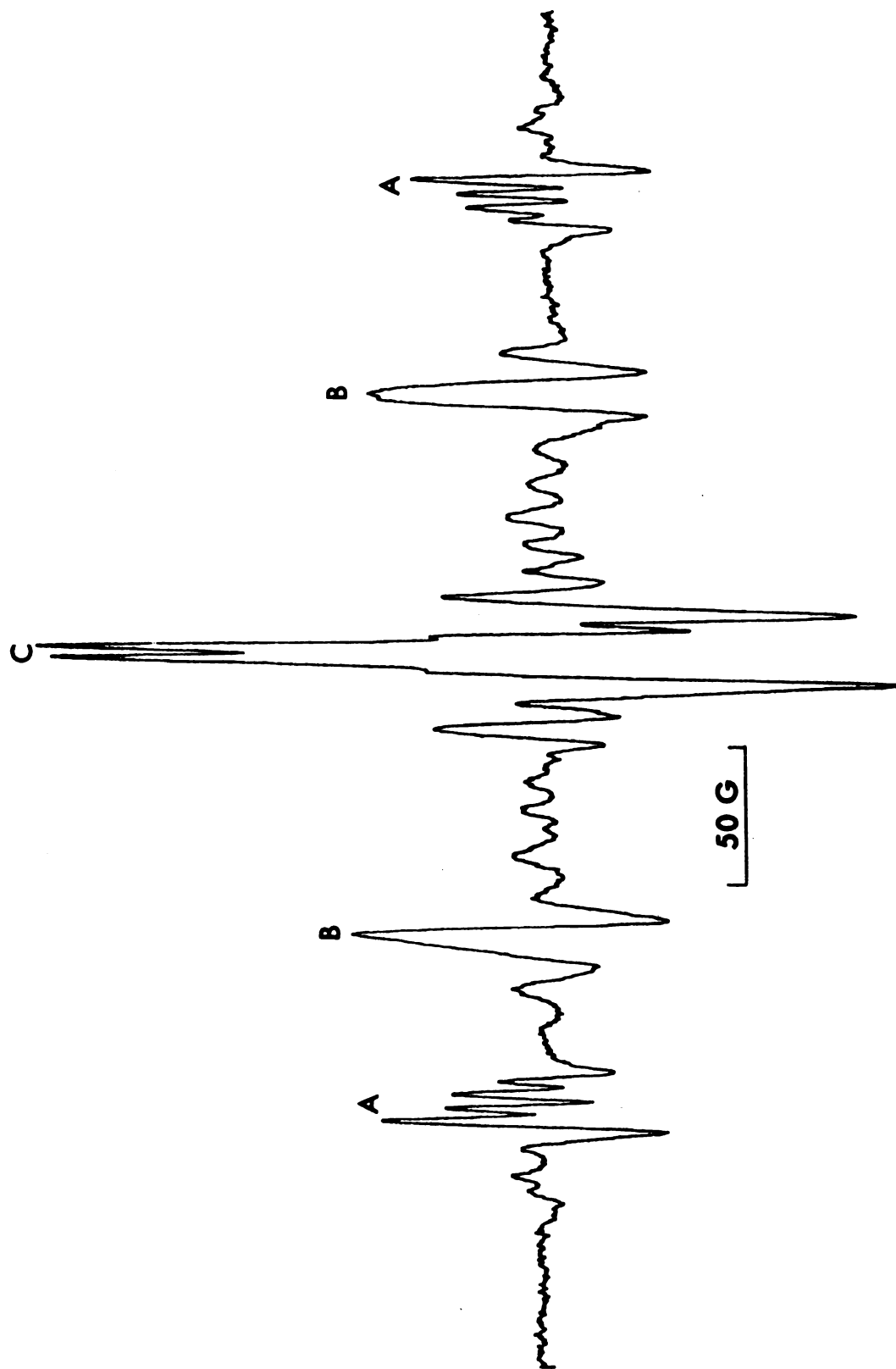


Figure 23. Second-derivative ESR spectrum of radicals produced in a single crystal of ammonium chlorodifluoroacetate by irradiation at 77° K. The orientation is that which gives maximum splitting of the outer multiplets.



$\text{CF}_3\text{COONH}_4$  and  $\text{CF}_2\text{ClCOONH}_4$  it appears that two processes are occurring on irradiation at  $77^\circ \text{K}$ ; carbon-carbon bond breaking and carbon-halogen bond breaking. There seems to be a preference for CF bond breaking over CH bond breaking, for example, in  $\text{CFH}_2\text{COONH}_4$ . One would expect to find twice as much  $\cdot\text{CFHCOO}^-$  if the loss of hydrogen and fluorine atoms were equally probable. However, approximately four times as much  $\cdot\text{CH}_2\text{COO}^-$  is found. And, in the difluoroacetate there is a large preference for  $\cdot\text{CFHCOO}^-$  at  $77^\circ \text{K}$ . On the other hand, the loss of chlorine appears to be favored over loss of fluorine in the ammonium chlorodifluoroacetate system. This is supported by the evidence reported for radicals produced in irradiated sodium chlorodifluoroacetate.<sup>89</sup>

Carbon-carbon bond breaking also appears to be one result of low-temperature irradiation. However, this seems to depend on the number and type of halogen substituents. That is, CC bond breaking takes place in the monofluoro system. However, successively larger amounts of radical are produced with successive fluorine substitution, with relatively large concentrations in the trifluoro system. It is interesting to note that the  $\cdot\text{CH}_3$  radical is the predominant radical formed on irradiation of  $\text{CH}_3\text{COONH}_4$  single crystals at  $77^\circ \text{K}$ .<sup>47</sup>

On warming, abstraction reactions appear to be taking place. For  $\text{CFH}_2\text{COONH}_4$ , the  $\cdot\text{CH}_2\text{COO}^-$  abstracts a proton from a neighboring molecule to give  $\cdot\text{CFHCOO}^-$  at room

temperature. In  $\text{CF}_2\text{COONH}_4$ , both  $\cdot\text{CF}_2\text{H}$  and some  $\text{CFHCOO}^-$  must abstract protons from the neighboring molecules to account for the relative abundance of  $\cdot\text{CF}_2\text{COO}^-$  at room temperature. Also, the  $\cdot\text{CF}_3$  radical abstracts a fluorine from the lattice to give  $\cdot\text{CF}_2\text{COO}^-$  in ammonium trifluoroacetate while  $\cdot\text{CF}_2\text{Cl}$  must abstract a chlorine from a neighbor to produce  $\cdot\text{CF}_2\text{COO}^-$  at room temperature in ammonium chlorodifluoroacetate.

## CHAPTER VI

### SUMMARY

Electron spin resonance studies of radicals in several irradiated acetates and halogen-substituted acetates have been carried out.

(I) Single crystals of  $\text{CH}_3\text{COONa}\cdot 3\text{D}_2\text{O}$  have been irradiated at  $77^\circ\text{ K}$  and  $300^\circ\text{ K}$  and the ESR spectra studied over a range of temperatures. Three radicals were found;  $\cdot\text{CH}_3$  predominates at  $77^\circ\text{ K}$ ,  $\cdot\text{CH}_2\text{COO}^-$  at  $198^\circ\text{ K}$  and  $\cdot\text{CO}_2^-$  at room temperature. The  $g$  tensor and proton hyperfine splitting tensors were determined by analysis of the spectra. In addition,  $\cdot\text{CD}_3$  was studied in irradiated single crystals of  $\text{CD}_3\text{COONa}\cdot 3\text{D}_2\text{O}$  at  $77^\circ\text{ K}$ .

A study of the ESR spectrum of methyl radical in the range  $4.2^\circ\text{ K}$  -  $77^\circ\text{ K}$  was made. At  $77^\circ\text{ K}$  the ESR parameters show that it is a  $\pi$ -electron radical with three equivalent hydrogens and that it is undergoing rotation about the threefold axis. At  $30^\circ\text{ K}$  relative intensities of the four lines were found to change from 1:3:3:1 to 1:1:1:1 indicating some restriction of rotation at low temperature.

The ESR parameters for  $\cdot\text{CH}_2\text{COO}^-$  and  $\cdot\text{CO}_2^-$  are similar to those observed for the same radicals in other matrices.

The mechanism by which  $\cdot\text{CH}_2\text{COO}^-$  is produced from  $\cdot\text{CH}_3$  appears to be hydrogen abstraction from a  $\text{CH}_3\text{COO}^-$  ion of the matrix.

(II) A study of the ESR spectra of  $\gamma$ -irradiated single crystals and powders of anhydrous sodium acetate was made at  $77^\circ\text{K}$ . The  $\cdot\text{CH}_2\text{COO}^-$  radical was obtained and the  $A(\text{H})$  tensors evaluated. In addition, a triplet spectrum was observed which was attributed to a radical pair. Although the components of the pair appeared to be different, the spectra did not permit their positive identification.

(III) The ESR spectra of  $\gamma$ -irradiated single crystals of ammonium monofluoroacetate were studied over the temperature range  $77^\circ\text{K} - 373^\circ\text{K}$ . It was found that the radicals  $\cdot\text{CH}_2\text{COO}^-$  and  $\cdot\text{CFHCOO}^-$  were produced in the approximate ratio 4:1 on irradiation at  $77^\circ\text{K}$ . On warming to room temperature only the  $\cdot\text{CFHCOO}^-$  radical was present.

The  $\cdot\text{CFHCOO}^-$  radical at room temperature was found to occupy two magnetically inequivalent sites. On cooling, the spectra were observed to change such that two  $\cdot\text{CFHCOO}^-$ , each with different  $A(\text{F})$ ,  $A(\text{H})$  tensors, were obtained and each occupied two magnetically distinct sites. The  $g$  and the fluorine and hydrogen hyperfine splitting tensors were evaluated for both radicals at  $-140^\circ\text{C}$  and for the room-temperature radical; for the room-temperature radical the  $^{13}\text{C}$  hyperfine interaction tensor was also obtained.

An oscillation of the CHF group of the radical about

the C-C bond was postulated to account for the dependence of the ESR spectra on temperature. However changes in crystal structure may also occur.

(IV) A study of the ESR spectra of  $\gamma$ -irradiated single crystals and powders of ammonium difluoroacetate was made at 77° K and at room temperature. Material irradiated and observed at 77° K gave complex spectra which could not be analyzed in detail but the powder spectra indicated that both  $\cdot\text{CF}_2\text{H}$  and  $\cdot\text{CFHCOO}^-$  were produced, the former in relatively low concentrations, and possibly a third radical.

On warming the  $\cdot\text{CF}_2\text{H}$  radical disappeared and at room temperature the spectra showed the presence of  $\cdot\text{CF}_2\text{COO}^-$  and  $\cdot\text{CFHCOO}^-$  in approximately equal proportions. Measurements of the maximum components of the  $^{13}\text{C}$  hyperfine splitting tensors were made for both radicals and from these the isotropic components were estimated. These values show that  $\cdot\text{CFHCOO}^-$  is a nearly planar  $\pi$ -electron radical while  $\cdot\text{CF}_2\text{COO}^-$  is bent about 8° out of the plane.

(V) An investigation of the radical species present in irradiated ammonium trifluoroacetate- $\text{d}_4$  ( $\text{CF}_3\text{COOND}_4$ ) was made. ESR spectra of single crystals irradiated and observed at 77° K show strong evidence that the  $\cdot\text{CF}_3$  radical is produced, along with  $\cdot\text{CF}_2\text{COO}^-$ . A long-range coupling from a neighboring atom was not eliminated in the deuterated salt as would have been expected from a study reported in the

literature in which the radical was assigned the structure  $[\text{CF}_3\text{COOH} \cdots \text{NH}_3]^-$  instead of  $\cdot\text{CF}_3$ .

(VI) Single crystals of ammonium chlorodifluoroacetate were irradiated and the ESR spectra observed at 77° K. These show the presence of at least two radicals, one showing chlorine and fluorine hyperfine splitting and the second fluorine hyperfine splitting only. The radicals were assigned the structures  $\cdot\text{CF}_2\text{Cl}$  and  $\cdot\text{CF}_2\text{COO}^-$ .

These studies have shown that irradiation of acetate salts yields radicals which undergo interesting reactions and motional changes with changes in temperature and whose behavior has served to illustrate many of the properties of radicals in solid matrices. In addition to the reactions and motional changes, examples of radical pair formation and structural changes of radicals in crystals have been found. The structures of a number of radicals have been deduced from the ESR parameters and comparisons with data for the same radicals in different crystal matrices have provided information concerning the effects of the host on radical structure and conformation. Acetates have been regarded here as model systems, a study of whose behavior on irradiation should lead to an insight into the behavior of more complex systems such as macromolecules and biological materials.



## LIST OF REFERENCES

## REFERENCES

1. E. Zavoisky, J. Phys. U.S.S.R. 9, 211 (1945).
2. P. W. Atkins and M. C. R. Symons, The Structure of Inorganic Radicals, Elsevier Pub. Co., New York, 1967.
3. E. T. Kaiser and L. Kevan, ed., Radical Ions, Interscience Publishers, New York, 1968.
4. K. D. J. Root and M. T. Rogers, in Spectroscopy in Inorganic Chemistry, C. N. R. Rao and J. R. Ferraro, ed., Academic Press, New York, 1971, Vol. 2, p. 115.
5. H. A. Kuska and M. T. Rogers, in Spectroscopy in Inorganic Chemistry, C. N. R. Rao and J. R. Ferraro, ed., Academic Press, New York, 1971, Vol. 2, p. 175.
6. H. A. Kuska and M. T. Rogers, in Radical Ions, E. T. Kaiser and L. Kevan, ed., Interscience Publishers, New York, 1968, p. 579.
7. R. W. Fessenden and R. H. Schuler, in Advances in Radiation Chemistry, M. Burton and J. L. McGee, Interscience Publishers, New York, 1970, Vol. 2, p. 1.
8. A. Hudson and G. R. Luckhurst, Chem. Rev. 69, 191 (1969).
9. H. A. Farach and C. P. Poole, in Advance in Magnetic Resonance, J. S. Waugh, ed., Academic Press, New York, 1971, Vol. 5, p. 229.
10. J. E. Wertz and J. R. Bolton, Electron Spin Resonance, McGraw-Hill Book Co., New York, 1972.
11. D. J. E. Ingram, Biological and Biochemical Applications of Electron Spin Resonance, Hilger and Watts Ltd., London, 1969.
12. A. Ehrenberg, B. G. Malmstrom and T. Vanngard, ed., Magnetic Resonance in Biological Systems, Pergamon Press, New York, 1967.
13. T. J. Stone, T. Buckman, P. L. Nordio and H. M. McConnell, Proc. Natl. Acad. Sci. U.S. 54, 1010 (1965).
14. O. H. Griffith and A. S. Waggoner, Accts. Chem. Res. 2, 17 (1969).



15. See, for example, M. Dole, ed., Radiation Chemistry of Macromolecules, Academic Press, New York, 1972.
16. See, for example, Chem. Eng. News, April 10, 1972, p. 14.
17. J. R. Mallard and M. Kent, Nature 204, 1192 (1964).
18. W. T. Dixon and R. O. C. Norman, J. Chem. Soc. 1963, 3119; R. O. C. Norman and B. C. Gilbert, in Advances in Physical Organic Chemistry, V. Gold, ed., Academic Press, New York, 1967, Vol. 5, p. 53.
19. T. Cole and H. C. Heller, J. Chem. Phys. 42, 1668 (1965).
20. J. R. Morton, Chem. Rev. 64, 453 (1964).
21. See, for example, R. M. Eisberg, Fundamentals of Modern Physics, J. Wiley and Sons, Inc., New York, 1961, p. 76.
22. H. C. Box, H. G. Freund and K. T. Lilga, J. Chem. Phys. 42, 1471 (1965).
23. J. W. Wells, J. Chem. Phys. 52, 4062 (1970).
24. H. C. Box, H. G. Freund and E. E. Budzinski, J. Chem. Phys. 57, 4290 (1972).
25. J. Sinclair and M. W. Hanna, J. Phys. Chem. 71, 84 (1967); J. Chem. Phys. 50, 2125 (1969).
26. A. Minegishi, Y. Shinozaki and G. Meshitsuka, Bull. Chem. Soc. Japan 40, 1549 (1967).
27. I. Miyagawa, N. Tamura and J. W. Cook, J. Chem. Phys. 51, 3520 (1969).
28. E. Friday and I. Miyagawa, J. Chem. Phys. 55, 3589 (1973).
29. N. Tamura, M. A. Collins and D. H. Whiffen, Trans. Faraday Soc. 62, 2434 (1966).
30. G. C. Moulton and M. P. Cernansky, J. Chem. Phys. 51, 2283 (1969).
31. H. M. Vyas, J. Janecka and M. Fujimoto, Can. J. Chem. 48, 2804 (1970).
32. M. Fujimoto and W. A. Seddon, Can. J. Chem. 48, 2809 (1970).

33. W. M. Tolles, R. A. Sanders and R. G. Gish, J. Chem. Phys. 54, 1532 (1971).
34. M. Iwasaki, B. Eda and K. Toriyama, J. Am. Chem. Soc. 92, 3211 (1970).
35. M. Fujimoto, W. A. Seddon and D. R. Smith, J. Chem. Phys. 48, 3345 (1968).
36. D. G. Cadena, R. E. Linder and J. R. Rowlands, Can. J. Chem. 47, 3429 (1969).
37. A. Minegishi, Y. Shinozaki and G. Meshitsuka, J. Chem. Phys. 56, 2481 (1972).
38. H. C. Box, K. T. Lilga and E. E. Budzinski, J. Phys. Chem. 74, 40 (1970).
39. J. Sinclair, J. Chem. Phys. 55, 245 (1971).
40. A. Horsfield, J. R. Morton and D. H. Whiffen, Mol. Phys. 4, 327 (1961); Nature 189, 481 (1961).
41. R. C. McCalley and A. L. Kwiram, J. Am. Chem. Soc. 92, 1441 (1970); J. Chem. Phys. 53, 2541 (1970).
42. K. Reiss and W. Gordy, J. Chem. Phys. 55, 5329 (1971).
43. M. Iwasaki, T. Ichikawa and T. Ohmori, J. Chem. Phys. 50, 1991 (1969).
44. M. Iwasaki and B. Eda, Chem. Phys. Lett. 2, 210 (1968).
45. M. Iwasaki, K. Minakata and K. Toriyama, J. Chem. Phys. 55, 1472 (1971).
46. J. S. Hyde, L. D. Kispert, R. C. Sneed and J. C. W. Chien, J. Chem. Phys. 48, 3824 (1968).
47. M. T. Rogers and L. D. Kispert, Advan. Chem. Series, Amer. Chem. Soc. 82, 327 (1968).
48. B. L. Bales, R. N. Schwartz and M. W. Hanna, J. Chem. Phys. 51, 1974, 5178 (1969).
49. K. Itoh and I. Miyagawa, J. Chem. Phys. 40, 3328 (1964).
50. K. Itoh, I. Miyagawa and C. S. Chen, J. Chem. Phys. 52, 1822 (1970).
51. R. C. Schoening and P. J. Hamrick, (unpublished results).

52. I. Miyagawa and K. Itoh, J. Chem. Phys. 43, 2915 (1965).
53. I. Miyagawa and K. Itoh, Nature 209, 504 (1966).
54. I. Miyagawa and K. Itoh, J. Chem. Phys. 36, 2157 (1962).
55. J. R. Morton, J. Am. Chem. Soc. 86, 2325 (1964).
56. T. Kato and R. Abe, J. Phys. Soc. Japan 26, 948 (1969); *ibid.* 29, 389 (1970).
57. W. M. Tolles, L. P. Crawford and J. L. Valenti, J. Chem. Phys. 49, 4745 (1968).
58. R. G. Hayes, D. J. Steible, W. M. Tolles and J. W. Hunt, J. Chem. Phys. 53, 4466 (1970).
59. H. Ohigashi and Y. Kurita, Bull. Chem. Soc., Japan, 41 275 (1968).
60. M. Fujimoto and J. Janecka, J. Chem. Phys. 55, 5 (1971).
61. E. A. C. Lucken and C. Mazeline, J. Chem. Soc. 1967 A , 439; Colloque Ampere XIV, North Holland Pub. Co., Amsterdam, 1967, p. 566.
62. R. P. Kohin and P. G. Nadeau, J. Chem. Phys. 44, 691 (1966).
63. S. Ohnishi, S. Sugimoto and I. Nitta, J. Chem. Phys. 37, 1283 (1962).
64. C. Corvaja, J. Chem. Phys. 44, 1958 (1966).
65. O. H. Griffith, J. Chem. Phys. 41, 1093 (1964).
66. M. Kashiwagi and Y. Kurita, J. Chem. Phys. 39, 3165 (1963).
67. C. Corvaja, Trans. Faraday Soc. 63, 26 (1967).
68. N. Tamura, M. A. Collins and D. H. Whiffen, Trans. Faraday Soc. 62, 1037 (1966).
69. E. W. Stone and A. H. Maki, J. Chem. Phys. 37, 1326 (1962).
70. A. Horsfield, J. R. Morton and D. H. Whiffen, Mol. Phys. 5, 115 (1962).

71. R. B. Davidson and I. Miyagawa, J. Chem. Phys. 52, 1727 (1970); *ibid*, 57, 1815 (1972).
72. G. Lassmann and W. Damerau, Mol, Phys. 21, 551 (1971).
73. W. L. Gamble, I. Miyagawa and R. L. Hartman, Phys. Rev. Lett. 20, 415 (1968).
74. J. W. Wells and H. C. Box, J. Chem. Phys. 48, 2542 (1968).
75. C. Heller, J. Chem. Phys. 36, 175 (1962).
76. S. Clough, M. Starr and N. D. McMillan, Phys. Rev. Lett. 25, 839 (1970).
77. M. Iwasaki, K. Nunome, H. Muto and K. Toriyama, J. Chem. Phys. 54, 1839 (1971).
78. M. Fujimoto, J. Chem. Phys. 39, 846 (1963).
79. J. R. Morton, J. Chem. Phys. 41, 2956 (1964).
80. H. C. Box and H. G. Freund, J. Chem. Phys. 44, 2345 (1966).
81. J. W. Wells and H. C. Box, J. Chem. Phys. 46, 2935 (1967).
82. S. Clough and F. Poldy, J. Chem. Phys. 51, 2076 (1969); Colloque Ampere XV, North Holland Pub. Co., Amsterdam, 1969, p. 274; Phys. Lett. 24A, 545 (1967); *ibid*, 25A, 186 (1967).
83. C. M. Bogan and L. D. Kispert, J. Chem. Phys. 57, 3109 (1972).
84. J. H. Freed, J. Chem. Phys. 43, 1710 (1965).
85. R. J. Cook, J. R. Rowlands and D. H. Whiffen, Mol. Phys. 7, 31 (1963).
86. R. J. Lontz and W. Gordy, J. Chem. Phys. 37, 1357 (1962).
87. M. T. Rogers and L. D. Kispert, J. Chem. Phys. 46, 3193 (1967).
88. F. D. Srygley and W. Gordy, J. Chem. Phys. 46, 2245 (1967).
89. M. T. Rogers and L. D. Kispert, J. Chem. Phys. 55, 2360 (1971).

90. F. G. Herring, W. C. Lin and M. R. Mustafa, Can. J. Chem. 48, 447 (1970).
91. F. G. Herring, W. C. Lin and M. R. Mustafa, J. Magn. Resonance 2, 9 (1970).
92. M. Iwasaki, S. Noda and K. Toriyama, Mol. Phys. 18, 201 (1970).
93. M. T. Rogers and D. H. Whiffen, J. Chem. Phys. 40, 2662 (1964).
94. L. D. Kispert and M. T. Rogers, J. Chem. Phys. 54, 3326 (1971).
95. R. J. Lontz, J. Chem. Phys 45, 1339 (1966).
96. L. D. Kispert and F. Meyers, J. Chem. Phys. 56, 2623 (1972).
97. R. W. Fessenden and F. H. Schuler, J. Chem. Phys. 43, 2704 (1964).
98. M. T. Rogers and L. D. Kispert, J. Chem. Phys. 46, 221 (1967).
99. D. L. Beveridge, P. A. Dobosh and J. A. Pople, J. Chem. Phys. 48, 4802 (1968).
100. J. A. Pople, D. L. Beveridge and P. A. Dobosh, J. Am. Chem. Soc. 90, 4201 (1968).
101. D. M. Schrader and M. Karplus, J. Chem. Phys. 40, 1593 (1964); D. M. Schrader, J. Chem. Phys. 46, 3895 (1967).
102. C. P. Poole, Electron Spin Resonance, Interscience Publishers, New York, 1967.
103. R. S. Alger, Electron Paramagnetic Resonance, Interscience Publishers, New York, 1968.
104. P. B. Ayscough, Electron Spin Resonance in Chemistry, Methuen and Co. Ltd., London, 1967.
105. A. Abragam and B. Bleaney, Electron Paramagnetic Resonance of Transition Ions, Clarendon Press, Oxford, 1970.
106. See, for example, Advances in Magnetic Resonance, J. S. Waugh, ed., Academic Press, New York, 1965.
107. A. Carrington and A. McLachlan, Introduction to Magnetic Resonance, Harper and Row Publishers, New York, 1967.



108. C. P. Poole and H. A. Farach, The Theory of Magnetic Resonance, Interscience Publishers, New York, 1972.
109. H. M. McConnell, C. Heller, T. Cole and R. W. Fessenden, J. Am. Chem. Soc. 82, 766 (1960).
110. H. M. McConnell and D. B. Chestnut, J. Chem. Phys. 28, 107 (1958).
111. A. D. McLachlan, Mol. Phys. 1, 233 (1958).
112. D. B. Chestnut, J. Chem. Phys. 29, 43 (1958).
113. D. Vorlander and O. Nolte, from Chem. Abs. 8, 342 (1914).
114. L. D. Kispert, Ph. D. Thesis, Michigan State University, 1965.
115. P. Groth, Chemisches Krystallographie III, Verlag von Wilhelm Engelmann, Leipzig, 1906.
116. J. C. Watson, Ph. D. Thesis, Michigan State University, 1970.
117. W. G. Waller, Ph. D. Thesis, Michigan State University, 1973.
118. W. G. Waller and M. T. Rogers, J. Magn. Resonance, 9, 92 (1973).
119. W. Snipes and W. Bernhard, J. Chem. Phys. 43, 2921 (1965).
120. G. T. Trammell, H. Zeldes and R. Livingston, Phys. Rev. 110, 630 (1958).
121. R. W. Fessenden, J. Phys. Chem. 71, 74 (1967).
122. T. Cole, H. O. Pritchard, N. R. Davidson and H. M. McConnell, Mol. Phys. 1, 406 (1958).
123. C. K. Jen, S. N. Foner, E. L. Cochran and V. A. Bowers, Phys. Rev. 112, 1169 (1958).
124. J. M. Riveros and S. Shih, J. Chem. Phys. 50, 3132 (1969).
125. H. N. Rexroad and W. Gordy, Phys. Rev. 125, 242 (1962); G. S. Jackel and W. Gordy, Phys. Rev. 176, 443 (1968).
126. B. Smaller and M. S. Matheson, J. Chem. Phys. 28, 1169 (1958).

127. M. Fujimoto, H. D. Gesser, B. Garbutt and M. Shimizu, *Science* 156, 1105 (1967).
128. G. B. Garbutt, H. D. Gesser and M. Fujimoto, *J. Chem. Phys.* 48, 4605 (1968).
129. J. Turkevitch and Y. Fujita, *Science* 152, 1619 (1966).
130. I. A. Zlochower, W. R. Miller and G. K. Fraenkel, *J. Chem. Phys.* 42, 3339 (1965).
131. P. Smith, J. T. Pearson, P. B. Wood and T. C. Smith, *J. Chem. Phys.* 43, 1535 (1965).
132. J. Janecka, H. M. Vyas and M. Fujimoto, *J. Chem. Phys.* 54, 3229 (1971).
133. G. Vincow, S. Y. Chang and E. R. Davidson, *J. Chem. Phys.* 54, 4121 (1971), and references cited therein.
134. K. Eben and R. W. Fessenden, *J. Phys. Chem.* 75, 1186 (1971).
135. H. C. Box, H. G. Freund and E. E. Budzinski, *J. Am. Chem. Soc.* 88, 658 (1966).
136. H. C. Box, E. E. Budzinski and H. G. Freund, *J. Chem. Phys.* 50, 2880 (1969).
137. D. W. Ovenall and D. H. Whiffen, *Mol. Phys.* 4, 135 (1961); *Mol. Phys.* 5, 189 (1962).
138. S. Schlick, B. L. Silver and Z. Luz, *J. Chem. Phys.* 54, 867 (1971).
139. P. W. Atkins, N. Keen and M. C. R. Symons, *J. Chem. Soc.* 1962, 2873.
140. O. Edlund, A. Lund and H. Tellgren, *Colloque Ampere XV*, North Holland Pub. Co., Amsterdam, 1969, p. 293.
141. S. A. Marshall, A. R. Reinberg, R. A. Serway and J. A. Hodges, *Mol. Phys.* 8, 225 (1964); J. A. McMillan and S. A. Marshall, *J. Chem. Phys.* 48, 467 (1968).
142. R. C. Hughes and Z. G. Soos, *J. Chem. Phys.* 52, 6302 (1970).
143. J. E. Bennett, B. Mile and A. Thomas, *Trans. Faraday Soc.*, 61, 2357 (1965).
144. R. W. Holmberg, *J. Chem. Phys.* 55, 1730 (1971).

145. R. N. Schwartz, M. W. Hanna and B. L. Bales, J. Chem. Phys. 51, 4336 (1969).
146. P. Premovic, O. Gale and B. Radak, J. Chem. Phys. 59, 987 (1973).
147. J. N. Herak, J. Chem. Phys. 52, 6440 (1970).
148. R. J. Cook and D. H. Whiffen, J. Phys. Chem. 71, 93 (1967).
149. D. Pooley and D. H. Whiffen, J. Chem. Soc. 1962, 366.
150. W. Gordy and R. Morehouse, Phys. Rev. 151, 207 (1966).
151. M. Iwasaki, T. Ichikawa and T. Ohmori, J. Chem. Phys. 50, 1984 (1969).
152. Y. Kurita, J. Chem. Phys. 41, 3926 (1964).
153. Y. Kurita, and M. Kashiwagi, J. Chem. Phys. 44, 1727 (1966).
154. M. Kashiwagi and Y. Kurita, J. Phys. Soc. Japan 21, 558 (1966).
155. H. Hayashi, K. Itoh and S. Nagakura, Bull. Chem. Soc. Japan 40, 284 (1967).
156. H. Ohigashi and Y. Kurita, Bull. Chem. Soc. Japan 40, 704 (1967).
157. G. C. Moulton, M. P. Cernansky and D. C. Straw, J. Chem. Phys. 46, 4292 (1967).
158. M. Iwasaki and K. Toriyama, J. Chem. Phys. 46, 4693 (1967).
159. K. Reiss and H. Shields, J. Chem. Phys. 50, 4368 (1969).
160. H. C. Box, E. E. Budzinski and W. Potter, J. Chem. Phys., 55, 315 (1971).
161. H. C. Box, J. Phys. Chem. 75, 3426 (1971).
162. M. Iwasaki and T. Ichikawa, J. Chem. Phys. 46, 2851 (1967).
163. D. Campbell and M. C. R. Symons, J. Chem. Soc. 1969 A, 1494.
164. P. D. Bartlett, Chem. Eng. News 44, 106 (1966).

165. D. A. Wiersma and J. Kommandeur, Mol. Phys. 13, 241 (1967); D. A. Wiersma, J. H. Lichtenbelt and J. Kommandeur, J. Chem. Phys. 50, 2794 (1969).
166. A. Davis, J. H. Golden, J. A. McRae and M. C. R. Symons, Chem. Commun. 1967, 398; J.A.McRae and M. C. R. Symons, J. Chem. Soc. 1968 B, 428.
167. P. W. Atkins, M. C. R. Symons and P. A. Trevalion, Proc. Chem. Soc. 1963, 222; S. B. Barnes and M. C. R. Symons, J. Chem. Soc. 1966 A, 66.
168. H. M. McConnell, J. Chem. Phys. 29, 1422 (1958).
169. D. Cruikshank, D. W. Jones and G. Walker, J. Chem. Soc. 255, 1303 (1964).
170. H. S. Gutowsky and C. H. Holm, J. Chem. Phys. 25, 1228 (1956).
171. C. H. Johnson, in Advances in Magnetic Resonance, J. S. Waugh, ed., Academic Press, New York, 1965, Vol. 1, p. 33.
172. R. G. Gordon and R. P. McGinnis, J. Chem. Phys. 49, 2455 (1968).
173. G. Binsch, Mol. Phys. 15, 469 (1958); J. Am. Chem. Soc. 91, 1304 (1969).
174. M. Iwasaki, K. Toriyama and B. Eda, J. Chem. Phys. 42, 63 (1965).

MICHIGAN STATE UNIVERSITY LIBRARIES



3 1293 03169 5137